Molecular analysis of the neuroprotective role of Norrin for photoreceptors in the mammalian retina

DISSERTATION

Zur Erlangung des Doktorgrades der
Naturwissenschaften (Dr. rer. nat.) der
Naturwissenschaftlichen Fakultät III
Biologie und vorklinische Medizin der
Universität Regensburg

vorgelegt von
Barbara Maria Braunger
aus Biberach an der Riß

Regensburg, 2013

Das Promotionsgesuch wurde eingereicht am:
8.10.2013

Die Arbeit wurde angeleitet von:
Prof. E.R. Tamm

Unterschrift:

The human being,

creature of eyes,

needs the image.

Leonardo da Vinci (1452 – 1519)

Meinen Eltern

Table of Contents

1 Introduction:

1.1 Retina

The vertebrate retina consists of several neuronal layers interconnected by synapses. From the vitreous side, the first neuronal layer is the ganglion cell layer (GCL) with the soma of retinal ganglion cells and aberrant amacrine cells. The axons of the retinal ganglion cells (RGC) form the optic nerve. The cells of the RGC layer are connected by synapses with the neurons of the inner nuclear layer (INL). Within the INL, there are several different neuronal populations: the amacrine, bipolar and horizontal cells. Additionally the cell somas of the Müller glia cells are located in the INL. The INL neurons are again interconnected by synapses with the light sensitive photoreceptor cells, their cell soma are located in the outer nuclear layer (ONL). Figure 1 shows a schematic of the retina and a corresponding semithin section of the retinal morphology.

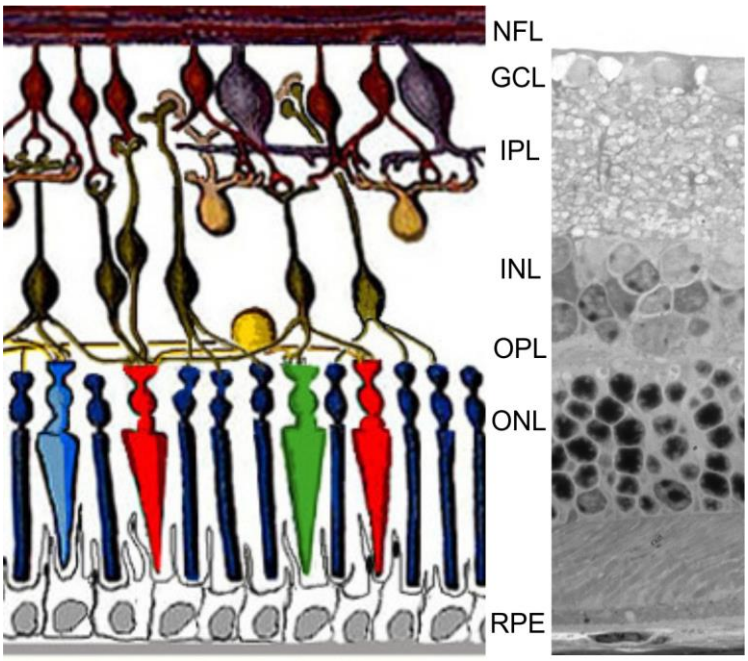

Figure 1: Morphology of the retina
Schematic and corresponding semithin section of retinal morphology. Abbreviations: NFL: nerve fiber layer, GCL: ganglion cell layer, IPL: inner plexiform layer, INL: inner nuclear layer, OPL: outer plexiform layer, ONL: outer nuclear layer, RPE: retinal pigment epithelium. Slightly modified after (1), semithin section (right hand side) by Barbara Braunger.

1.1.1 Retinal neurons and glia cells

1.1.1.1 Retinal ganglion cells

The retinal ganglion cells are located in the innermost neuronal layer of the retina. The axons of the retinal ganglion cells form the nerve fiber layer (stratum opticum) which is situated on top of the retinal ganglion cell soma, next to the side of the vitreous. These axons conjoin in the central retina as optic nerve head and form thereafter the optic nerve, which extend after the optic chiasm as optic

tract in the optic center of the brain (2). There are different subpopulations of retinal ganglion cells (3) that use different neurotransmitter gamma-aminobutyric acid (GABA), glycine or glutamate (4).

The retinal ganglion cells have different functions, apart from sending photoreceptor derived signal into the optic center of the brain. For example, photosensitive retinal ganglion cell are involved in the pupillary reaction and circadian rhythm (5,6).

1.1.1.2 The inner nuclear layer (INL):

The inner nuclear layer (INL) is composed of various different cell types. One has to distinguish between neuronal cells like amacrine, bipolar and horizontal cells and Müller glia cells (see 1.1.1.4.).

1.1.1.3 Neurons of the INL: amacrine cells, bipolar cells and horizontal cells

Amacrine cells are located in the retinal ganglion cell layer, where they are called aberrant amacrine cells and in the inner aspect of the inner nuclear layer (2). There are various subtypes (> 30 different subtypes) of amacrine cells (7,8). Amacrine cells have large dendrites that extend laterally in the inner plexiform layer. They modulate ganglion cell function by utilizing inhibitory neurotransmitters like GABA or glycine, but also the excitatory neurotransmitter acetylcholine (9). Additionally, amacrine cells with extensive ramified dendrites are thought to support the function of horizontal cells by sending inhibitory feedback to bipolar cells and ganglion cells.

Bipolar cells are the major neuronal cell population in the inner nuclear layer (2). They are interneurons, transporting the signals from the photoreceptor cells to the ganglion cells. One distinguishes between cone and rod bipolar cells and the way they mediate the electric excitation as on- and off-bipolar cells (10). In the mouse retina, there is one class of rod driven bipolar cell and 11 subtypes of cone driven bipolar cells (11). Bipolar cells use the neurotransmitters glutamate and to a small extend glycine (4). After light induced hyperpolarization of photoreceptor cells, the on-bipolar cells depolarize resulting in an excitation of the subsequent retinal ganglion cell. In contrast off-bipolar cells hyperpolarize after photoreceptor hyperpolarization leading to an inhibition of the consecutive retinal ganglion cell.

Horizontal cells are situated at the outer aspect of the inner nuclear layer with large ramified dendrites in the outer plexiform layer (2). Depending on the species, there are up to 3 different subtypes of horizontal cells which release the inhibitory neurotransmitter GABA (12). Although the detailed mode of how horizontal cells mediate their effects is still under discussion (10,13), in the end horizontal cells sum up the light responses across a wide retinal region and subtract it from the local signal. This results in an improved contrast vision and allows seeing properly under dim as well as under bright light conditions (14).

1.1.1.4 Retinal glia cells: astrocytes, Müller glia cells and microglia

The retinal astrocytes are found in the optic nerve fiber layer of the retina (15). Together with the Müller glia end feet they form the inner limiting membrane (16). Astrocytes play an important role during vasculogenesis for the proper guiding of the vessels towards the periphery of the retina. Later in development, they are part of the inner blood retinal barrier, which is composed of astrocytes, endothelial cells and pericytes (17). They also secrete the neuroprotective and angiogenic factor vascular endothelial growth factor (VEGF). This factor expressed from astrocytes turned out to be more important for the maintenance of vessel stability than the guiding of the vessels during vasculogenesis (18).

Müller glia cells span the retina vertically (19). Their cell bodies are located in the inner nuclear layer (2), of which they comprise 16% of all the cells present in the INL (15). Müller glia end feet give rise to the outer and inner limiting membrane (16). The outer limiting membrane lies between the outer nuclear layer and the inner segments of the photoreceptors, whereas the inner limiting membrane lies on top of the nerve fiber layer. During angiogenesis, Müller glia cells build up a gradient of the angiogenic factor vascular endothelia growth factor (VEGF) that guides endothelial cells towards their designated localization. Additionally, Müller glia cells are of major importance for the maintenance of the retina in general. They express growth factors, neurotransmitter transporters and antioxidant agents to prevent retinal neurons from excitotoxic damage (16,19). The various Müller cell functions are shown as a schematic in Figure 2. The ability of Müller cells to secrete neuroprotective factors is of major importance for this project.

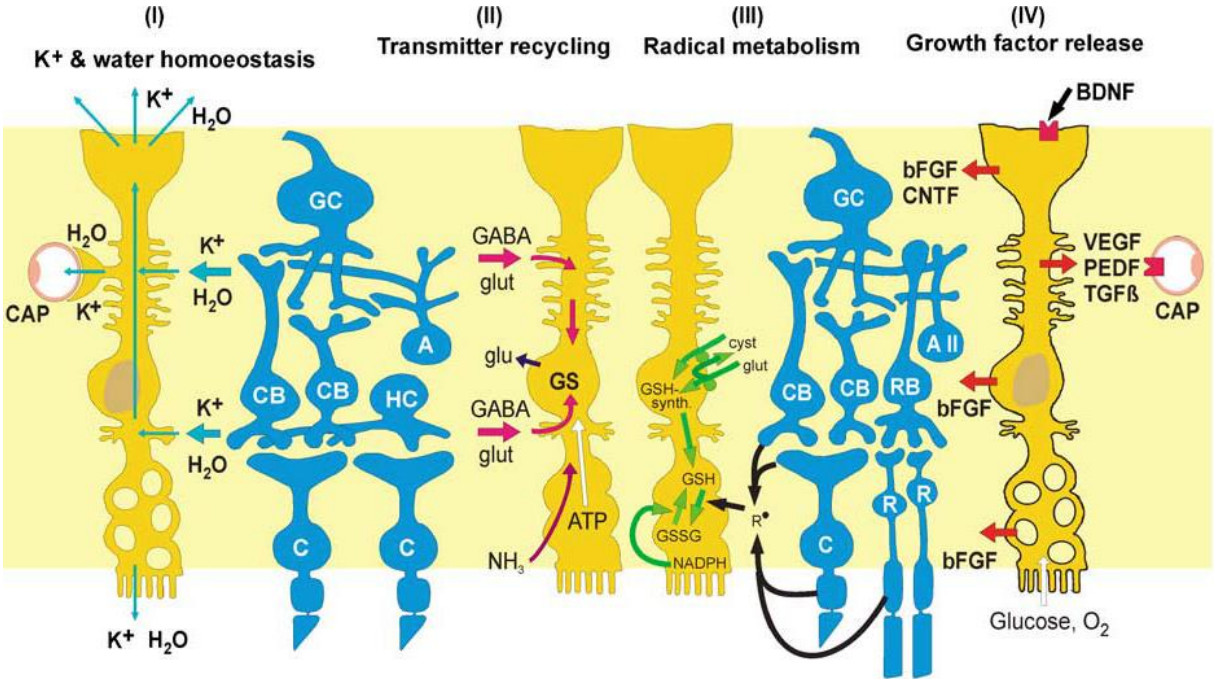

Figure 2: Schematic of the different Müller cell functions
Role of Müller glia cells in potassium (K^+) and water homeostasis (I), neurotransmitter clearing (II), protection from oxygen free radicals (III) and the secretion of neuroprotective factors (IV). Picture taken from (20).

Microglia cells are the third glial population in the retina. Microglia cells represent the mononuclear phagocyte population of the nervous system (21). In the retina, they are located in the inner and outer plexiform layer and have important functions in immune surveillance and neuronal homeostasis (22–25).

1.1.1.5 Cells of the outer nuclear layer (ONL): photoreceptors

There are two types of photoreceptor cells: rod and cones. Rod photoreceptor cells are specialized for vision in dim light and provide black and white vision, whereas the cones operate during bright light, like daylight, and provide color vision (10).

In the dark, the photoreceptor cells permanently release the neurotransmitter glutamate (4), which is thought to be the neurotransmitter of the vertical neurons in the retina (photoreceptor cells, bipolar cells and retinal ganglion cells). When light hits the rhodopsin molecule in the photoreceptor cell this results in a closure of ion channels (Na^+ and Ca^{2+}) which in turn results in a hyperpolarization of the photoreceptor cell and subsequently a diminished release of its neurotransmitter glutamate. (The detailed process of phototransduction is described in 1.1.2.1).

Regarding the photoreceptor`s morphology one speaks of an inner and an outer segment, a cell body, which is situated in the outer nuclear layer (ONL) containing the nucleus of the photoreceptor cell, and the synaptic terminal, which is situated in the outer plexiform layer (OPL) where neurotransmission to downstream neurons occurs (2). The inner segment of the photoreceptors contains cell organelles like mitochondria, golgi apparatus, endoplasmatic reticulum and ribosomes (26). A cilium connects the inner with the outer segment of the photoreceptor. Figure 3 shows the ultrastructure of a rod and cone photoreceptor and a membranous disc stack. Photoreceptor cells have an outer segment composed of membranous discs (rod) or membrane enfolding (cones) that contain the photopigment (26).

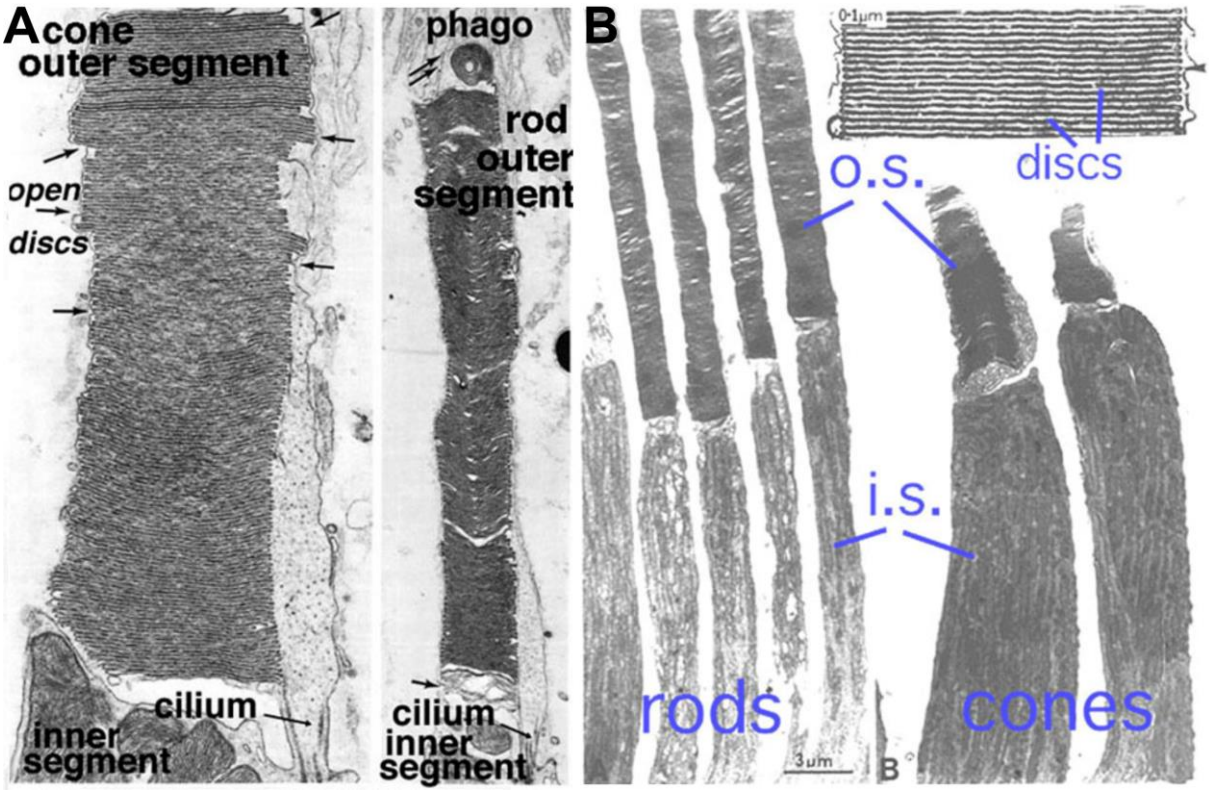

Figure 3 Ultrastructure of photoreceptors

A. Electron microscopy of rod and cones photoreceptors of a squirrel retina with the connecting cilium between the inner and the outer segments and an example of disc shedding in the retinal pigment epithelium. **B.** Electron microscopy of rod and cone photoreceptors of a monkey retina with enlargement of the outer segment discs. o.s.: outer segment, i.s.: inner segment. Slightly modified after (27).

The opsin part is a membrane receptor that is assembled in the photoreceptor cell organelles of the inner segment and transported through the connecting cilium to their final destination in the membrane of the outer segment. In rod outer segments the final destination is in intracellular membrane disc stacks. These stacks are without contact to the plasma membrane (see Figure 3 and Figure 4). In cones, the disks are in contact with the plasma membrane (28,29), which is called 'membrane enfolding' (30).

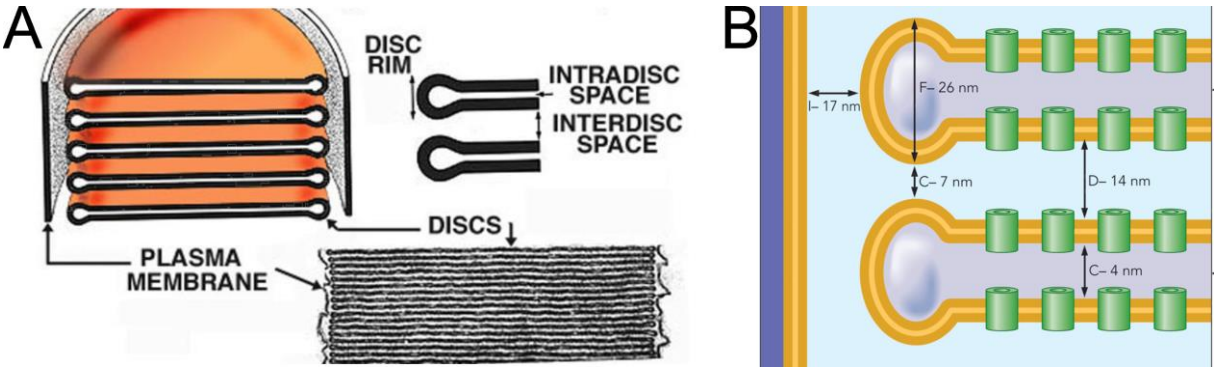

Figure 4: Schematic of rod outer segment disc

A. The rod outer segment is filled entirely with discs of folded double membranes. These membranes do not contact the plasma membrane of the photoreceptor cell. The light sensitive visual pigment is embedded in the intracellular disc membrane. Picture taken from (29).

B. Schematic that illustrates the continuous distance between the plasma membrane and the intracellular situated membranous discs stacks. Picture taken from (28).

The complete renewal of a photoreceptor disc occurs about every 10 days. Newly formed discs are located at the base of the outer segment and within 10 days the discs displace progressively towards the retinal pigment epithelium. When they reach the RPE they are phagozytosed (26). This process is called shedding. To facilitate this process, the outer segments lay folded in the microvilli of the retinal pigment epithelium (1). The retinal pigment epithelium plays an essential role in removing and recycling the photoreceptor discs.

To be precise, there is a third, but rare type of photoreceptor cell: the light sensitive ganglion cells that contain melanopsin as the photopigment. These cells are important for the circadian physiology, they are involved in the pupillary reaction to light by reflecting signals into brain regions like the olivary pretectal nucleus and they respond to blue spectral light (~ 480nm) independent of rod and cones (31).

The arrangement of the photoreceptor cells lying at the very end of the light entering the retina seems to be counteractive. But apart from its formation during retinal development, there may also be functional reasons in the context of regeneration, as supported by the special relationship that exists between the outer segments of the photoreceptor and the retinal pigment epithelium..

1.1.1.6 The retinal pigment epithelium

The retinal pigment epithelium has many different and very important functions for the maintenance of the eye (outlined in Figure 5). Among these are the secretion of growth factors (vascular endothelial growth factor (VEGF), pigment epithelium derived growth factor (PEDF), the epithelial transport to uphold the ion homeostasis for glia cells, the phagocytosis of sorted photoreceptor disks (shedding) and its ability of light absorption (32).

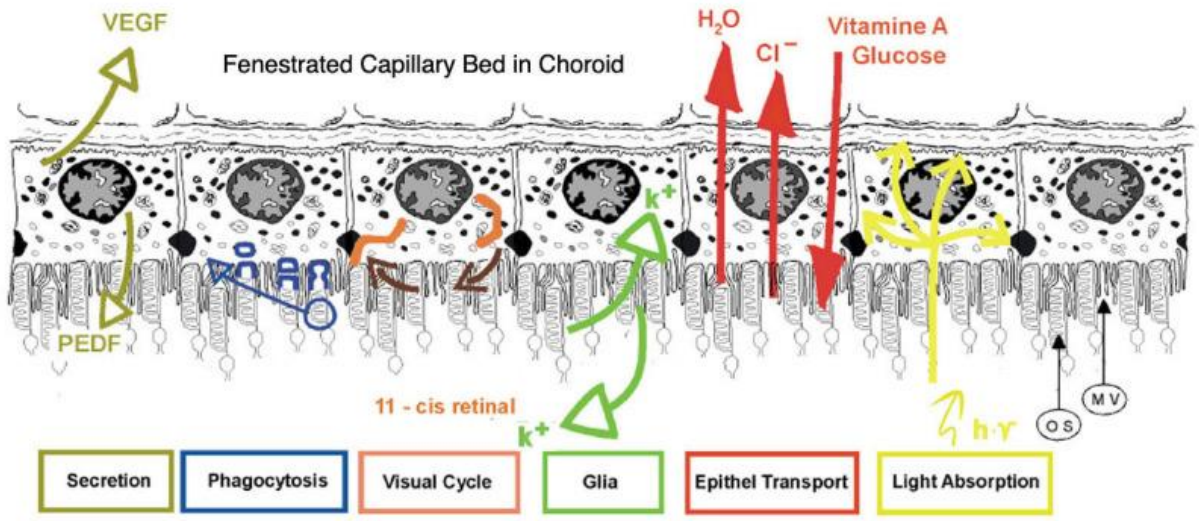

Figure 5: The retinal pigment epithelium and its functions.
Picture taken from (32). For details see main text.

One of its functions which is of major importance for the current project, lies in the biochemical machinery for the regeneration of the photopigment molecules, after they have been exposed to light. This process is called visual cycle.

1.1.2 Phototransduction and visual cycle

1.1.2.1 Phototransduction

Vision starts with the conversion of light in an electric signal in the photoreceptor cells. This process is called phototransduction (Figure 6). After light (photon) absorption in the photopigment of the photoreceptor cell, a signaling cascade is initiated that changes the membrane potential of the receptor and leads in the end to a change of the amount of the neurotransmitter glutamate released by the photoreceptor synapses onto the cells in the inner nuclear layer (4).

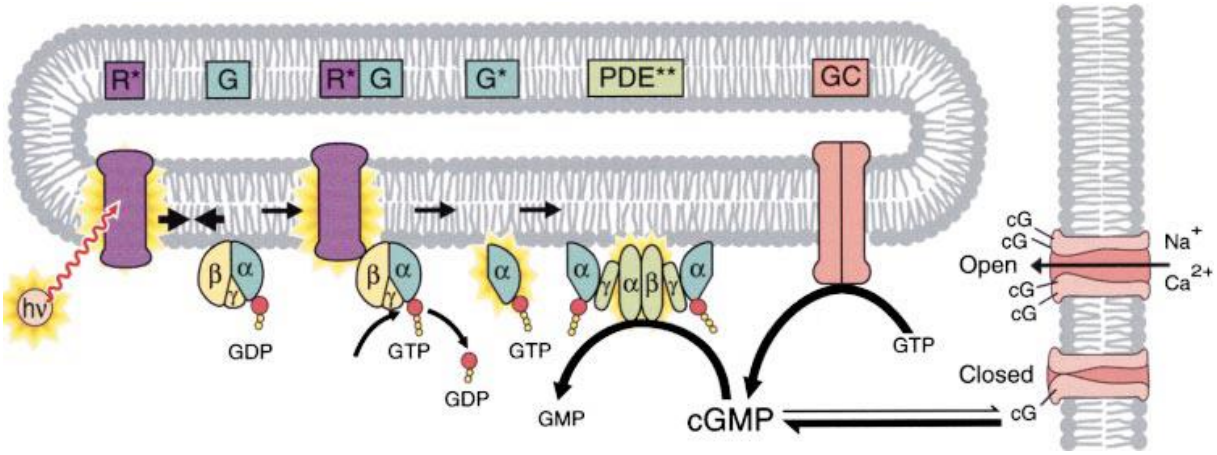

Figure 6: Phototransduction
Photon absorption (hv) activates the rhodopsin molecule (R*) in the disk membrane. The activated rhodopsin initiates the exchange of the G-protein (transducin, G) bound GDP to a GTP. The activated α-subunit (G*) of the G-protein binds to phosphodiesterase (PDE) which results in its activation (PDE**) and hydrolysis of cGMP to GMP. This leads to closure of the cation ion channels (Na^+, Ca^{2+}) and the photoreceptor cell membrane hyperpolarizes. GDP= guanosine diphosphate; GTP= guanosine triphosphate; cGMP/cG= cyclic guanosine monophosphate; GMP= guanosine monophosphate. Figure taken from (34).

The signaling cascade is mediated via G-proteins. The photopigment opsin itself is a membrane-bound G-coupled receptor. The chromophore is 11-cis retinal, which is covalently bound to the opsin part. The opsin molecule is generated in the inner segment of the photoreceptor whereas the chromophore 11-cis retinal is delivered via interphotoreceptor matrix carrier molecules (retinal binding proteins, IRBP) from the retinal pigment epithelium (32). When a light photon hits the G-coupled receptor, the 11-cis retinal changes its conformation into all-trans retinal – a phenomenon called photo isomerization. Subsequently the G- coupled receptor changes its conformation, resulting in its activation. Then the light activated photopigment activates the GTP-binding protein transducin. Transducin stimulates cyclic guanosine monophosphate (cGMP) phosphodiesterase (PDE). The PDE enzyme hydrolyzes cGMP to 5`GMP. Subsequently the cGMP gated ion (Na^+ and Ca^{2+})

channels in the cell surface membrane close. This results in the hyperpolarization of the photoreceptor cell and modulation of the neurotransmitter release at the synaptic terminal (33).

1.1.2.2 Visual cycle

The visual cycle describes the regeneration process of all-trans retinal. As mentioned above (in 1.1.2.1) when 11-cis retinal is photo isomerized, it changes its conformation into all-trans retinal. During the visual cycle, a "used" all trans-retinal is recovered back into the active 11-cis-retinal using several enzymatic recovery steps. This process takes place in the outer segments of the photoreceptors and the retinal pigment epithelium (see Figure 7). Between these structures and in the interphotoreceptor matrix, the retinal is transported using carrier proteins.

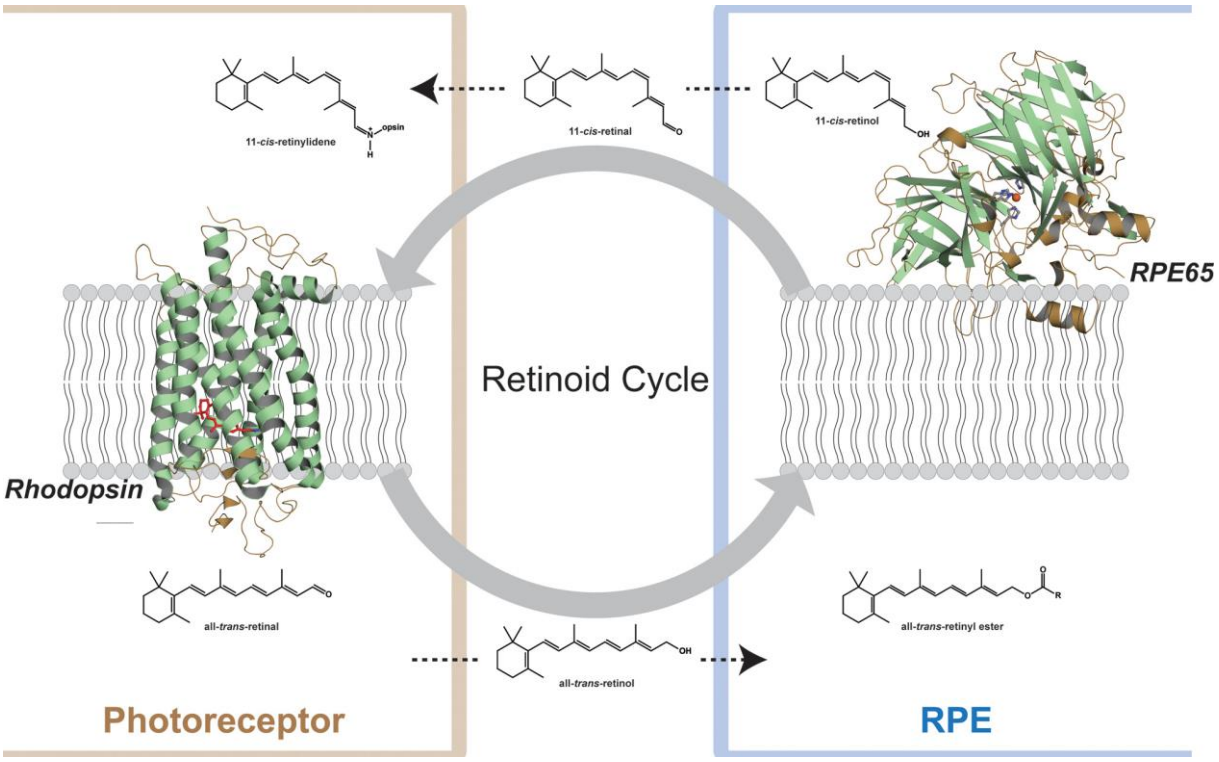

Figure 7: Visual cycle
Schematic showing the visual cycle with its light induced conformation change of 11-cis retinal into all-trans retinal and the following regeneration process in the interphotoreceptor matrix and retinal pigment epithelium, respectively. Figure taken from (28).

The 11-all-trans retinal is released from the opsin protein, reduced to all-trans retinol and esterified by lecithin retinol acyltransferase (LRAT), converted to 11-cis retinol by the protein RPE65. Finally, 11-cis retinol is oxidized to 11-cis retinal and moved back to the rod outer segment, where it is reconjugated to an opsin. A new functional visual pigment (opsin) is formed (28).

In the context of light damage experiments (see 1.3.2) the proper function of the visual cycle is essential. Animal experiments with *RPE65* knockout ($RPE65^{-/-}$) mice and animals that did not express opsin in photoreceptors ($Rho^{-/-}$ mice) showed that these mice both are not sensitive to intense light exposure (35). $RPE65^{-/-}$ and $Rho^{-/-}$ animals did not develop any kind of light induced damage. These

results highlight the importance of rhodopsin in the context of light damage and its main impact on retinal degeneration, indicating that the G-coupled receptor is the receptor mediating the damaging effects of light (35). Additionally, the publication of Grimm and co-workers showed the importance of the RPE65 protein (visual cycle, see 1.1.2.2 and Figure 7) in the context of light induced photoreceptor damage. RPE65 deficiency protected against early signs of light mediated damage (vesiculation of photoreceptor rod outer segments), as well as against late effects (photoreceptor apoptosis). The authors pointed out the importance of "excessive" adsorption of photons by rhodopsin that induces a death cascade leading to apoptosis (35).

Another observation highlights the importance of the visual cycle and the *RPE65* gene in the context of light susceptibility. A point mutation at position 450 in the *RPE65* gen has been shown to be of major important for the susceptibility of the animals to light damage. This mutation results in an amino acid exchange from methionine to leucine (36–38). Animals carrying the leucine variant of the Rpe65 protein are about 120-fold more sensitive to intense light than methionine carrying animals. In the current thesis, experimental animals were tested for the mutation and leucine carriers only were used for the experiments.

1.1.3 Electrophysiology: Electroretinography (ERG)

The electroretinography (ERG) method is used to *in vivo* evaluate the activity of the retinal neurons. In a standard ERG one distinguishes between a- and b-wave amplitude (see Figure 8). The negative a-wave amplitude provides information about photoreceptor function and reflects their hyperpolarization upon activation, while the b-wave amplitude is indicative for the function of the neurons of the inner retina (post synaptic second and third order neurons). Using different light stimuli one can selectively activate either the rod or the cone pathway. In the current project, we used the ERG methods to analyze the neuronal function in the retina of our animals before and after light exposure.

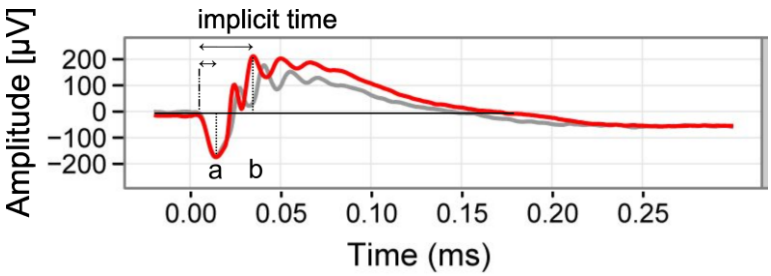

Figure 8: ERG response and parameters that are measured for diagnosis
The a-wave indicates the activation of the photoreceptor cells, whereas the b-wave is the response of post-synaptic second and third order neurons. The implicit time is the time between the light stimulus to the peak. Experiment performed by Barbara Braunger in cooperation with Prof. H. Jägle.

1.1.4 Retinal vessels in development and adulthood

In the adult retina 3 different vascular layers can be distinguished. These layers are called plexus and named according to their localization in the retina: superior/superficial, intermediate and inferior/deep (39). The superior plexus lies on top of the retinal ganglion cell layer next to the vitreous; the intermediate vascular layer is situated in the inner plexiform layer next to the inner aspect of the inner nuclear layer. The inferior vascular plexus is localized in the outer plexiform layer next to the outer aspect of the inner nuclear layer (see Figure 9) (2,39).

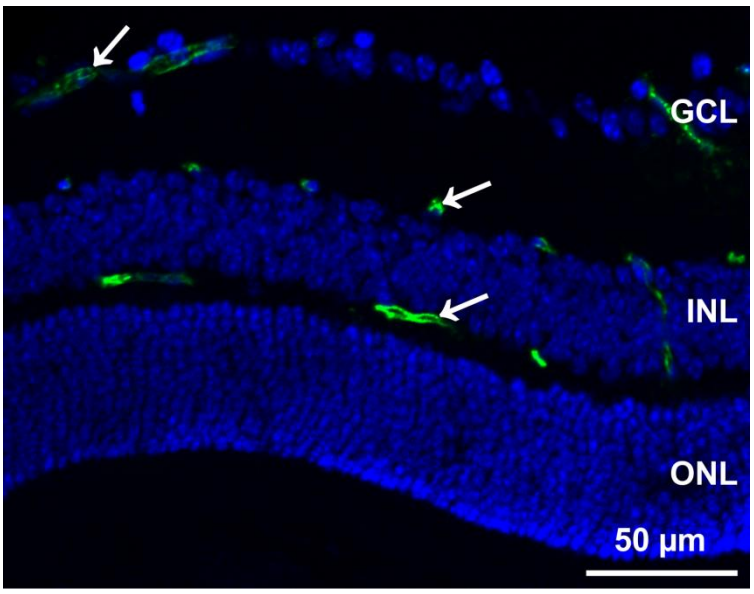

Figure 9: FITC- coupled Dextran perfusion showing intra-retinal vessel localization
Retinal vessels of a 3 weeks old 129SV wild-type mouse. The vessels are perfused with high molecular FITC-Dextran (green) that stays in the vessel lumen due to its high molecular weight, which does not allow a passage through the blood retinal barrier. Cell nuclei are stained with DAPI (blue).The white arrows indicate the correct position of the superior, intermediate and inferior vascular plexus. GCL: ganglion cell layer, INL: inner nuclear layer, ONL: outer nuclear layer.

In contrast to humans, retinal vessel development in the murine retina starts postnatally. This process in the mouse retina is thought to be restricted to angiogenesis (humans: vasculogenesis and angiogenesis) (40). During murine angiogenesis vessel sprouting starts at the optic nerve head (see Figure 10).The immature vessels sprout from the optic nerve head into the periphery following the guidance of astrocytes on the very top of the retina. At postnatal day (P) 8 the vessels reach the periphery (Figure 10). Then, in the further process of angiogenesis, the vessels start to grow into the retina as early as P9. They form the deep vascular plexus in the outer plexiform layer. The intermediate vascular plexus begins to develop starting at P12 (39). In contrast, in the human retina, the plexus are formed in the following order: superior, intermediate and inferior plexus).

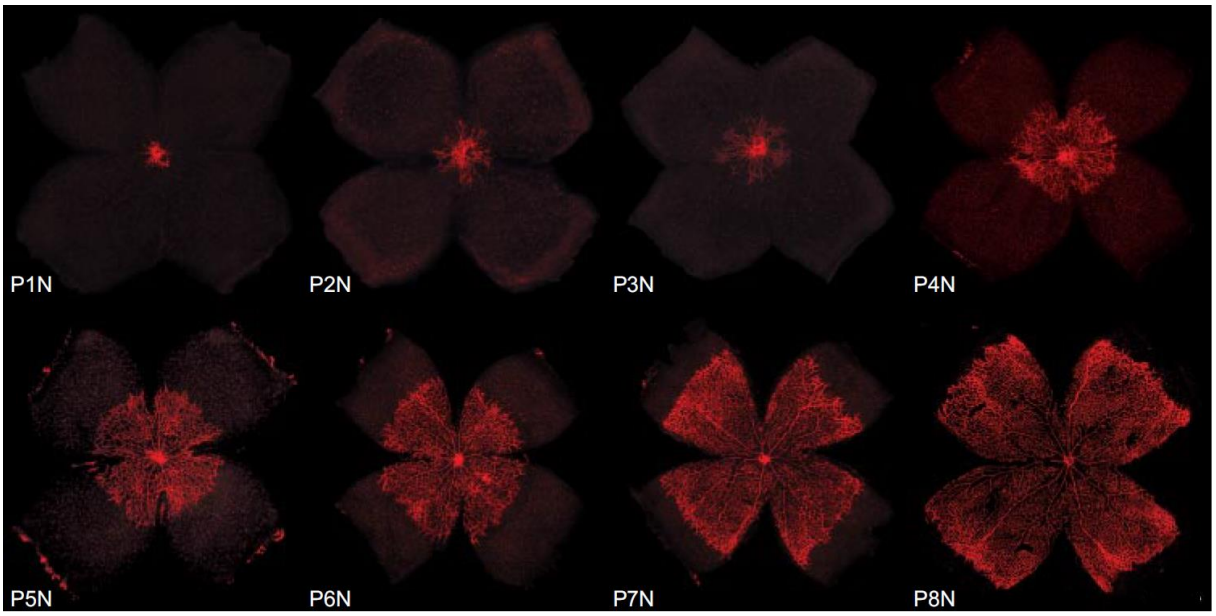

Figure 10: Retinal vessel development – superior vascular plexus
Superior vascular plexus development of C57Bl6 mice retinae. The endothelial cells are labeled using isolectin B4-Alexa 496 (red). At postnatal day 1 (P1N), the vessels are only present at the optic nerve head. From there, they extend radial, reaching the periphery at P8N. Figure taken from (39).

1.2 Norrin

1.2.1 Norrie disease: symptoms and genetics

The Norrie syndrome is a congenital X linked recessive disease. The major symptoms of this disease are ophthalmological findings such as atrophic irides, corneal clouding, cataract and retinal dysplasia with early vascular proliferation (pseudoglioma) followed by bulbar atrophy. Additionally, the affected patients show progressive sensorineural hearing loss, psychotic features and one third of the patients demonstrate mental retardation (41–47). The localization of the Norrie disease gene on the proximal short arm of the X chromosome (Xpll.3) was assigned using deletion and linkage analysis (48–52). The gene is located 60 kilobases (kb) proximal of the monoamine oxidase B (MAOB) gene and its 5`end is oriented towards the centromere. The Norrie gene is evolutionary-conserved (53). Interestingly, two other ophthalmologic diseases are either genetically linked to the same region (familial exudative vitreoretinopathy, FEVR) (54–59) or linked to the receptor which binds Norrin, the frizzled 4 receptor (autosomal-dominant familial exudative vitreoretinopathy) (60). The X-linked form of familial exudative vitreoretinopathy (FEVR) is caused by missense mutations in Norrin (54–59), while the autosomal-dominant familial exudative vitreoretinopathy is caused by mutant frizzled-4 and is characterized by incomplete vascularisation of the peripheral retina (61).

1.2.2 The protein Norrin

The Norrin gene contains three exons that are transcribed into an mRNA of 2.1 kb (52). The murine Norrin gene encodes for a secreted protein of 131 amino acids with a molecular weight of about 17 kDa (62). Based on multiple sequence alignments of Norrin with TGFβ and the resulting similarities one assumes Norrin has a cysteine rich domain. *In silico* analyses of its tertiary protein structure predict a cysteine knot motif (63,64).

Norrin, or Norrin disease pseudoglioma (*Ndp*), is expressed in retinal neurons (outer nuclear layer (ONL), inner nuclear layer (INL), ganglion cell layer (GCL), Müller glia cells, the choroid, the fetal brain (cerebellar granular layer, hippocampus, olfactory bulb and cortex), the stria vascularis of the cochlea, decidua, uterus and human placenta. It is expressed in fetal, as well as in adult stages. (51,52,67–71). Recent data coming from a Norrin knock-in mouse that carries the coding sequence of human placental alkaline phosphatase (AP) as a reporter gene inserted at the *Ndp* locus (*Ndp*(AP)) further elucidated the expression pattern of Norrin during mouse embryonic development (72). These mice showed distinct AP-staining, which indicated Norrin expression, in the central nervous system (CNS) starting from E10.5. Postnatally, the expression in the CNS is restricted to astrocytes in the forebrain and midbrain, the Bergmann glia in the cerebellum and in the retina, the Müller glia cells. In the cochlea, the *Ndp*(AP) expression is associated with two compactly vascularized regions

the first is the stria vascularis and the second a capillary plexus between the Corti organ and the spiral ganglion (72).

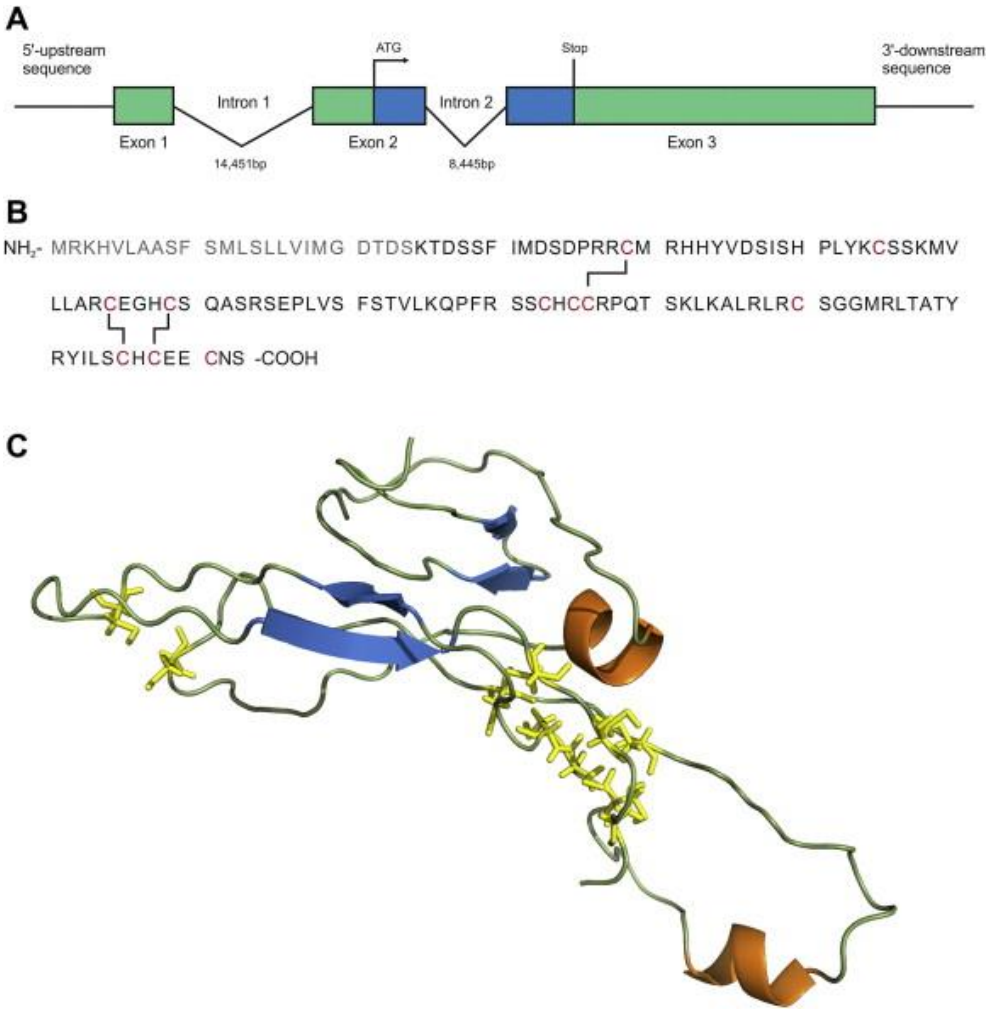

Figure 11: Structure of the Norrin gene and protein
(A) The genomic structure of the Norrin gene. **(B)** The protein sequence of Norrin. The 3 braces indicate putative evolutionarily conserved disulfide bonds. They are expected to form the cysteine knot motif. **(C)** Predicted 3D structure of the human Norrin protein. The yellow stick models show the cysteine residues of the cysteine-rich domain. This domain is predicted to adopt a cysteine knot motif. Figure taken from (65,66).

1.2.3 The biological functions of Norrin

1.2.3.1 Angiogenic properties of Norrin

Norrin deficient (*Ndp*$^{y/-}$) mice show a prominent retinal phenotype. It is mainly characterized by the complete absence of the intermediate and inferior vascular plexus and the formation of vascular membranes at the vitreal surface of the retina (73). The number of blood vessels in the interface of the ganglion cell layer and the nerve fiber layer was significantly increased in *Ndp*$^{y/-}$ mice. In contrast, a drastic decrease was observed in the vessel number of the inner and outer plexiform layers in 9 day old *Ndp*$^{y/-}$ mice (74). Vessels were adjacent to the inner limiting membrane, which they penetrated occasionally and the hyaloid vessels were still present. Electron microscopy revealed fenestrations of

the vessels (74). Taken together, these observations in *Ndp*$^{y/-}$ mice demonstrated angiogenic malformations in the absence of Norrin, comparable to those observed in humans with Norrie disease (75). This indicates that Norrin is essential for vascular development of the inner retinal layers, especially for the development of inferior vascular plexus, and for the atrophy of hyaloid vessels (74,76). Vascular changes are also described for the auditory system, where the stria vascularis of *Ndp*$^{y/-}$ mice is the most affected structure (69). Taken together, this implies the important role for Norrin in basic vascular biology.

To further investigate the angiogenic properties of Norrin, Ndp$^{y/-}$ mice were crossed with transgenic Norrin animals (Nor-29). Nor-29 mice overexpress Norrin lens-specifically under the control of the βB1-crystallin promoter (73). The ectopic Norrin expression in the lens restored retinal structure and function in *Ndp*$^{y/-}$ mice. Additionally, double transgenic animals (Nor-29/*Ndp*$^{y/-}$) also developed both retinal capillary beds. The capillaries were covered by pericytes and surrounded by a complete basal lamina and they showed typical ultrastructural characteristics of retinal capillaries. In summary, the ectopic transgenic expression of lens-derived Norrin completely restored normal vascular development of the retina, compared to *Ndp*$^{y/-}$ mice (73).

1.2.3.2 Neuroprotective properties of Norrin

Ndp$^{y/-}$ mice showed disorganized retinal ganglion cells which migrate into the inner plexiform layer. Quantification of the number of retinal ganglion cells in *Ndp*$^{y/-}$ mice compared to wild-type demonstrated a decreased number of retinal ganglion cells in knockout animals (74). In contrast, the cell number (retinal ganglion cells and during retinal development: neurons in the marginal and ventricular zone) in the transgenic Norrin overexpressing Nor-29 animals was significantly increased. Furthermore, double transgenic animals (Nor-29/*Ndp*$^{y/-}$) showed a rescue of retinal ganglion cells loss in cell number (73).

Ndp$^{y/-}$ mice showed sporadic variations the inner and outer nuclear layer cell morphology. Those regions that were severely affected exhibited a degeneration of the outer plexiform layer and the outer segments of the photoreceptors. Furthermore, in these regions the retinal pigment epithelium (RPE) was hyperpigmented (77). Loss of the anti-apoptotic functions of Bcl-2 interacting death suppressor (Bis) and Fas apoptosis inhibitory molecule (Faim) in *Ndp*$^{y/-}$ mice may contribute to the degeneration of photoreceptor cells during disease progression (78).

Taken together, these findings support the idea of a neuroprotective activity of Norrin. Cell culture experiments with RCG-5 cells, treated with only staurosporine (SS) resulted in cell death, whereas RCG-5 cells treated with SS and Norrin showed less apoptosis (79). In another approach, the possible neuroprotective role of Norrin was investigated using an animal model, in which an exitotoxic (using

N-methyl-D-aspartic acid (NMDA)) retinal ganglion cell death was induced. To this end, intravitreal Norrin injections in N-methyl-D-aspartic acid (NMDA) treated animals provided the evidence for a protective role of Norrin for retinal ganglion cells (RGC) survival (80). The double treated animals (NMDA+Norrin) demonstrated a minor loss of axons in the optic nerve and the area of glial scarring appeared to be considerable smaller, compared to eyes treated with NMDA alone. TUNEL labeling confirmed the significant inhibition of the RGC apoptosis after NMDA+Norrin injections (80). Norrin injections into NMDA damaged eyes resulted in Müller glia cell activation and enhanced Endothelin-2 (EDN2)/leukemia inhibitory factor (LIF) signaling. Experiments with an inhibition of the Wnt/β-catenin pathway using Dickkopf-1 indicated that the neuroprotective effect of Norrin is most probably mediated by the Wnt/β-catenin pathway (80). In summary, this study showed that Norrin is part of an endogenous protective system in the retina which is important for RGC survival during and after injury (80). The endogenous protective system appears to act largely independent from the effects of Norrin on vascular development and repair (71,80).

1.2.3.3 Norrin in reproduction and development

The expression of Norrin in murine deciduae was confirmed using RNA in situ hybridization (70). Transcripts of the *NDP* gene could be detected in decidua and uteri of wild-type mice and in human placentae, indicating an additional role for Norrin in reproduction (70). The distinct reduction of decidualization in female $Ndp^{-/-}$ mice resulted in an impaired female fertility. Compared to wild-type mice, the deciduae were also smaller in female $Ndp^{-/-}$ mice and did not reach as deep into the endometrium (70). In addition, fibrocytes of the deeper endometrial zone did not show transition to large roundish decidua cells and they were separated from each other by wide intercellular spaces (70). In summary, Norrin affects reproduction in two possible ways: on the one hand it impairs the correct vascularization of the deciduae resulting indirectly in a decreased female fertility. On the other hand, Norrin deficiency resulted in the malformation of endometrial fibrocytes, which implicates a more direct role of Norrin in decidualization.

During retinal development, Norrin stimulates the proliferation of neurons. This has been shown in Norrin overexpressing animals (Nor-29 mice) that exhibited a significant higher number of bromo-desoxyuridine (BrdU) positive cells in the retina at E14.5. During DNA synthesis, BrdU incorporates in the DNA of the replicating cell and is therefore used for the detection of cell proliferation in living tissue. The increased number of BRDU positive cells in Nor-29 mice indicated a growth stimulatory effect of Norrin on retinal neurons. The increased proliferation led to a thicker retina and an increased cell number of retinal ganglion cells and other neurons at P2. However, Norrin most probably does not influence the rate of apoptosis directly, since no significant difference

was found in the number of apoptotic cells (TUNEL, see 5.1.5.4) at P7 between Nor-29 and wild-type littermates (73).

1.2.4 Norrin signaling and the Wnt/β-catenin pathway

In the absence of a Wnt (Wingless-related integration site) ligand (inactive Wnt pathway, see Figure 12, left hand side), β-catenin forms a complex composed of APC (Adenomatous polyposis coli), GSK-3β (Glycogen synthase kinase-3β), CK1 (Casein kinase 1, alpha 1) and Axin in the cytosol (81,82). In this situation β-catenin is phosphorylated, ubiquitinylated through the E3-ubiquitin-ligase β-Trcp (β-transducin repeat containing) and degradated by the proteasome (81). In summary, an inactive Wnt pathway results in a constant degradation of the intracellular β-catenin levels.

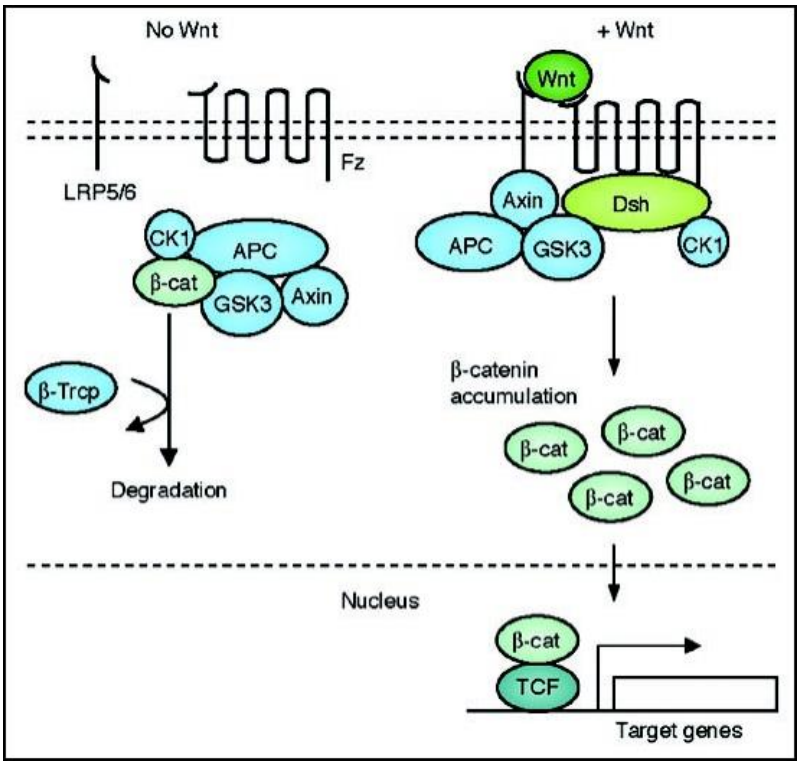

Figure 12: Schematic of the canonical Wnt pathway.
Left: in the absence of Wnt ligand, a complex of Axin, APC, GSK3-β, CK1 and β-catenin is located in the cytosol. β-catenin is phosphorylated by CK1 and GSK3-β and degraded by the proteosomal machinery mediated by β-Trcp.
Right: Wnt signaling through the Fz receptor and LRP5/6 co-receptor complex induces the phosphorylation of LRP6 and this leads to a translocation of the protein complex containing Axin from the cytosol to the plasma membrane. Dsh is also recruited to the membrane and binds to Fz. This results in a stabilization of β-catenin, which subsequently translocates into the nucleus. There it complexes with Lef/Tcf family members to mediate the transcription of target genes. APC= Adenomatous polyposis coli). GSK-3β= Glycogen synthase kinase-3β. CK1= Casein kinase 1, alpha 1. β-Trcp= β-transducin repeat containing. Dsh= dishelved. Figure taken from (83).

Wnt pathway activation (see Figure 12, right hand side) leads to a phosphorylation of Lrp5/6, which in turn results in a translocation of the some proteins from the β-catenin complex from the cytosol to the plasma membrane. Axin binds to phosphorylated Lrp5/6 and Dsh is recruited to binds to the Fz receptor (81). This complex formed of Fz/Lrp5/6 induces the stabilization of β-catenin in the cytosol either through sequestration and/or degradation of Axin. β-catenin translocates into the nucleous

where it forms a complex with Lef/Tcf family members resulting in the transcription of Wnt- signaling target genes (81,82).

Despite the canonical Wnt/β-catenin pathway, which results in a β-catenin accumulation in the cell, there are two other possible Wnt-pathway activations that do not result in an intracellular β-catenin accumulation: the non-canonical planar cell polarity pathway and the non-canonical Wnt/Ca^{2+} pathway (83).

Norrin shows specific and strong affinity binding to the frizzled 4 receptor (Fz4) (84). In consequence Norrin and fz4 mutations in both, human and mice (see 1.2.3.1 and 1.2.3.2) result in very similar morphological phenotypes (60,84,85). After Norrin binds to the Fz4 receptor, the canonical Wnt/β-catenin pathway is activated as shown in Figure 13, B (84).

Dickkopf-1 (DKK1) binds with high affinity to Lrp5 and 6 and is used in the current thesis to inhibit the Norrin mediated Wnt/β-catenin pathway activation (86,87).

A recent study showed that the transmembrane protein Tspan12 (Tetraspanin 12) is able to enhance specific the activity of Norrin/β-catenin signaling and not Wnt/ β-catenin signaling (88). Tspan 12 is expressed in the retinal vasculature, but not in other neuronal cell types. The authors discuss a Tspan 12 mediated enhanced clustering of Fz4 receptor complexes (receptor multimerization) thus also enhancing Norrin/β-catenin activity. Consistently, the phenotype of Tspan 12 knockout mice is comparable to those of the *Ndp*$^{y/-}$ (see 1.2.3.1), *Fz4*$^{-/-}$ and *Lrp5*$^{-/-}$ knockout (88).

Norrin is in addition able to bind to the Lgr4 receptor (Leucine-rich repeat containing G protein-coupled receptor 4) and stimulates the canonical Wnt signaling though Lgr4 binding and its activation (89). However, binding studies using AP (alkaline phosphatase) coupled Norrin showed a higher Norrin binding affinity to Fz4 than to Lgr4 (89). In a study using xenopus as a model, Norrin interacted with the TGFβ (transforming growth factor β) signaling ligands BMP4 (bone morphogenic protein 4) and Nodal1 resulting in an inhibition of the TGFβ signaling pathway (90). Similar results were obtained in mammal cell culture assays, where Norrin acted as an antagonist of BMP2 and 4, resulting in a BMP signaling pathway inhibition (affecting intracellular Smad1/5/8) (89). Taken together, Norrin is considered as a multifunctional ligand to three receptor/binding proteins that are of major importance for Wnt and BMP signaling pathways.

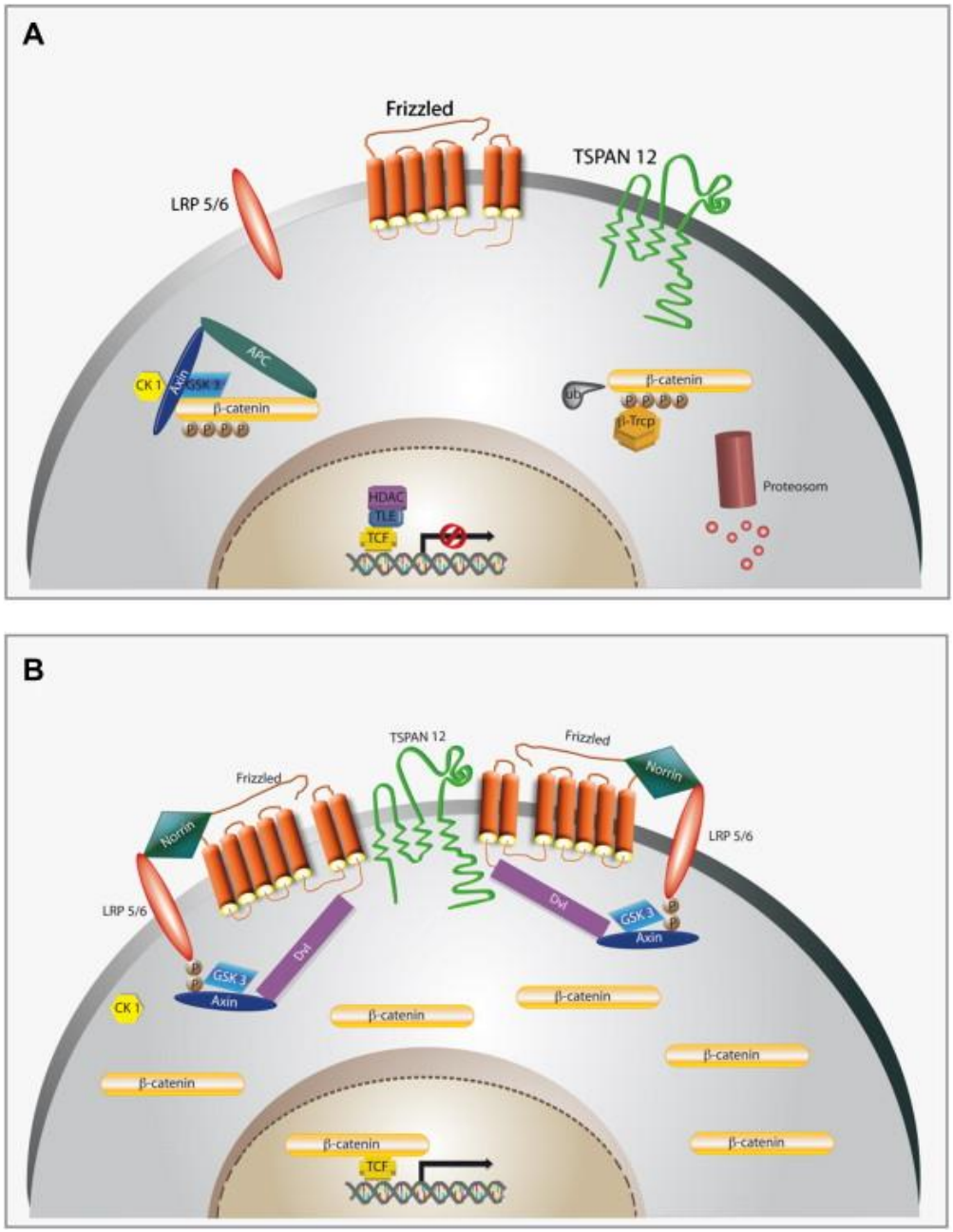

Figure 13: Schematic of Norrin binding to frizzled 4/LRP5/6 receptors

A. Inactive: β-catenin is part of a complex composed of APC (Adenomatous polyposis coli), GSK-3β (Glycogen synthase kinase-3β), CK1 (Casein kinase 1, alpha 1) and Axin in the cytosol. β-catenin is phosphorylated, ubiquitinylated processed to proteasomal degradation.

B. Active: Wnt pathway activation leads to a phosphorylation of Lrp5/6, which allows a translocation of Axin to the phosphorylated Lrp5/6. Dsh is recruited to bind to the Fz receptor. β-catenin is stabilized in the cytosol and translocates in the nucleous. There β-catenin and Lef/Tcf family members induce the transcription of Wnt-signaling target genes.

APC= Adenomatous polyposis coli). GSK-3β= Glycogen synthase kinase-3β. CK1= Casein kinase 1, alpha 1. β-Trcp= β-transducin repeat containing. Dsh= dishelved. Figure taken from (66)

1.3 Animal models to induce cell specific stress

1.3.1 The retinopathia of prematurity (ROP) model

The disease retinopathia of prematurity (ROP) in humans is characterized through 2 phases: a time period of vaso-obliteration followed by retinal neovascularization (91,92). The ROP animal model reflects the pathogenesis of the human disease. This animal model is used to investigate vascular conditions in which vascular development becomes unbalanced (93). In the ROP model, mice are exposed to high levels of oxygen (75%) for a designated duration (detailed methodical explanation: see 5.1.6.1). The high levels of oxygen induce a vaso-obliteration and growth arrest of the developing retinal vessels (93). Relocalization of the experimental animals back to normal room air leads to a relative hypoxia in the tissue (due to the former growth arrest) and this results in uncontrolled vessel growths (neovascularizations: due to the expression of vascular endothelial growth factor (VEGF) and insulin growth factor (IGF)) (91,93). In the current thesis, we used this model to investigate the influence of Norrin on vessel growth and retinal vascularization.

1.3.2 A damage model for photoreceptor degeneration: light damage

Exposure of rat or mouse eyes to bright, visible light leads to death of their rod photoreceptors (94). This vulnerability to light has been used to establish the experimental model of light-induced damage. Photoreceptors exposed to excessive amounts of light die through apoptosis, a scenario that is quite similar to their apoptotic death seen in inherited retinal dystrophies or in age-related macular degeneration (AMD) (95,96). Animal models for inherited retinal dystrophies or AMD are available and commonly show photoreceptor apoptosis over a relative long period of time, with only a few neurons entering apoptotic cell death each day. In contrast, photoreceptor death induced by excessive light leads to a large number of photoreceptors dying at the same time. Accordingly, studies on the molecular mechanisms of photoreceptor apoptosis and/or on neuroprotective signaling pathways preventing apoptotic death are considerably easier. Light damage can be induced in an acute or chronic way, by exposing animals to light for a short or longer period of time. In addition, different qualities of light can be used, such as fluorescent white light with an emission spectrum similar to that of daylight, or energy-rich blue light (94,97,98). In the current thesis, light exposure was used to investigate whether Norrin has neuroprotective effects on photoreceptor cells and which molecular mechanism may mediate this effect.

1.3.3 Neuroprotective signaling pathways in the context of photoreceptor degeneration

In the context of light damage and neuroprotection several neuroprotective factors are discussed. Microarray analysis revealed a relatively small number of genes activated after light exposure (99). Among those transcripts *endothelin 2 (Edn2)* was highly upregulated (99). Its localization in the ONL was determined using in situ hybridization (99). In addition, the *endothelin receptor type B (Ednrb)*

was upregulated in Müller glia cells indicating that photoreceptor derived *Edn2* signals to Müller glia cells to probably increase their sensitivity to *Edn2* as part of the retinal tissue response to the light damage (99).

It was also shown that photoreceptor cell death in VPP mice (a model for inhereditary photoreceptor degeneration) strongly induced the expression of leukemia inhibitory factor (LIF) in Muller glia cells (100). *Lif*$^{-/-}$ animals revealed accelerated photoreceptor degeneration in the VPP mouse model without activating the Müller glia cells (100). Similar to the situation in light damaged retinae, *Edn2* was significantly upregulated in VPP retinae as well (99,100). Intravitreal injections of recombinant LIF in turn induced molecular factors like *Edn2, signal transducer and activator of transcription (Stat3), fibroblast growth factor 2 (Fgf2)* and *glial fibrillary acidic protein (Gfap)* in wild-type, VPP and interesstingly in *Lif*$^{-/-}$ mice, too. These findings strongly indicate that the upregulation of those factors are mediated through LIF. The fact that *Edn2* levels in *Lif*$^{-/-}$ animals were reduced to the level of 2% compared to wild-types and that VPP;*Lif*$^{-/-}$ double mutants did not reveal an upregulation of *Edn2* (although VPP animals did) further indicates that *Edn2* expression is dependent on LIF.

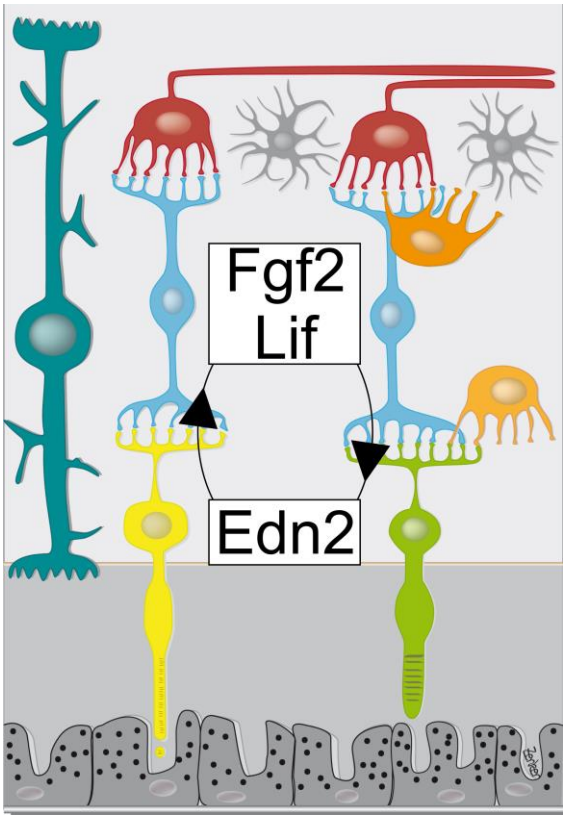

Figure 14: The response of photoreceptors to injury: EDN2, LIF and FGF2
Light or genetically induced photoreceptor cell stress results in the upregulation of LIF. Strikingly, Lif induction leads to an upregulation of EDN2 in photoreceptor cells and FGF2 in Müller glia cell. Since EDN2 itself further stimulates the expression of LIF, a positive feed forward loop is very likely.

FGF2 is upregulated in different models of photoreceptor degeneration and it is speculated that endogenous FGF2 may function in a parakrine way, secreted from the Müller glia cells, as a protective factor activated in response to photoreceptor cell stress (101,102). When *Fgf2* and Müller glia cell activation marker *Gfap* were studied in *Lif*$^{-/-}$ and VPP;*Lif*$^{-/-}$ mice respectively, again, the *Fgf2* and *Gfap* levels in *Lif*$^{-/-}$ animals were reduced to a level of 38% (*Fgf2*) and 11% (*Gfap*), respectively. VPP;*Lif*$^{-/-}$ double mutants did not reveal an upregulation of *Fgf2* or *Gfap* (although VPP animals did) (100). This further indicates that the expression of FGF2 and GFAP is dependent on LIF as well.

Taken together LIF/EDN2/FGF2 signaling pathways (see Figure 14) seem to play an essential and early role in the retinal response to photoreceptor injury.

1.4 Aim of the current work

The main focus of this thesis is to investigate the neuroprotective role of Norrin on photoreceptor survival and maintenance. To this end, we will use a transgenic mouse line that overexpresses Norrin specifically in the retinal pigment epithelium (RPE).

First, we will carefully characterize the overexpression of Norrin in the transgenic animals using various molecular biology techniques. Then we will analyze the effect of Norrin on photoreceptor survival in untreated animals. To this end, we will characterize the morphology of the animals at different timepoints, followed by morphometric analysis. For morphometry, we will measure the thickness of the photoreceptor cell layer (outer nuclear layer, ONL) at 20 measure points throughout the entire retina and blot these measure points in a so called spider diagram. We will evaluate the different measure points in the spider diagram using Student's t-test. This will give us a good indication, if Norrin has proliferative effects on the outer nuclear layer (ONL). Since Norrin has strong angiogenic properties, the retinal vasculature will be examined by dextran perfusion, *in vivo* fluorescence angiography and immunohistochemical staining (Isolectin B4, plasmalema associated protein (PLVAP)).

To investigate a possible neuroprotective function of Norrin for photoreceptors, we will consequently establish a light induced damage model for photoreceptor apoptosis. Using the established model, we will treat transgenic animals and littermate controls. TUNEL labeling for apoptotic cells will show, if the transgenic overexpression of Norrin might have a protective effect on photoreceptor survival (less apoptosis). These results will be confirmed with an ELISA, which detects free nucleosomes as a sign for apoptosis. Additionally, we will focus on the morphology and use Spider diagrams and Student's t-test to compare the thickness of the ONL of light exposed animals. To learn more about the underlying molecular mechanisms, transcript levels of different neuroprotective factors (leukaemia inhibitory factor (Lif), fibroblast growth factor 2 (Fgf-2), endothelin-2 (Edn-2), brain derived neurotrophic factor (Bdnf), lens epithelium derived growth factor (Ledgf), ciliary neurotrophic factor (Cntf), pigment epithelium derived growth factor (Pedf)) and as a marker for Müller glia cell activation: glial fibrillary acidic protein (GFAP) will be determined before and after light exposure. Western blot analysis and immunohistochemical staining will be performed to confirm realtime-PCR data on the protein level. *In vivo* examinations like, e.g. ERG-, OCT- and SLO-analysis will be performed in cooperation with Prof. Seeliger (Tübingen) to complete the dataset with a functional aspect.

Finally we will investigate in detail the possible mechanism by which Norrin mediates its neuroprotective effects. Norrin can activate the canonical Wnt/β-catenin pathway (103). Hence, Western blot analysis for β-catenin will be performed. In addition, crossbreeding of transgenic Norrin

animals with TopGal mice (Wnt signaling reporter mice, see 5.1.1.3) will reveal if the Wnt pathway is more active in the transgenic animals. Wnt signaling is neuroprotective (80,104,105). Consequently, if transgenic animals show neuroprotective effects following light damage, we will investigate, if this effect might be mediated through the classical Wnt/β-catenin pathway. To this end, we will inhibit Wnt signaling using vitreal Dkk-1 injections. We will inject Dkk-1 into the vitreous of the left eye; the right eye will be injected with PBS only, followed by light damage experiments. Spider diagrams of PBS and Dkk-1 injected transgenic and wild-type control animals will be constructed and statistical analysis will be performed. The expression levels of possible target genes of Norrin and Wnt/β-catenin signaling will be investigated after injection of Dkk-1 in untreated and light exposed animals. Possible downstream signaling pathways of the target genes will be analyzed using Western Blot analysis and immunohistochemical staining.

2 Results

2.1 Characterization of Rpe65-Norrin-2 mice

2.1.1 Southern Blot: successful genomic insertion of the transgene construct

To analyze if the transgene construct was successfully integrated into the genome of Rpe65-Norrin mice, southern blot analysis was used. To this end, genomic DNA was cut with the restriction enzyme EcoRV, transferred on a agarose gel on which the DNA fragment were separated by their size. Subsequently, the DNA was blotted onto a positively charged nitrocellulose membrane. After membrane hybridization with the digoxygenin (DIG) labeled RNA-probe, a RNA-DNA hybrid was formed, which was detected using the DIG easy system with alkaline phosphatase as chemiluminescence.

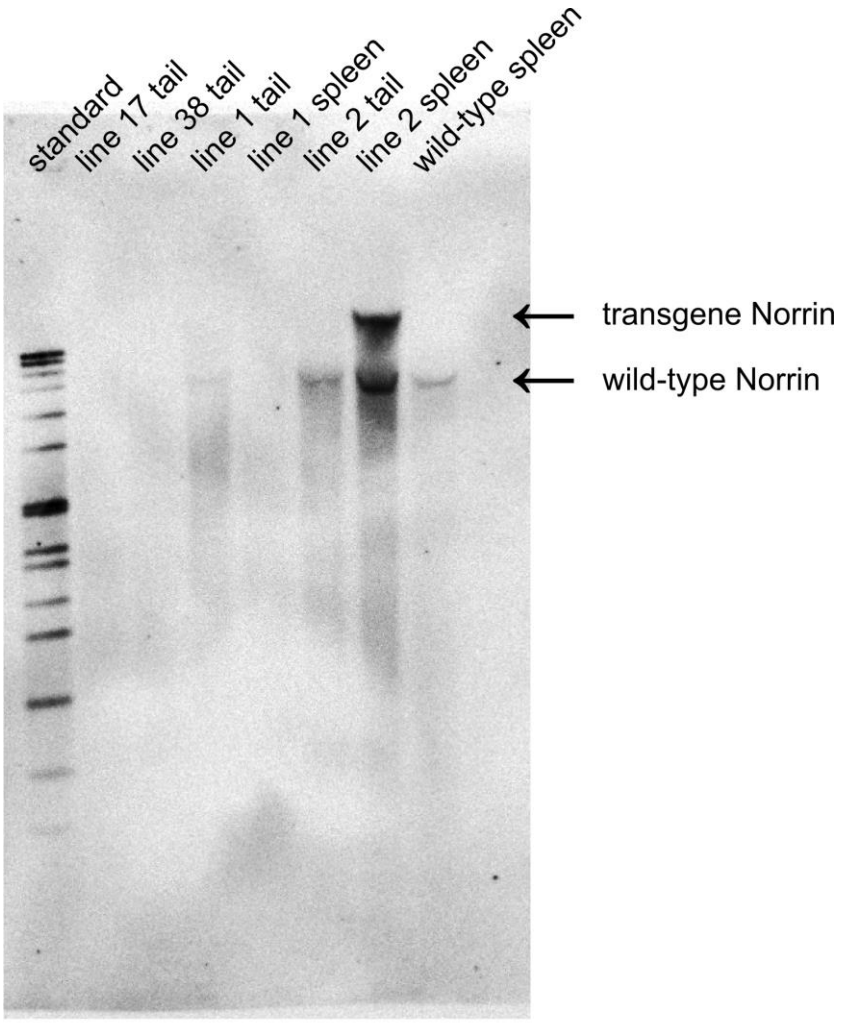

Figure 15: Southern blot analysis of the different Rpe65-Norrin founder mouse lines
Southern blot analysis showed a distinct signal for wild-type Norrin DNA. Line 25 showed a second band positive for the Norrin probe indicating a successful insertion of the transgene construct into the genomic DNA.

Rpe65-Norrin-line 2 animals showed a distinct second signal in addition to the wild-type Norrin signal, which was detectable in control animals (wild-type) and Rpe65-Norrin-line 1 animals (second transgene mouseline) (Figure 15). Mentioning the fact that the lanes are obviously not equally loaded, one might have the impression of a very weak additional second signal above the wild-type signal in the Rpe65-Norrin-line 1 tail DNA (Figure 15, lane 4).

2.1.2 Northern blot analysis: effective transcription of the construct

Northern blot analysis was used to further verify if the successfully integrated Norrin transgene construct is being transcribed in the eye. To this end carefully isolated RNA samples from the posterior bulb (sample containing the retina, RPE, choroid and sclera) were pretreated as described in 5.1.3.5, loaded on an agarose gel and separated by size. The RNA in the gel was transferred on a positively charged nitrocellulose membrane, hybridized with the same probe as used for Southern blot analysis and the RNA-RNA Hybrid was detected using DIG easy system with alkaline phosphatase as chemiluminescent reagent. Rpe65-Norrin-2 animals showed a signal on the same height as the positive control (βB1-Norrin). The signal in Rpe65-Norrin-2 retinae appeared weaker compared to controls, a phenomenon which is not surprising at all, because it is well known, that the promoter (βB1-crystallin) in these positive controls is far more effective than the RPE65 promoter used in our mouse line in this project (Figure 16).

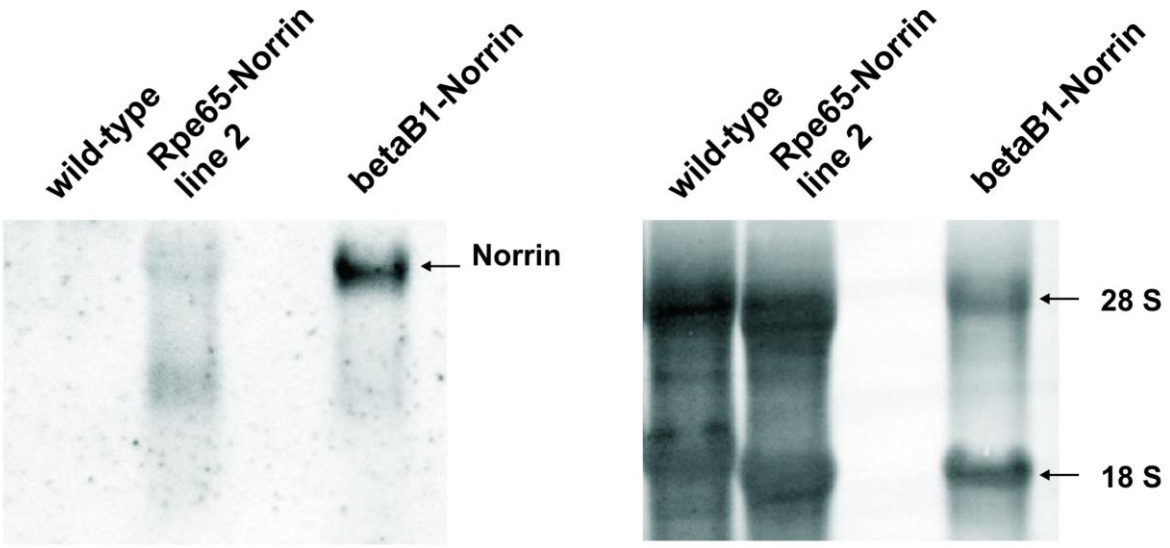

Figure 16: Northern Blot analysis of Rpe65-Norrin-2
Rpe65-Norrin-2 animals show a distinct signal at the appropriate size. On the right: coomassie blue staining of the membrane to show equally loaded lanes, especially for the wild-type, since there was no signal visibly in the northern blot. 28 S and 18 S indicate the large and small ribosomal RNAs. Experiment published in (106), performed by Barbara Braunger.

2.1.3 Western blot analysis: effective protein translation

To further confirm, whether the RNA was successfully translated into Norrin protein, which in the end would stand for a successful overexpression of Norrin protein in the retina, Western blot analysis was performed. After statistical evaluation of the Western blot densitometry, Rpe65-Norrin-2 animals had indeed a significant, about 2-fold increase of Norrin protein in the retina (Figure 17).

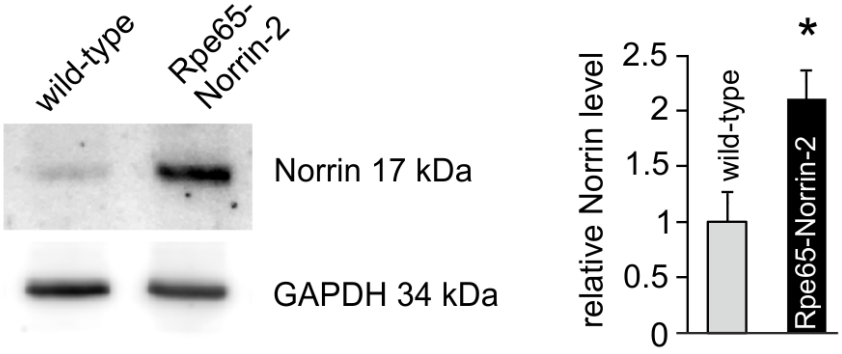

Figure 17: Western blot for Norrin in Rpe65-Norrin-2 mice
Left: Western blot analysis for Norrin protein in retinal lysates of Rpe65-Norrin-2 mice compared to wild-type littermates.
Right: statistical evaluation (students t-test) of the densitometric analysis.
Rpe65-Norrin-2 animals showed a significant increase of Norrin in the retina compared to their wild-type littermates. Mean and SEM are shown; n= 8; *p<0.05. Experiment published in (107), performed by Barbara Braunger.

2.1.4 Immunohistochemistry: retinal localization of the transgenic Norrin protein

To investigate in which region or cellular layer of the retina the significant overexpressed Norrin was localized, immunohistochemical staining was performed (Figure 18). In adult control animals, specific immunostaining for Norrin was weak and barely detectable in the outer retina. In contrast Rpe65-Norrin-2 animals showed an intense staining for Norrin in the inner and outer segments of the photoreceptors, the ONL and the outer plexiform layer. This strongly indicated that Norrin was secreted from the retinal pigment epithelium into the retina.

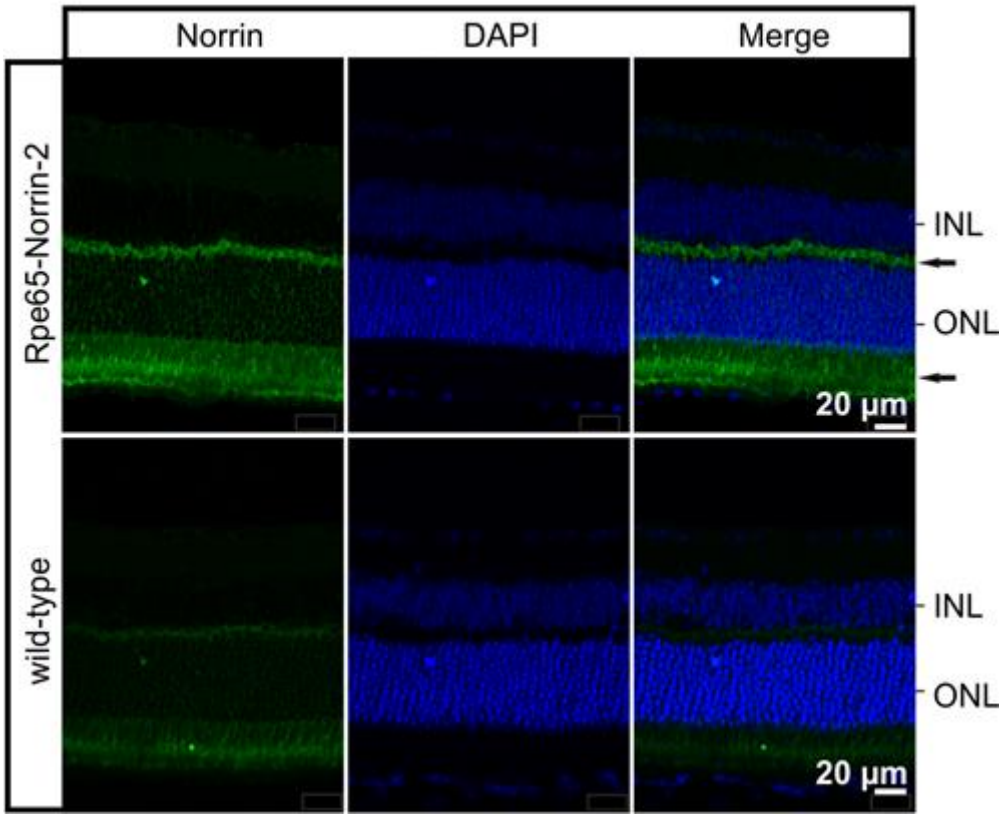

Figure 18: Immunohistochemical staining for Norrin in the retina
Rpe65-Norrin-2 showed an intense staining for Norrin (green) in the outer and inner segments of the photoreceptors, the ONL and the outer plexiform layer (arrows). Cell nuclei were stained with DAPI (blue). INL= inner nuclear layer; ONL= outer nuclear layer. Experiment published in (107), performed by Barbara Braunger.

2.1.5 Rpe65-Norrin-2 mice and Wnt/β-catenin activation

Norrin activates the canonical Wnt/β-catenin pathway by binding to the Frizzled-4 receptor (see Figure 13) (60,85,103). To investigate whether the Wnt/β-catenin pathway was activated in the transgenic Rpe65-Norrin-2 animals, western blot analysis of β-catenin levels was performed. Densitometric and statistic evaluation showed that Rpe65-Norrin-2 animals had a significant increase in β-catenin protein in the retina compared to control wild-type littermates (Figure 19).

Figure 19: Western blot analysis for β-catenin in Rpe65-Norrin-2 animals
Rpe65-Norrin-2 animals had a significant increase for β-catenin protein in the retina. Mean and SEM are shown; n≥7; *p>0.05. Experiment published in (107), performed by Barbara Braunger.

To investigate if the increase in retinal β-catenin in the retina correlated with an activation of the canonical Wnt/β-catenin signaling pathway, Wnt reporter mice (TOPGAL) were crossed to the Rpe65-Norrin-2 line and β-galaktosidase staining was performed.

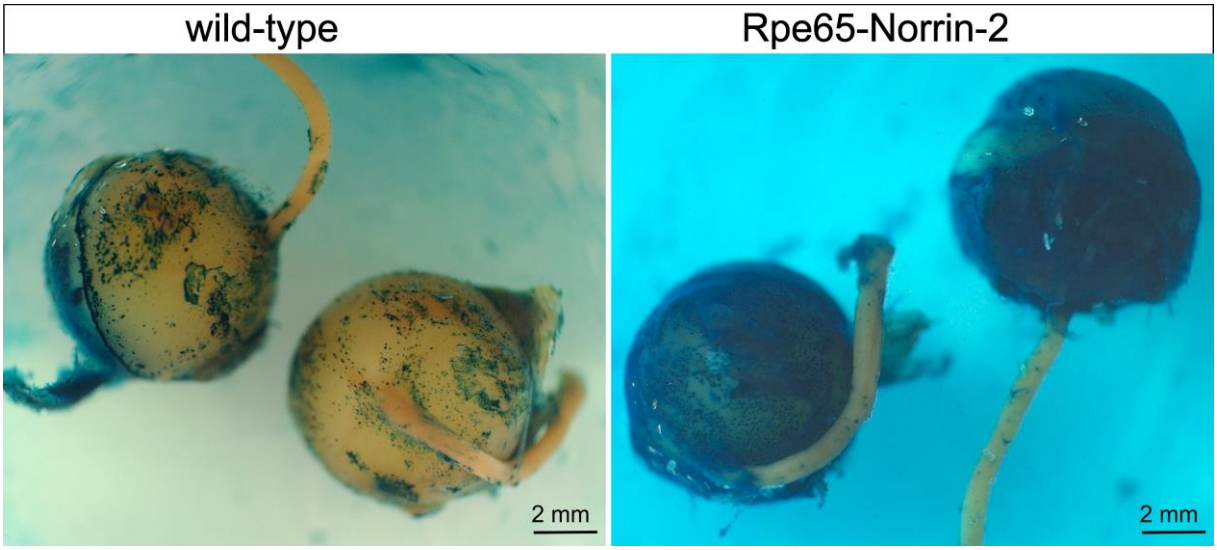

Figure 20: Wnt pathway reporter mice (TOPGAL): macroscopic picture of β-galactosidase stained eye.
Macroscopic pictures of the eyes of Lac-Z stained TOP-Gal;wild-type and TOP-Gal; Rpe65-Norrin-2 animals. The sample of Rpe65-Norrin-2 mice showed a strong β-galactosidase reactivity compared to wild-types.

In control animals only a weak positive signal was detected in the innermost layers of the retina, in contrast double transgenic Rpe65-Norrin-2 X TOP-Gal animals showed an intense β-galaktosidase signal (Figure 20) throughout the retina (Figure 21), which indicates an active Wnt/β-catenin pathway. Taken together, these experiments strongly pointed out that the canonical Wnt/β-catenin pathway was activated in the retina of transgene Rpe65-Norrin-2 animals.

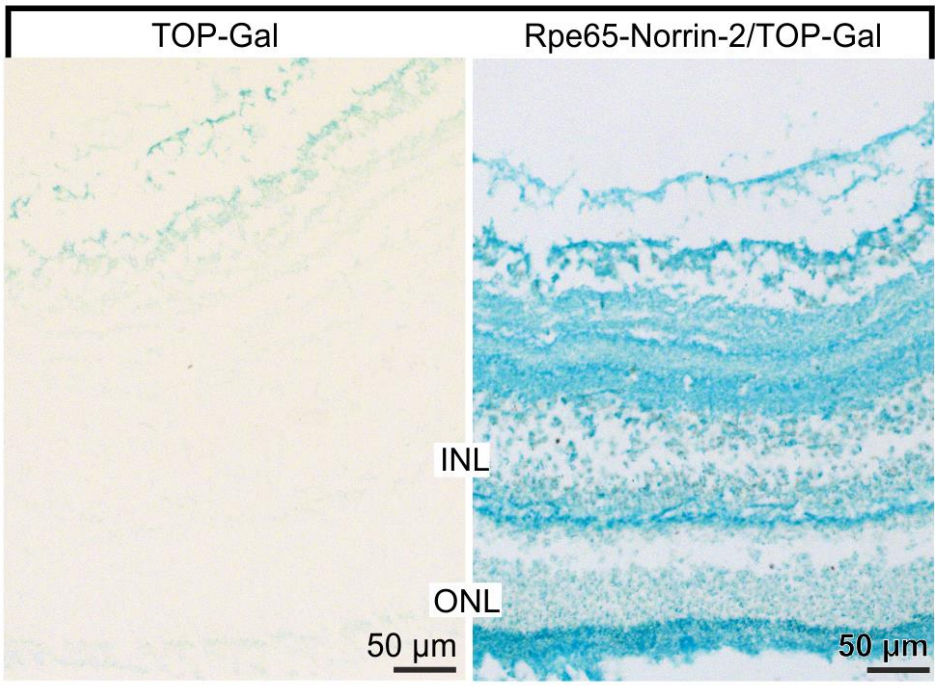

Figure 21: Wnt pathway reporter mice (TOPGAL): β-galactosidase staining
Rpe65-Norrin animals showed an intense β-galactosidase staining, which indicates an active Wnt/β-catenin pathway. INL= inner nuclear layer; ONL= outer nuclear layer. Experiment published in (107), performed by Barbara Braunger.

2.2 Phenotype analysis of Rpe65-Norrin-2 animals

2.2.1 Retinal morphology

Conventional light microscopy was used to analyze the morphology of Rpe65-Norrin-2 animals and wild-type littermates at different time points by using Richardson stained semithin sections. Although we observed a strong overexpression of Norrin from the retinal pigment epithelium into the retina, the phenotype of the transgenic animals showed no morphological differences. The sizes of wild-type and transgenic eyes were similar, the anterior segment of the eye was regular formed, and the retinae showed a normal architecture with all layers present from the optic nerve to the periphery. The retinal pigment epithelium (RPE) looked normal with no visible alterations (Figure 22).

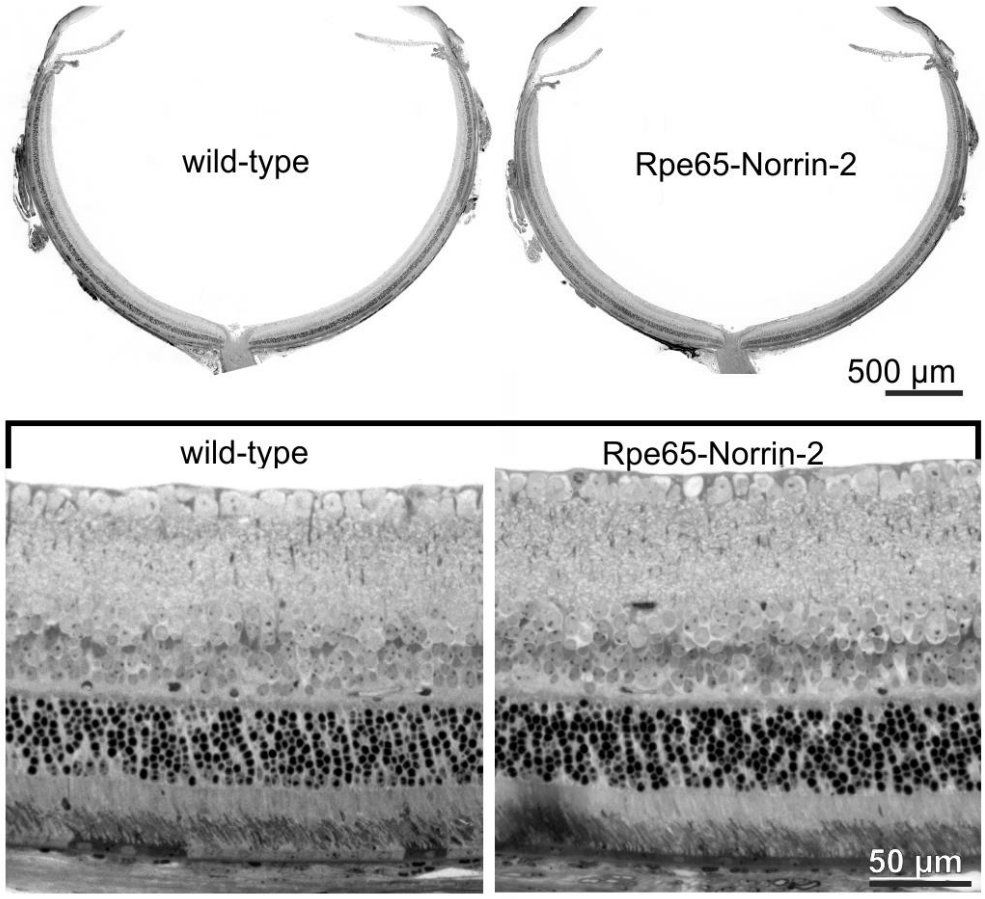

Figure 22: Semithin sections of adult Rpe65-Norrin-2 and control wild-type littermates eyes
Semithin (1 µm thick) horizontal sections of eyes of a 6 week-old Rpe65-Norrin-2 mouse and its wild-type littermate. The eyes were of similar sizes and the architecture of the retina was normal with all layers present from the optic nerve to the periphery. Lower panel shows higher magnification of the central retina Rpe65-Norrin-2 animals. There was no obvious morphological change compared to control wild-type littermates. Experiment published in (107), performed by Barbara Braunger.

Because the thickness of the outer nuclear layer is the major read out data point for morphometric analysis of light damage experiments, prior to the actual light damage experiments the thickness of the outer nuclear layer throughout the entire retina was measured. The ONL thickness did not differ

between transgenic mice and wild-type littermates (Figure 23). Consequently, the ONL thickness could be used it as read out following light exposure without any further normalization.

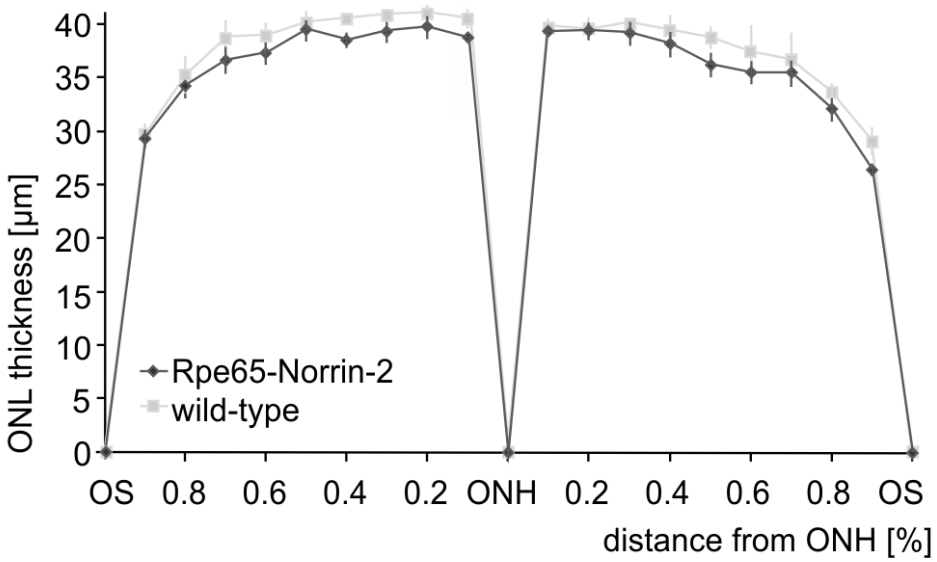

Figure 23: Spider diagram of untreated animals
The thickness of the outer nuclear layer (ONL) was measured on horizontal semithin sections of eyes of untreated Rpe65-Norrin-2 animals and wild-type littermates. To this end, the distance between the ora serrata (OS) and the optic nerve head (ONH) was divided into tenths and the thickness of the ONL was measured at each tenth. Data is mean ± SEM, n=5 per group. Experiment published in (107), performed by Barbara Braunger.

2.2.2 Ultrastructure of Rpe65-Norrin-2 animals

Since the overexpression of Norrin protein in Rpe65-Norrin-2 animals was driven by a RPE specific promoter, transmission electron microscopy was performed of the very region to confirm the normal structure and morphology of the RPE. More specifically, transmission electron microscopy did not detect differences in the ultrastructure of RPE and adjacent photoreceptor outer segments (Figure 24).

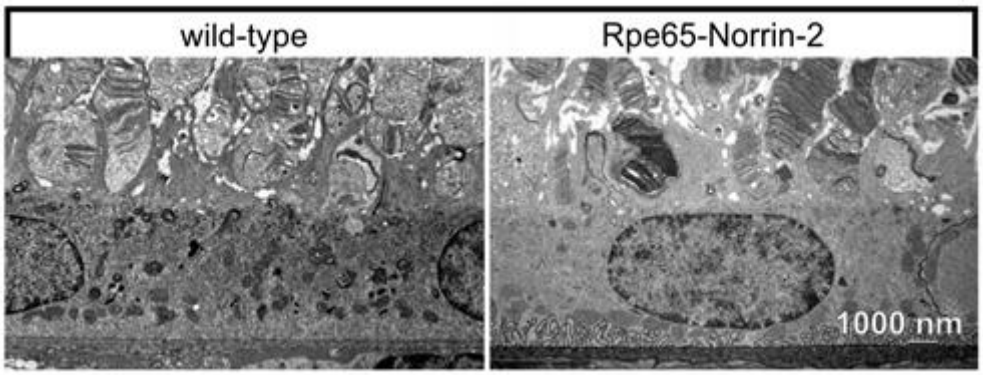

Figure 24: Ultrastructure of the RPE in Rpe65-Norrin-2 animals
Transmission electron microscopy of the retinal pigment epithelium and photoreceptor outer segments. No morphological ultrastructural difference was detected. Experiment published in (107), performed by Barbara Braunger.

2.2.3 Vascular phenotype

We subsequently analyzed the retinal vasculature of Rpe65-Norrin-2 mice, because Norrin is important for retinal angiogenesis during development. Transgenic overexpression of Norrin in the lens leads to a persistence of the tunica vasculosa lentis and the hyaloid vasculature (73). *In vivo* funduscopy and angiography was performed and a normal configuration of the retinal vasculature was observed in wild-type controls and transgenic Rpe65-Norrin-2 littermates (Figure 25).

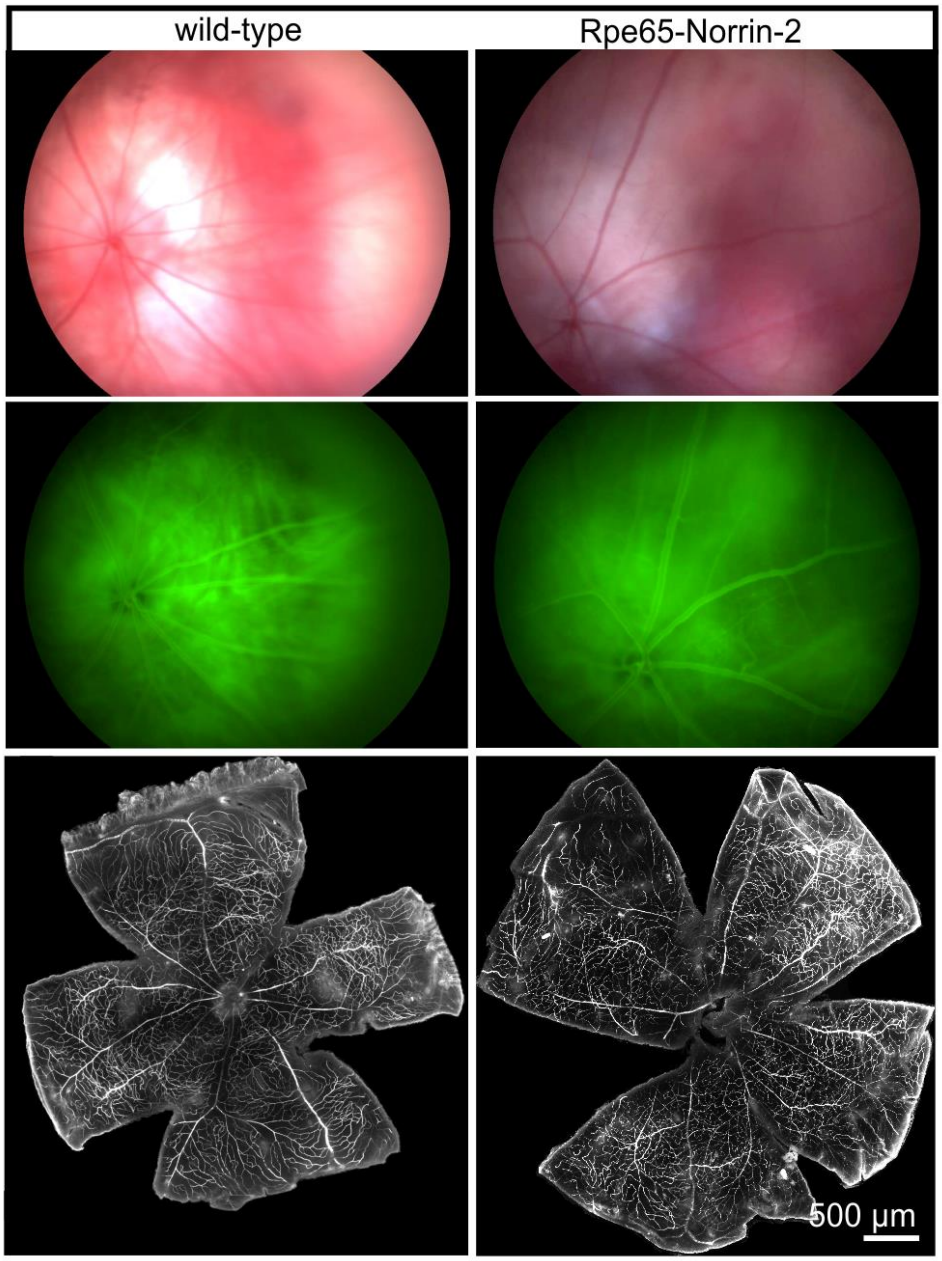

Figure 25: *In vivo* funduscopy and angiography in Rpe65-Norrin-2 animals
Rpe65-Norrin-2 animal showed a comparable vascular phenotype than the wild-type control littermates. *In vivo* funduscopy (top row) and fluorescein angiography (middle row) did not show obvious differences between the eye of a 2-month-old Rpe65-Norrin-2 mouse and its wild-type littermate. FITC–dextran perfused retinal whole mounts (lower row) of a 6-week-old Rpe65-Norrin-2 mouse and its wild-type littermate show a normal pattern of the retinal vasculature. *In vivo* funduscopy and angiography was performed in cooperation with Prof. H. Jägle. FITC-dextran perfusion and whole mount preparation were performed with the help of Andreas Ohlmann. Figure published in (107).

Additionally, no evidence for the persistence of hyaloid vessels or capillaries of the tunica vasculosa lentis was observed. Furthermore, in FITC–dextran perfused retinal whole mounts the pattern of the vascular plexus on the inner surface of the retina was comparable in Rpe65-Norrin-2 mice and their wild-type littermates with no signs for retinal neovascularization or pre-retinal tufts (Figure 25).

To investigate the vascular phenotype in more detail, the vascular endothelium of transgenic and wild-type animals was labeled with isolectin B4 and visualized. In addition to the already analyzed capillaries on the retinal surface, a regular deep and intermediate capillary plexus on the inner and outer aspects of the inner nuclear layer was observed (Figure 26, upper panel). Finally, the choriocapillaris was labeled with an antibody against plasmalemma vesicle associated protein (PLVAP), which is a marker for fenestrated capillaries and characteristic for the endothelium of the choriocapillaris (Figure 26, lower panel). Again no differences were detected between Rpe65-Norrin-2 mice and wild-type littermates.

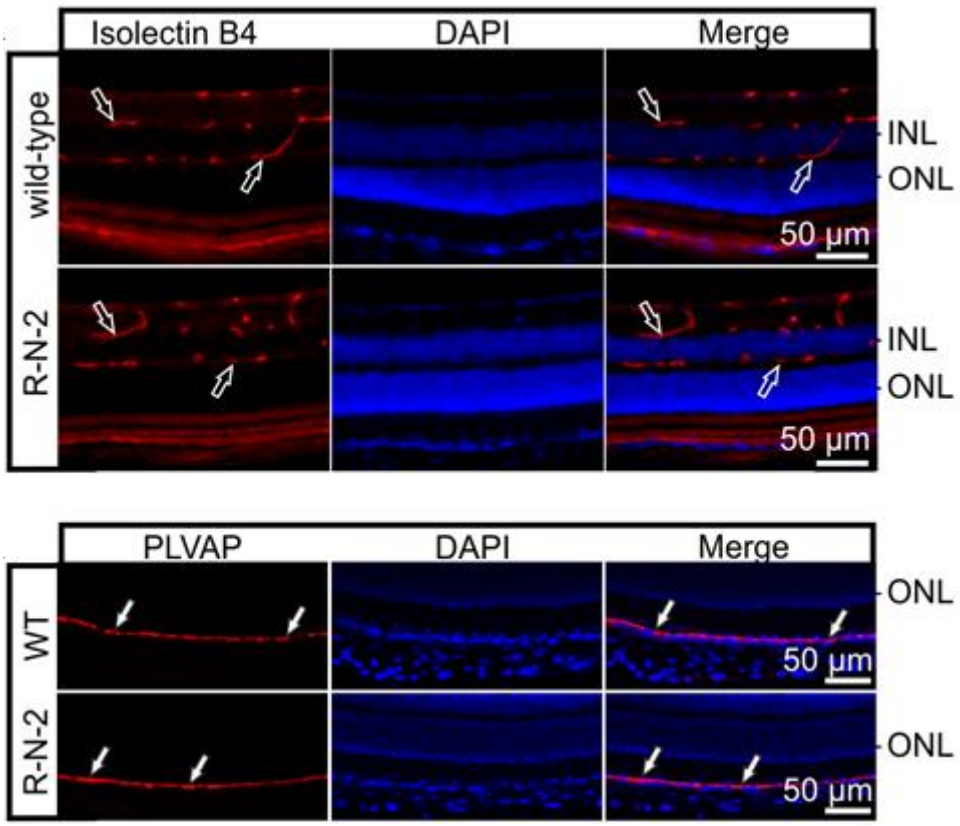

Figure 26: Vascular endothelial staining in Rpe65-Norrin-2 animals
Upper panel: Isolectin B4-labeling (red) in sections through the central retina of a 2-month-old Rpe65-Norrin-2 and wild-type mouse. The capillaries of both deep and intermediate capillary plexus (open arrows) were visualized. Nuclei were stained with DAPI (blue). Lower panel: Labeling of choriocapillaris endothelium (white arrows) with PLVAP (red) showed no differences between the Rpe65-Norrin-2 mouse and its wild-type littermate. Nuclei were stained with DAPI (blue). INL= inner nuclear layer; ONL= outer nuclear layer. Experiment published in (107), performed by Barbara Braunger.

2.3 The retinopathia of prematurity (ROP) model

Additional to the neuroprotective aspect of Norrin, the angiogenic function of Norrin was analyzed using the ROP model. This part of the thesis was performed in cooperation with Andreas Ohlmann and the data are published in (106).

To induce the vascular phenotype reflecting retinopathia of prematurity, pubs of βB1-Crystallin Norrin and Rpe65-Norrin-2 mice were exposed to high levels of oxygen from P7 - P12. Since the retina is well supplied with oxygen during this period of hyperoxia (75% oxygen), the retinal vessels stop to proliferate further which results in areas of vaso-obliteration. The subsequent exposure to normal room air leads to a relative hypoxia due to the non-perfused areas in the retina. In consequence of this, angiogenic factors are secreted. They induce an uncontrolled proliferation of the retinal vessel, resulting in preretinal tufts and leaky abnormal vessels (see also 1.3.1).

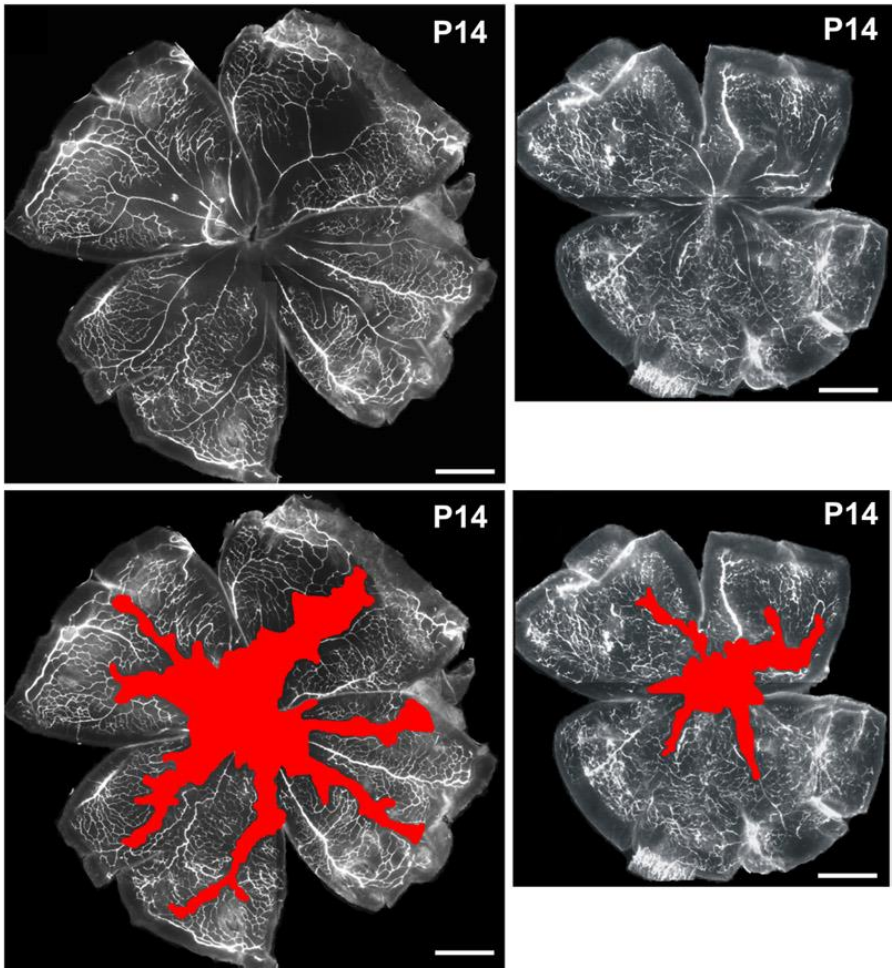

Figure 27: Overexpression of Norrin protects against obliteration and loss of vessels in βB1-Crystallin Norrin animals
Upper panel: FITC- dextran perfused wild-type (left) and βB1-Crystallin Norrin (right) retinae at P14 after induction of oxygen induced retinopathy.
Lower panel: The area of obliterated vessels in wild-type (left) and βB1-Crystallin Norrin (right) retinae labeled in red. (scale bars: 500 µm). Experiment published in (73), performed by Barbara Braunger.

In animals with a Norrin overexpression from the lens (βB1-Crystallin Norrin), the area of obliterated vessels compared to wild-type littermates was significantly reduced (Figure 27, quantified in Figure 28).

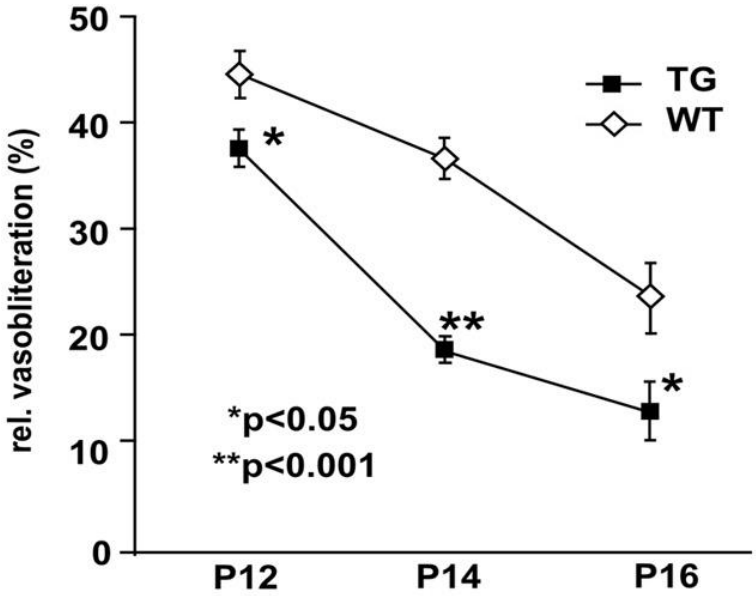

Figure 28: Quantification of ROP induced vaso-obliteration
The area of vaso-obliteration was quantified and plotted as percentage of total retinal area. P12, P14 and P16 was analyzed. Data is mean ± SEM, n>10. TG= βB1-Crystallin Norrin mice; WT= wild-type controls. Experiment published in (106), performed by Barbara Braunger and Andreas Ohlmann.

In addition to the better re-vascularisation of the superficial vascular plexus after ROP in βB1-Crystallin Norrin animals, their intraretinal vascularization also better compared to wild-type littermates. At P16, after ROP regime from P7-P12 wild-type animals showed predominantly vessels of the superficial plexus. In contrast, βB1-Crystallin Norrin mice showed abundant deep retinal capillaries (Figure 29, quantified in Figure 30).

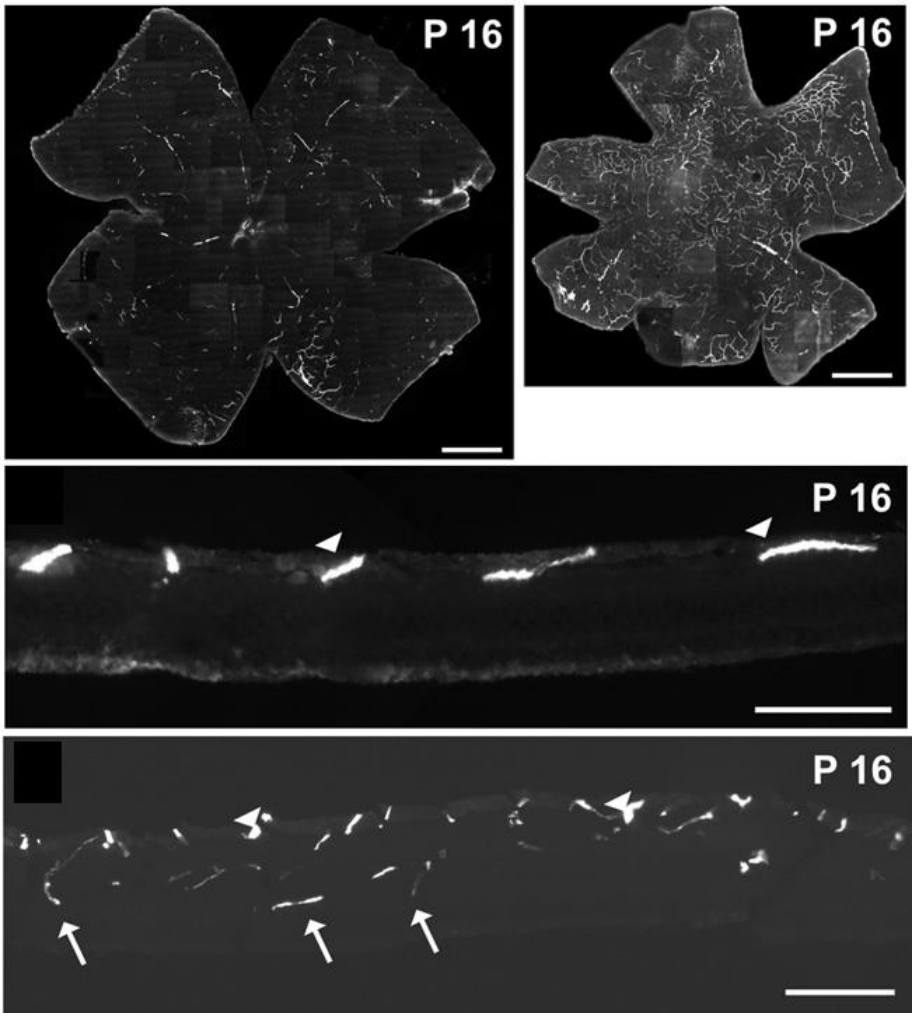

Figure 29: Norrin stimulated growth of intraretinal vessels after oxygen-induced retinopathy in βB1-Crystallin Norrin animals

Top: Representative FITC-labeled retinal whole mounts showing the intraretinal capillaries at P16. **Middle:** FITC- dextran labeled sagittal sections through retinal whole mount of wild-types at P16 following induction of oxygen-induced retinopathy. In wild-type animals, predominantly vessels of the superficial plexus were detectable (arrowheads).

Bottom: FITC- dextran labeled sagittal sections through retinal whole mount of B1-Crystallin-Norrin mice at P16 following induction of oxygen-induced retinopathy. In βB1-Crystallin Norrin mice deep retinal capillaries are abundant (arrows). Scale bars: 500 µm (top), 100 µm (middle and bottom). Experiment published in (106), performed by Barbara Braunger.

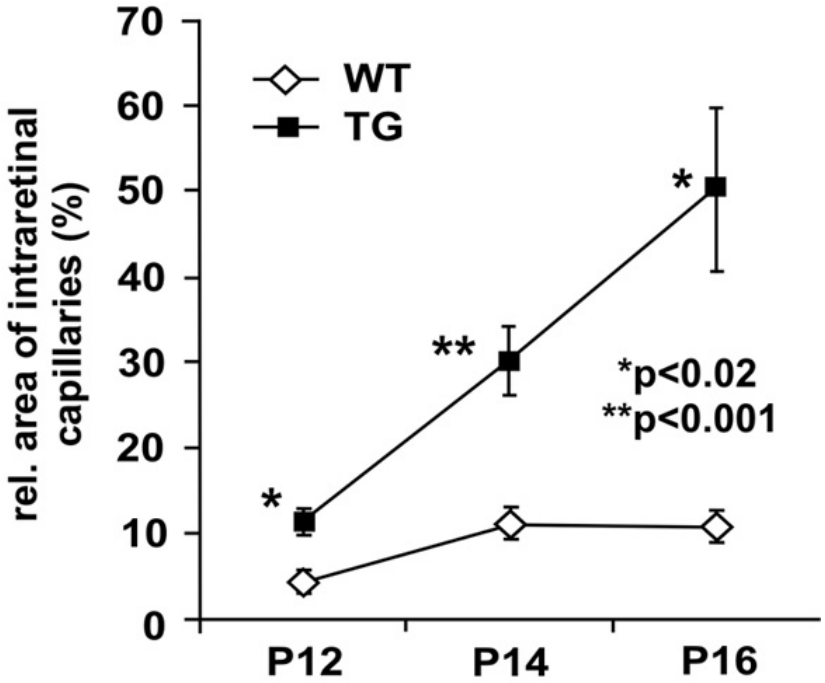

Figure 30: Quantification of relative area of intraretinal capillaries
The area covered by deep retinal capillaries was quantified at P12, P14, and P16 for βB1-Crystallin Norrin mice and controls and plotted as percentage of total retinal area. In βB1-Crystallin Norrin animals, the area of intraretinal vessels was significantly higher compared to wild-type pubs. Data is mean ± SEM; n>10. TG= βB1-Crystallin Norrin mice; WT= wild-type controls. Experiment published in (106), performed by Barbara Braunger and Andreas Ohlmann.

In the following, the results obtained so far, using βB1-Crystallin Norrin animals (Norrin overexpression in the lens), were confirmed with a second, independent mouse line, the Rpe65-Norrin-2 mice. In these animals Norrin is overexpressed in the retinal pigment epithelium and secreted into the retina (see Figure 18). In summary, Rpe65-Norrin-2 animals showed comparable effects to the βB1-Crystallin Norrin animals. However, the effects were less drastic in the Rpe65-Norrin-2 line (Figure 31 A and B). A possible explanation for this might be the different levels of Norrin overexpression due to the different promoters between βB1-Crystallin Norrin and Rpe65-Norrin-2 animals (see Figure 16).

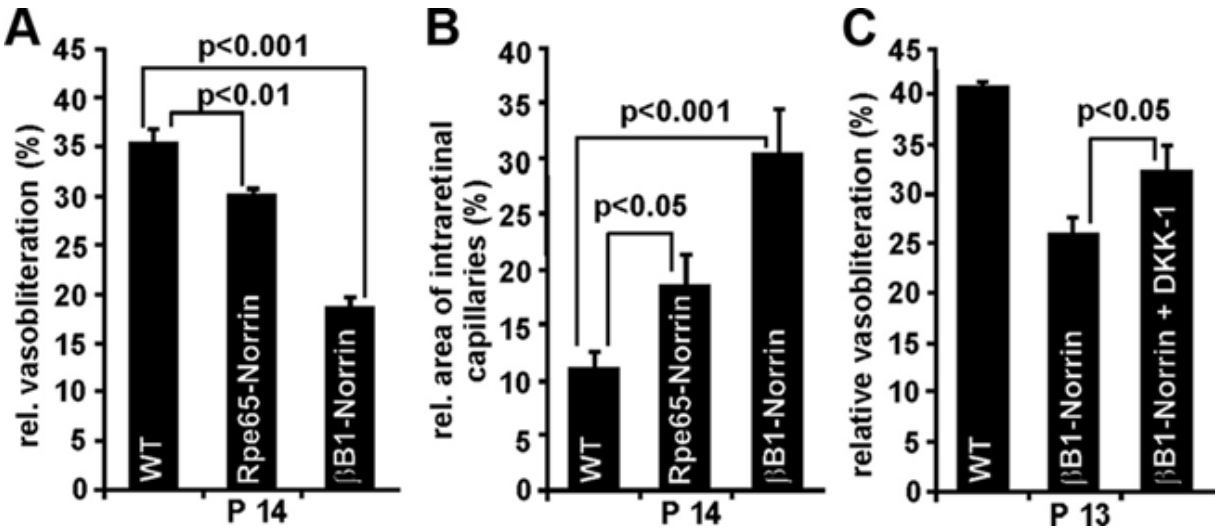

Figure 31: Quantification of the influence on vessel growth in βB1-Crystallin Norrin and Rpe65-Norrin-2 animals.

A. The area of relative vaso-obliteration was quantified at P14. Rpe65-Norrin-2, as well as βB1-Crystallin Norrin animals showed a significant reduction in the area of vaso-obliteration compared to wild-type littermates.

B. The area of relative intraretinal capillaries was quantified at P14. Rpe65-Norrin-2, as well as βB1-Crystallin Norrin animals showed significant more intraretinal vessels compared to wild-type littermates.

C. The area of relative vaso-obliteration was quantified at P13. Again, βB1-Crystallin Norrin animals showed a significant reduction in the area of vaso-obliteration compared to wild-type littermates. However, when the Wnt/β-catenin- pathway was blocked in βB1-Crystallin Norrin animals using DKK1 injections into the vitreous, the area of vaso-obliteration significantly increased compared to uninjected βB1-Crystallin Norrin animals. Data is mean ± SEM; n = 10; WT= wild-type. Experiment published in (106), performed by Barbara Braunger and Andreas Ohlmann.

Finally, the Wnt/β-catenin pathway was blocked after ROP using Dickkopf1 (DKK1) injections into the vitreous of βB1-Crystallin Norrin animals. The area of vaso-obliteration increased significantly in βB1-Crystallin Norrin animals, indicating that the positive influence of Norrin in the βB1 -Norrin animals is mediated through the Wnt/β-catenin pathway.

2.4 Light damage experiments

To investigate if overexpression of Norrin in the retinal pigment epithelium and subsequent Norrin secretion into the retina would have neuroprotective effects on the survival of photoreceptors, light damage experiments were performed.

2.4.1 Morphometric analysis

To this end, adult (6-9 weeks old) Rpe65-Norrin-2 and wild-type littermates were placed in transparent plastic cages and illuminated with cool white light coming from the top, with an intensity of 5000 lux. The analyses were performed 7 or 14 days after light exposure. For morphometric analysis, horizontal semithin sections stretching from the nasal to temporal side were investigated (for detailed explanation, see Figure 70). As expected, the major light induced damage on photoreceptor cells was localized in the central retina. However, in Rpe65-Norrin-2 animals, this effect was reduced compared to wild-type controls (see Figure 32) and the remaining outer nuclear layer (ONL) in the central part of the retina in Rpe65-Norrin-2 animals was remarkably thicker compared to control wild-type littermates (Figure 33).

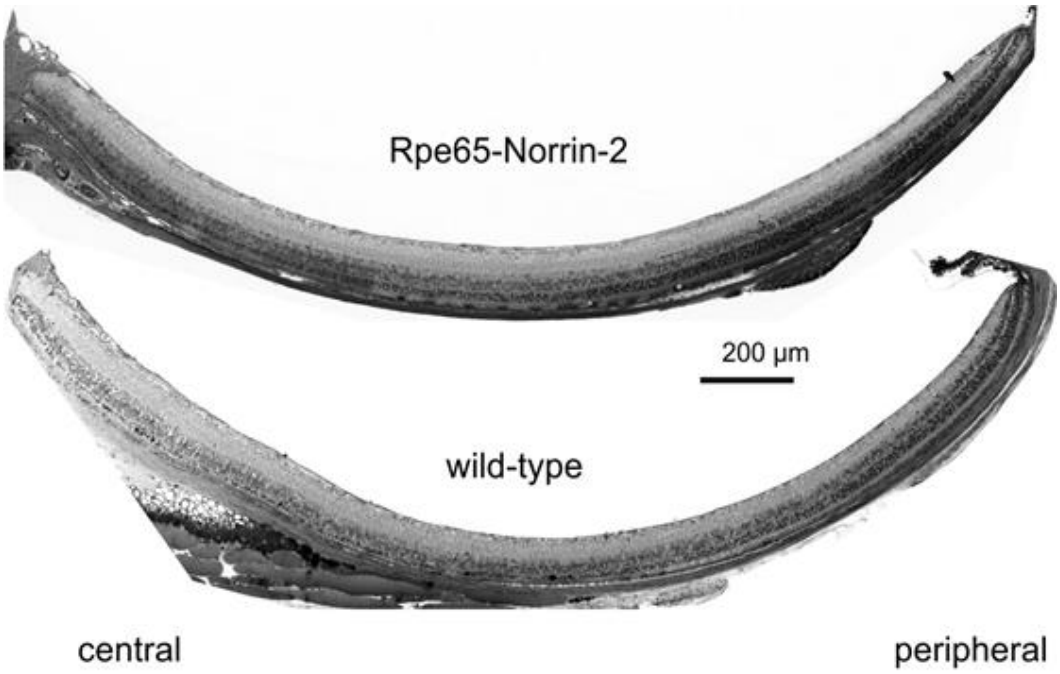

Figure 32: Semithin section of light exposed Rpe65-Norrin-2 and wild-type littermates.
Seven days after light exposure, the thickness of the ONL is noticeably reduced in the central retina, around the optic nerve head, whereas it is hardly thinned in the peripheral retina near the ora serrata. However, the ONL layer in the central retina was remained markedly thicker in Rpe65-Norrin-2 animals compared to wild-type controls. Experiment published in (107), performed by Barbara Braunger.

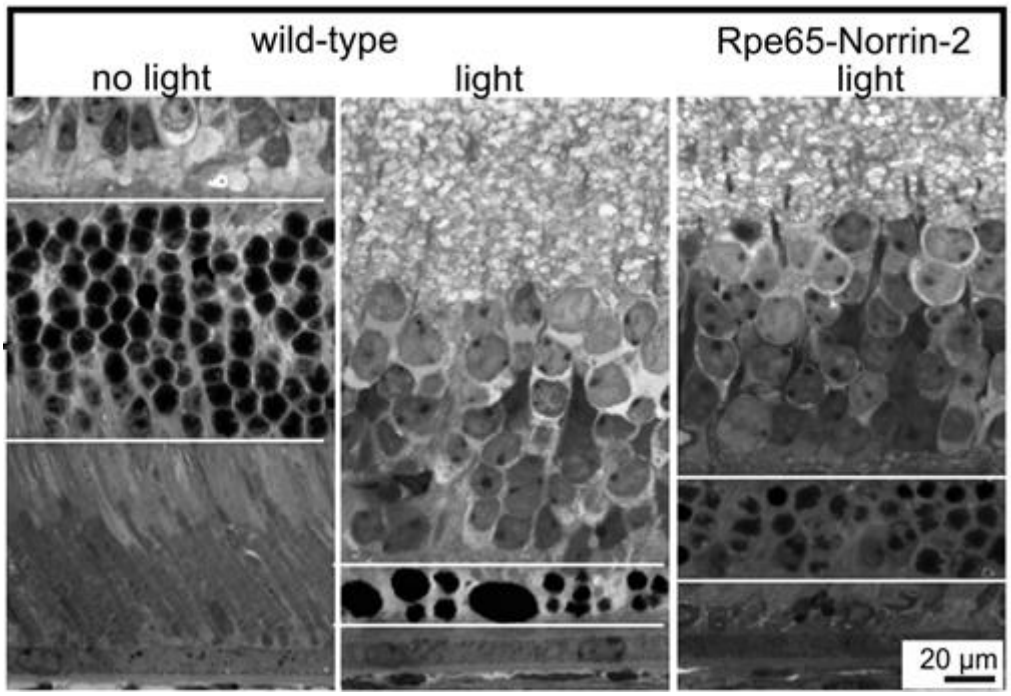

Figure 33: Higher magnification of the central retina after light exposure
The white bars which embrace the ONL show the thickness of this layer and additional indicate the measure technique for spider diagrams.
Left: control wild-type retina.
Middle: light damaged wild-type animal, 7 days after light exposure.
Right: light damaged Rpe65-Norrin-2 retina, 7 days after light exposure.
The ONL in control animals was reduced to 2 rows of photoreceptor cell nuclei, whereas in Rpe65-Norrin-2 animals 3 to 4 rows of cell nuclei remained. Experiment published in (107), performed by Barbara Braunger.

For morphometric analysis, the thickness of the outer nuclear layer was measured at 21 measure points across the entire retina and illustrated in spider diagrams (for spider diagram creation see Figure 70). Statistical evaluation 7 days after light exposure of Rpe65-Norrin animals revealed a significant thicker outer nuclear layer at 6 measure points throughout the retina compared to their wild-type littermates (Figure 34), indicating a neuroprotective effect of the Norrin overexpression in the RPE and its secretion into the retina.

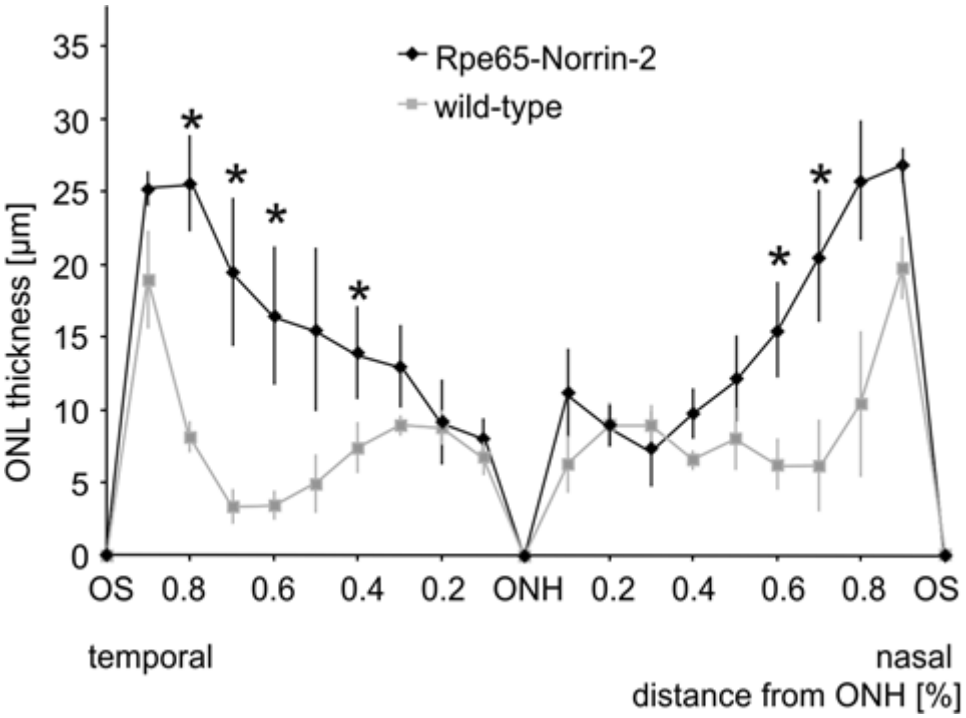

Figure 34: Spider diagram: ONL thickness 7 days after light exposure
The thickness of the outer nuclear layer (ONL) was quantified at 21 measure points on horizontal sections stretching from the nasal to temporal side through the optic nerve head (ONH). The results are illustrated in this spider diagram. Data is mean ± SEM, n=6, *p<0.05, 7 days after light exposure. Experiment published in (107), performed by Barbara Braunger.

14 days after light exposure this neuroprotective effect was even more pronounced. Again, the remaining thickness of the outer nuclear layer was quantified by morphometric analyses, followed by statistical evaluation. The results were plotted in spider diagrams (Figure 35). 14 days after light exposure Rpe65-Norrin-2 showed a significant thicker ONL at 12 measure points throughout the retina compared to their wild-type control littermates. Apparently, the clearance of the apoptotic cells after light exposure was not fully completed after 7 days, which might explain the pronounced effect at the later time point.

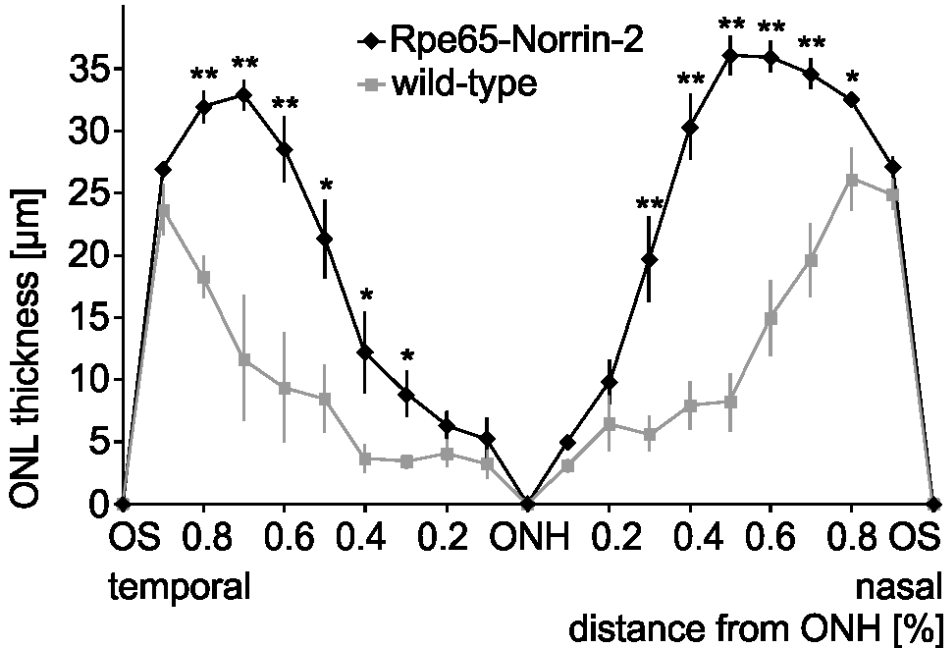

Figure 35: Spider diagram: ONL thickness 14 days after light exposure.
Thickness of the outer nuclear layer (ONL), quantified at 21 measure points on horizontal sections stretching from the nasal to temporal side through the optic nerve head (ONH). The results are illustrated in the spider diagram. Data is mean ± SEM, n=6. *p<0.05, **p<0.01. Experiment published in (107), performed by Barbara Braunger.

2.4.2 *In vivo* SLO and OCT imaging before and after light damage

Laser scanning ophthalmoscopy (SLO) and optical cohaerence tomography (OCT) were used to visualize the fundus and retina of untreated as well as light exposed Rpe65-Norrin-2 and wild-type littermates *in vivo*. In untreated Rpe65-Norrin-2 and wild-type animals, fundus SLO (Figure 32 A, upper row) imaging showed a normal fundus with the regular distribution of the retinal vessels. Additionally, blue light fundus-autofluorescence SLO imaging was performed to investigate whether autofluorescence of the RPE was present (Figure 32 A, upper row, right). RPE autofluorescence is due to the content of lipofuscin in the RPE. Lipofuscin accumulates if photoreceptor outer segments are depleted incompletely. Excessive lipofuscin accumulation is characteristic for various retinal degenerations. Lipofuscin has an excitation spectrum between 300 - 600 nm and an emission spectrum of 480 - 800 nm (108–110). SLO autofluorescence showed a normal fundus in both untreated Rpe65-Norrin-2 animals and wild-types littermates. The optic nerve head appeared black, because of the absence of RPE and its lipofuscin at this very point, and the blood vessels appeared also dark, because of the light absorption of the blood. In contrast in light damaged animals, a huge area of autofluorescence was visible, indicating a thinning of the retina, which is more pronounced in wild-types compared to Rpe65-Norrin-2 animals (Figure 32 B, upper row, right). This result confirmed the morphological data points and again indicated a neuroprotective role for Norrin overexpression from the RPE into the retina.

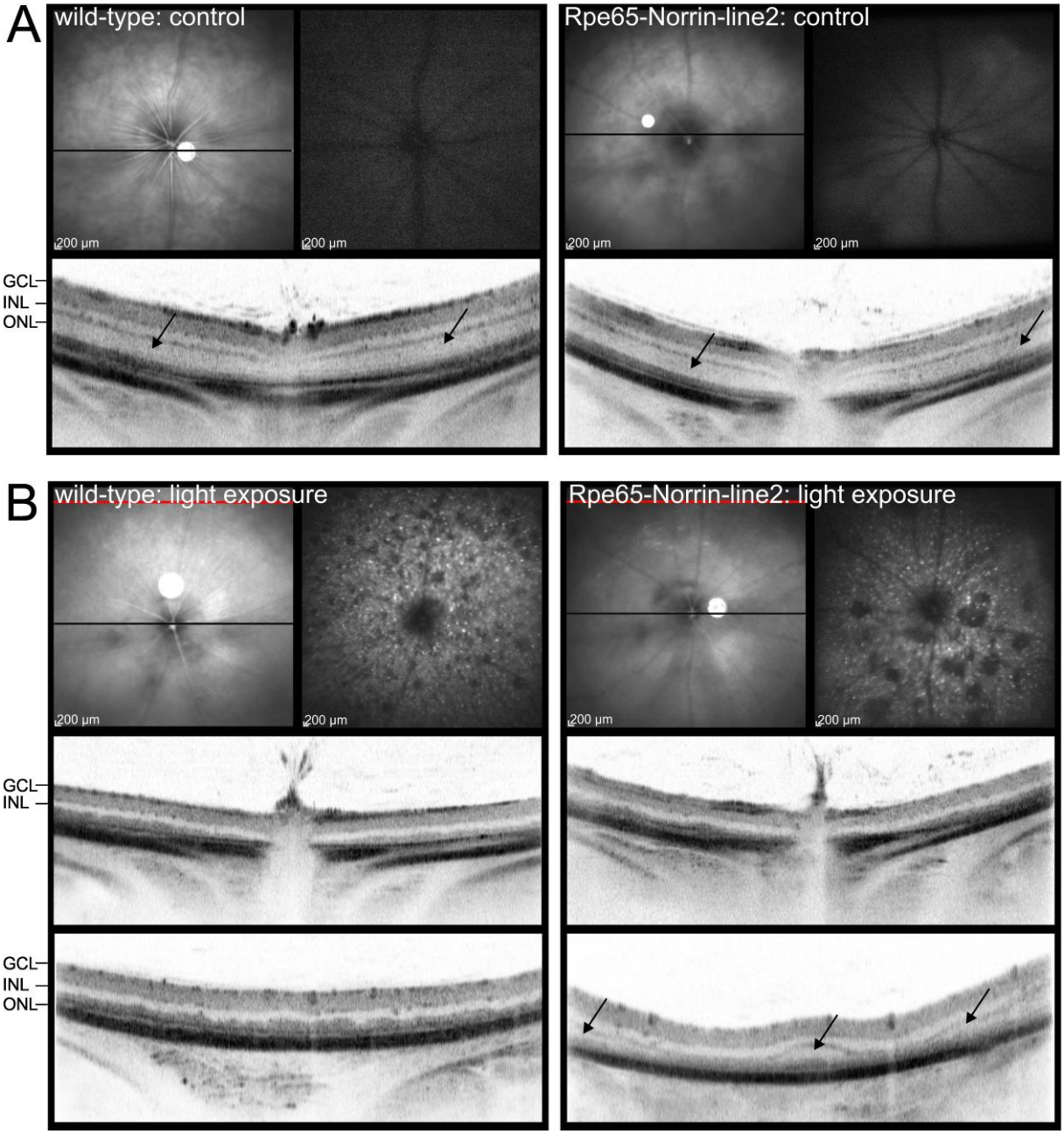

Figure 36: *In vivo* SLO and OCT imaging

A. Laser scanning ophthalmoscope (SLO – upper row) and optic coherence tomography (OCT – lower row) of untreated wild-type and Rpe65-Norrin-2 animals. **B**. Laser scanning ophthalmoscope (SLO – upper row) and optic cohaerence tomography (OCT – middle (central retina) and lower (mid-peripheral retina) row) of light exposed wild-type and Rpe65-Norrin-2 animals. The area of auto-fluorescence of the RPE is a sign for light-induced retinopathy and was visualized with SLO imaging. In SLO *in vivo* imaging, wild-type animals revealed more auto-fluorescence compared to their Rpe65-Norrin-2 littermates. Additionally, OCT *in vivo* imaging detected a reduced ONL thickness in light exposed wild-type animals compared to transgenic Rpe65-Norrin-2 animals in the mid-peripheral retina. The black arrows point to the ONL. GCL= ganglion cell layer, INL= inner nuclear layer, ONL= outer nuclear layer. OCT and SLO analysis were performed in cooperation with Prof. Seeliger, Tübingen.

In untreated Rpe65-Norrin-2 and wild-type animals, optic coherence tomography (OCT) imaging revealed a normal layering of the retina with comparable thickness between the specimens. The ONL layer was well defined (Figure 36 A, second row, black arrows). Light exposed animals showed a markedly thinned ONL in the central retina in both, wild-type animals and Rpe65-Norrin-2 animals.

This phenomenon changed in the periphery (Figure 36 B, lower panel, black arrows). In Rpe65-Norrin-2 animals, the ONL was already visible (Figure 36 B, lower panel, black arrows), whereas in wild-types hardly any ONL layer was visible in OCT analysis, again indicating an intense occurrence of damage in wild-types compared to Rpe65-Norrin-2 animals.

2.4.3 Functional analysis: electroretinography (ERG) analysis

ERG analysis was used to further investigate, if the morphometric and *in vivo* imaging (SLO and OCT) differences between light exposed wild-type and Rpe65-Norrin-2 animals would also result in function alterations. First, ERG analysis of untreated Rpe65-Norrin-2 mice (Figure 37, blue lines) and their wild-type (Figure 37, black lines) littermates was performed. There was no difference apparent, neither under dark-adapted (scotopic), nor in light-adapted (photopic) conditions (Figure 37, top and middle row). However, a severe loss of a- and b-wave components of the scotopic ERGs was observed in wild-type animals (Figure 37, green lines, top and middle row) two weeks following light damage. In contrast, Rpe65-Norrin-2 mice (Figure 37, red lines, top and middle row) showed a much better preservation in both a- and b-waves. As expected the amplitudes were to a certain degree lower than before light damage. For photopic conditions comparable results were observed. After statistical analysis (Figure 37, lower row) Rpe65-Norrin-2 mice revealed significantly better preservation of both the maximal a-wave, as well as the b-wave of the specific rod system and the specific cone system compared to wild-type mice. This results again indicated that overexpression of Norrin protects both rod and cone photoreceptors from light damage.

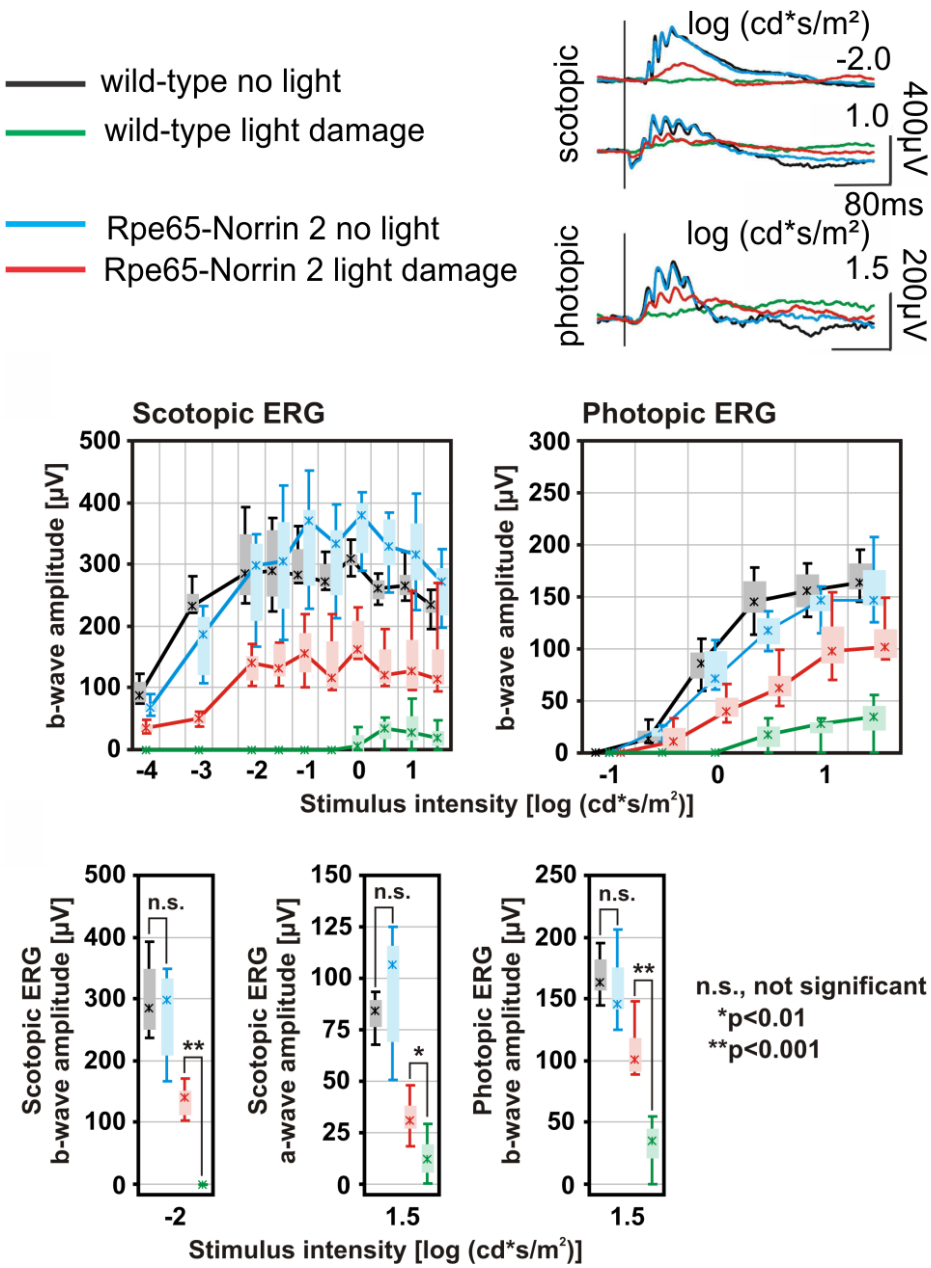

Figure 37: Functional ERG analysis

Top: Color legend of the 4 different experimental groups and representative single flash ERG recordings. **Middle:** Evaluation of single flash ERG b-wave amplitudes, scotopic (left) and photopic (right) in Box-and-whisker plots. The boxes indicate the 25 and 75% quantile range; whiskers indicate the 5 and 95% quantiles; and the asterisks indicate the median of the data. (n=4 each).

Bottom: Box-and-whisker plots of scotopic ERG b-wave amplitudes at −2.0 log cd s/m2 (left), scotopic ERG a-wave amplitudes at 1.5 log cd s/m2 (middle), and photopic ERG b-wave at 1.5 log cd s/m2 (right). (n.s. = not significant, * p<0.01, ** p<0.001; Mann–Whitney rank sum test). (n=4 each). The ERG analysis was performed in cooperation with Prof. Seeliger, Tübingen. Figure published in (107).

2.4.4 Analysis of the visual cycle

A normal function of the visual cycle is essential to be able to set a light damage (see 1.1.2.2). To analyze the state of the visual cycle, rhodopsin Western blots and immunohistochemical staining were performed. The total amount of rhodopsin, determined with Western blot analysis and immunohistochemical staining, was not altered in Rpe65-Norrin-animals compared to their control wild-type littermates (Figure 38). Immunohistochemical staining showed a strong immunoreactivity for rhodopsin in the photoreceptor segments and the retinal pigment epithelium in both, Rpe65-Norrin-2 animals and wild-types.

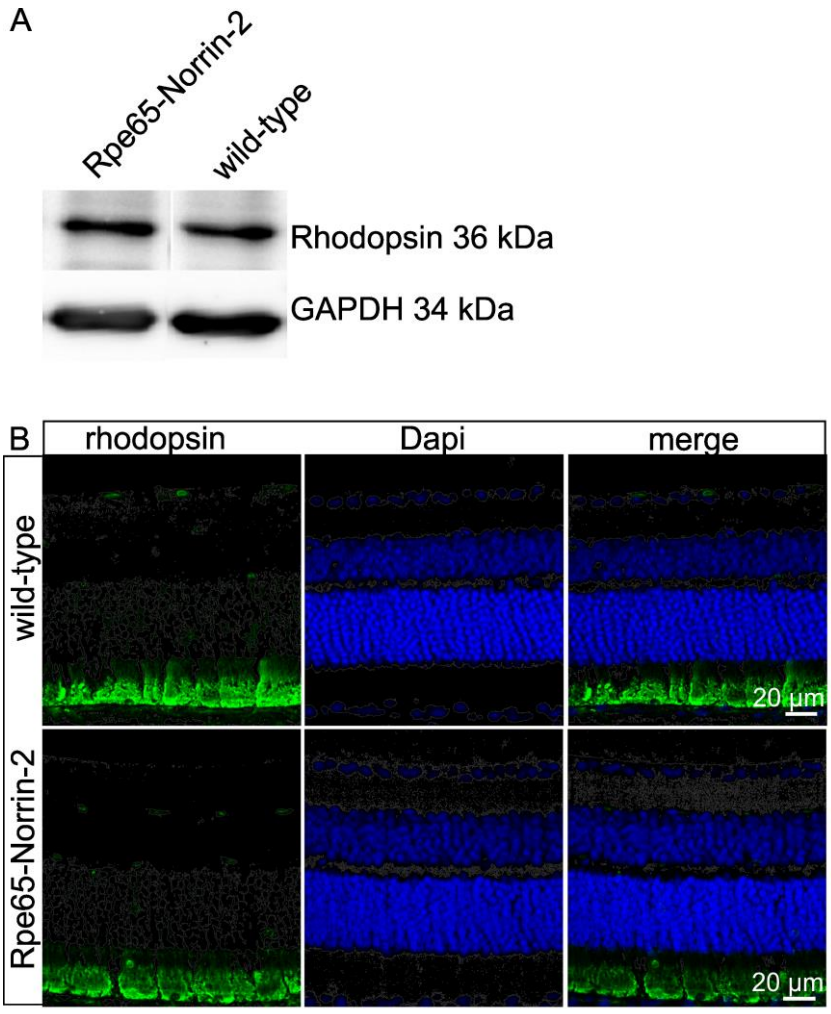

Figure 38: Rhodopsin: Western blot and immunohistochemistry
A. Western blot analysis for rhodopsin. Gapdh was used as loading control.
B. Immunohistochemical staining for rhodopsin (green). Cell nuclei are stained with Dapi (blue).

Additionally, western blot analyses for RPE65 protein were performed. RPE65 protein is an essential protein in the visual cycle (see 0). There was no difference in the protein level of RPE65 protein in Rpe65-Norrin-2 animals compared to controls (Figure 39). The results obtained so far did not show a difference in the amount of two major factors of the visual cycle (rhodopsin and RPE65). The total amount of them did not vary between the Rpe65-Norrin-2 and wild-type animals.

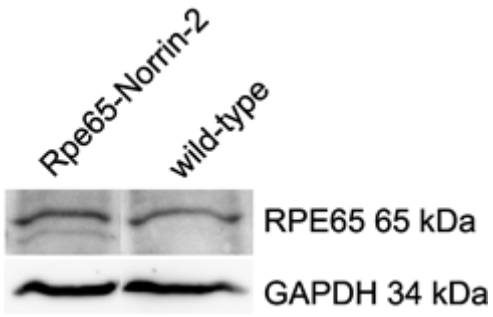

Figure 39: RPE65 (protein) Western blot
Western blot analysis for RPE65 protein in posterior halves of the eye. Tissue contained retina, RPE and sclera. Gapdh was used as loading control.

Furthermore, the rhodopsin recovery kinetics after illumination in Rpe65-Norrin-2 and wild-type littermates was analyzed. Here Rpe65-Norrin-2 animals showed a significant reduction in the capacity of rhodopsin recovery after illumination in the retinae harvested immediately after light exposure, 3h and 6h after light exposure with a meantime recovery period in the dark (Figure 40).

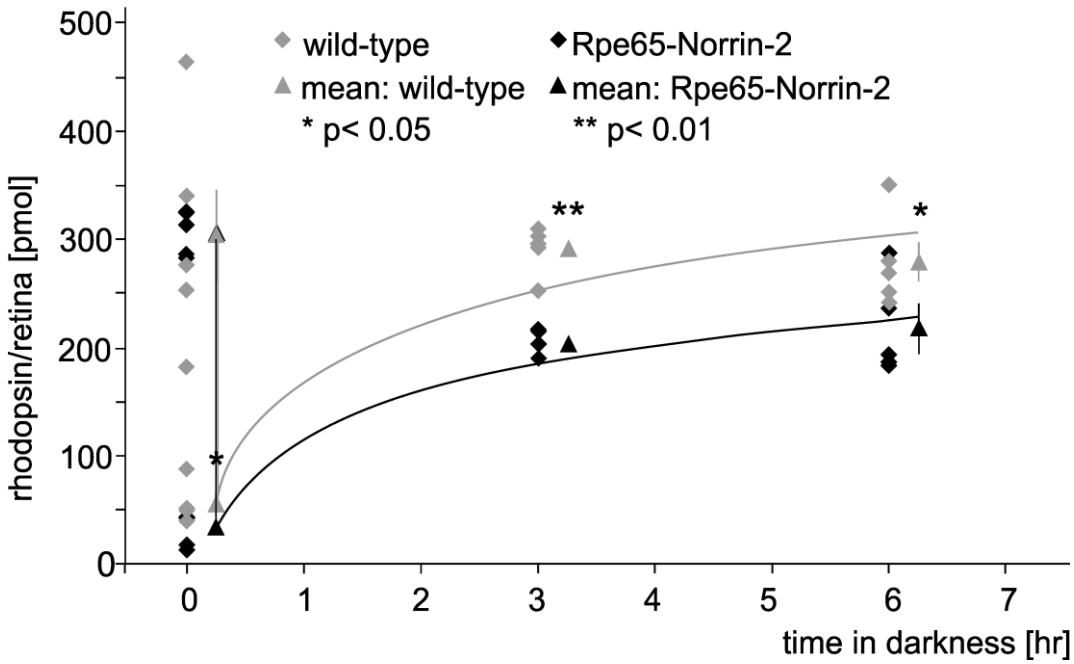

Figure 40: Rhodopsin recovery kinetics in darkness
Rpe65-Norrin-2 animals (dark: square and triangle) show a significant reduced capacity of rhodopsin recovery compared to wild-types (light grey: square and triangle). The content of rhodopsin in retinal samples was investigated at 4 different time-points: un-treated, only dark adapted animals (0 h, upper symbols), animals killed direct after light exposure (0 h, lower symbols), or 3 h and 6 h after light exposure. The two curves only highlight the approximate progress of the recovery kinetic. The amount of rhodopsin was investigated using photometer analysis at 500 nm wave length as described in 5.1.6.8. Square: data point of the single animals, triangle: mean and SEM (per time-point); n ≥ 4 per time-point; *p<0.05;**p<0.01.

Taken together, Rpe65-Norrin-2 animals showed normal protein expression levels of RPE65 and rhodopsin in Western Blot analysis. However, their rhodopsin recovery kinetic in darkness was impaired

2.4.5 Light exposure and apoptosis

Subsequently, TUNEL labeling, which indicates apoptotic cells, was performed to investigate if the differences in ONL thickness between Rpe65-Norrin-2 mice and their wild-type littermates might be the result of a different amount of photoreceptors entering apoptotic cell death following light exposure. Numerous TUNEL-positive cells were detected in the central retina in both Rpe65-Norrin-2 mice and their wild-type littermates. While some TUNEL-positive cells were detected in the peripheral retina of wild-type mice, only a very small number of apoptotic cells was detected in Rpe65-Norrin-2 mice the in the peripheral retina (Figure 41).

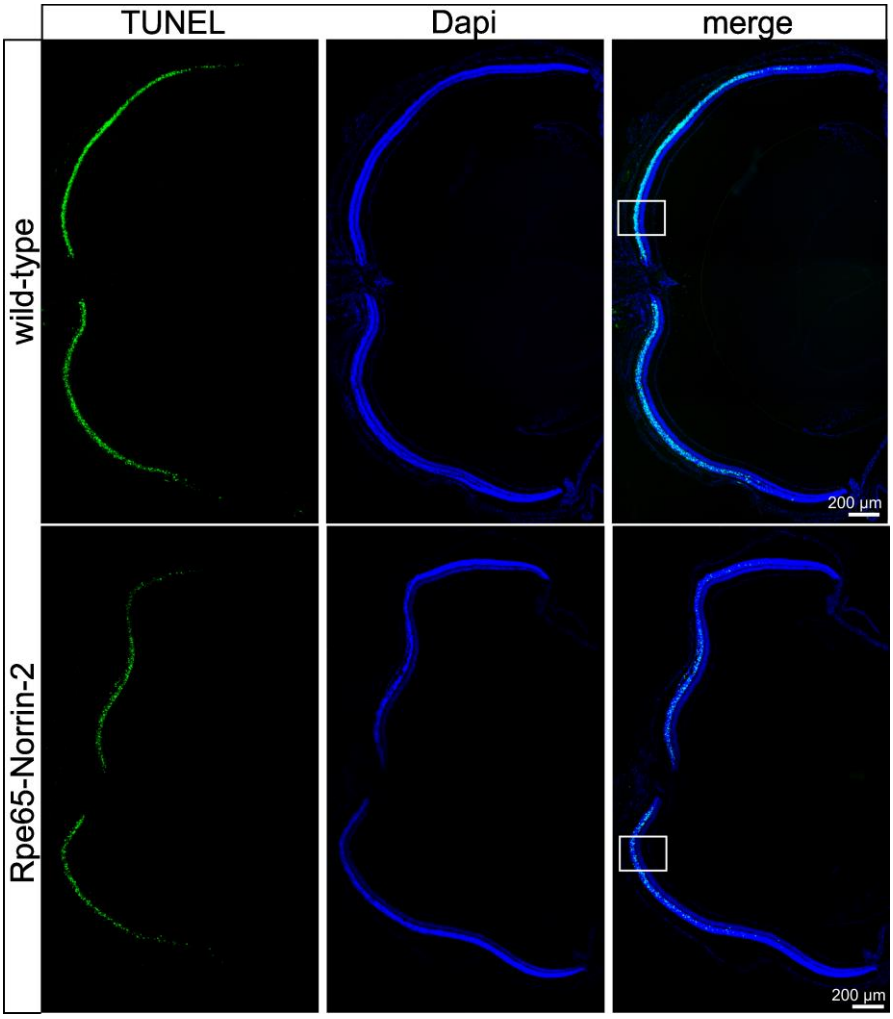

Figure 41: Norrin overexpression protects photoreceptors from light damage.
Horizontal TUNEL stained (green) sections of retinae 30 h after light damage. Nuclei are stained with Dapi (blue). Boxed areas in the merged picture indicate positions of panels in Figure 42 A. The distribution of the photoreceptor apoptosis throughout the retina with the major amount of apoptosis in the central part and less in the peripheral retina is characteristic for light damage. Experiment published in (107), performed by Barbara Braunger.

Next, the total number of TUNEL-positive nuclei in mid-horizontal sections in the outer nuclear layer was counted and normalized to the area of the outer nuclear layer. 1.76 ± 0.013 cells per 1000 µm^2 area outer nuclear layer were counted in wild-type mice versus 1.23 ± 0.066 cells per 1000 µm^2 in Rpe65-Norrin-2 transgenic mice ($p<0.05$) (Figure 42 A and B). These results were further validated

with a second independent assay. An ELISA that determined the relative amounts of cytoplasmic histone-associated DNA fragments (mono- and oligonucleosomes) was used to this end. The rate of cytoplasmic nucleosomes was 1.79 ± 0.24-fold higher in wild-type animals when compared to Rpe65-Norrin-2 mice ($p<0.05$) (Figure 42 C).

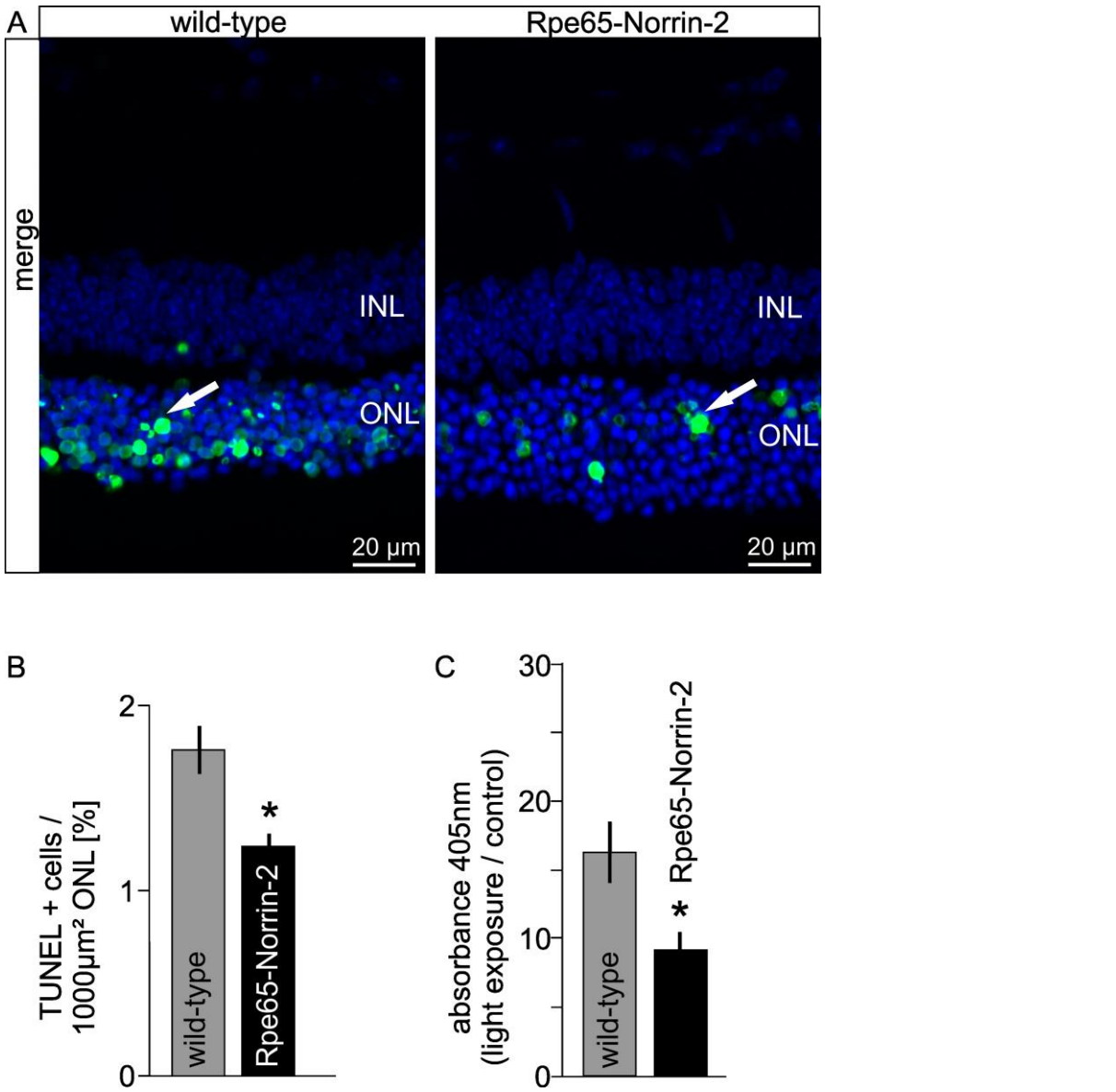

Figure 42: Norrin overexpression protects photoreceptors from light damage induced apoptosis
A. Higher magnification of the central retina (indicated area in Figure 41). Apoptotic cells were TUNEL labeled (green) 30 h after light exposure. Cell nuclei are labeled with Dapi (blue). **B.** Quantification of TUNEL positive cells per 1000 µm² ONL. The number of TUNEl positive cells is significant reduced in Rpe65-Norrin-2 animals. **C.** Cell death detection ELISA 30 h after light exposure. Rpe65-Norrin-2 animals showed significant less amounts of free histones compared to wild-types.
Data is mean ± SEM; TUNEL: n= 6, ELISA: n≥ 12; *$p<0.05$. INL= inner nuclear layer, ONL= outer nuclear layer. Experiment published in (107), performed by Barbara Braunger.

2.4.6 Wnt-/β-catenin signaling and Norrin mediated neuroprotection

To analyze if the neuroprotective effect in Rpe65-Norrin-2 animals might be mediated through Wnt-/β-catenin signaling, Dickkopf-1 (DKK1), an inhibitor of the Wnt-/β-catenin pathway, was injected in the vitreous of both Rpe65-Norrin-2 and wild-type littermates. In an initial experiment Western blotting for β-catenin was performed to assay the retinal protein levels in Rpe65-Norrin-2 animals and control littermates (Figure 43 A). Densitometric analysis of Western blots revealed a significant ($p<0.05$) increase in the amount of β-catenin in sham injected (PBS) Rpe65-Norrin-2 mice compared to wild-types (Figure 43 B). This result is quite comparable to the effects seen in uninjected animals (Figure 19). However, DKK1 injection reduced β-catenin protein levels significantly in Rpe65-Norrin-2 mice to levels seen in wild-type animals, whereas the injection of DKK1 into the vitreous of wild-type mice did not cause any alteration in the amounts of retinal β-catenin (Figure 43 B).

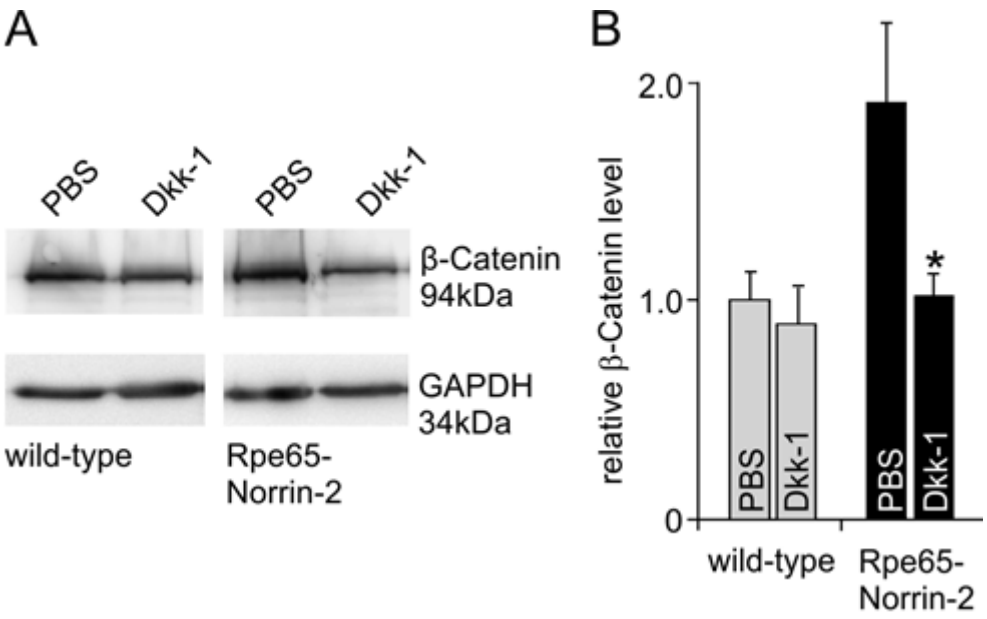

Figure 43: β-catenin Western blot analysis after DKK1 injections
A. β-catenin Western blot analysis of PBS and DKK1 injected eyes.
B. Densitometric analysis of Western blots for β-catenin levels in retinae of DKK1- or PBS-injected wild-type and Rpe65-Norrin-2 eyes.
Data is mean ± SEM, n≥ 4, *$p<0.05$. Experiment published in (107), performed by Barbara Braunger.

Subsequently, Wnt-/β-catenin signaling was blocked by DKK1 injections in Rpe65-Norrin-2 mice and wild-type littermates, 12 h before and 2 or 4 days after light exposure. One eye was injected with DKK1, while the contralateral eye was sham injected with PBS only. 7 days after light exposure, the eyes were harvested and semithin sections were analyzed using spider diagrams. In general, in light damaged, PBS-injected eyes, the thinning of the ONL was less severe than in non-injected eyes. However, the outer nuclear layer in the central retina of PBS-injected Rpe65-Norrin-2 eyes was still significantly thicker than the ONL of the PBS-injected wild-type littermates (Figure 44, upper panel).

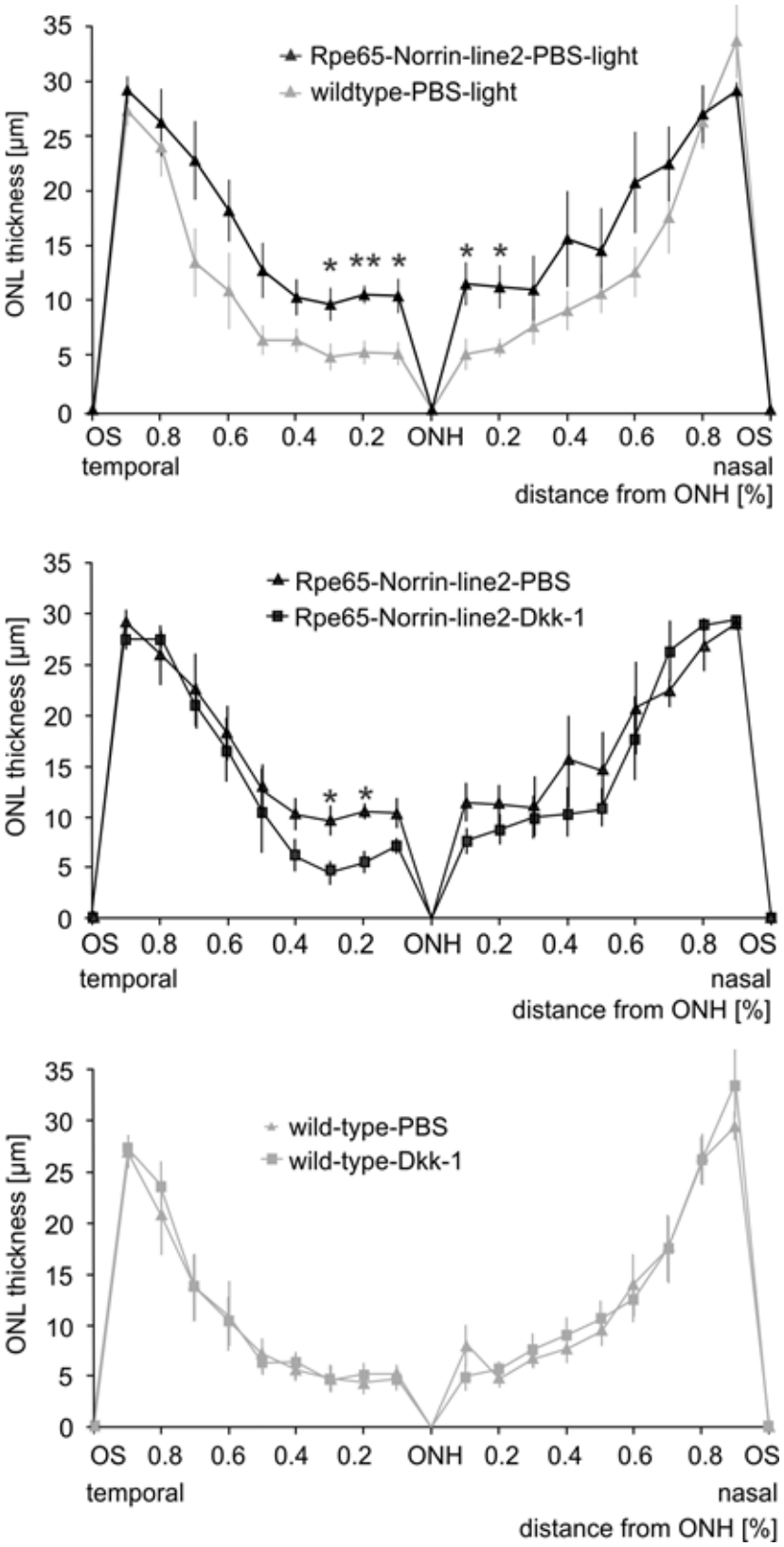

Figure 44: Spider diagrams: light exposure and Wnt/β-catenin signaling inhibition

Top: Spider diagram reflecting the thickness of the outer nuclear layer (ONL) of sham injected (PBS) wild-type and Rpe65-Norrin-2 mice 7 days after light exposure.

Middle: Spider diagram of the outer nuclear layer (ONL) thickness of DKK1- or PBS-injected contralateral eyes of Rpe65-Norrin-2 mice.

Bottom: Spider diagram of the outer nuclear layer (ONL) thickness of DKK1- or PBS-injected fellow eyes of wild-type littermates. Data is mean ± SEM, n= 6; *p<0.05 . Experiment published in (107), performed by Barbara Braunger.

After comparing the outer nuclear layer thickness of PBS and DKK1 injected eyes of Rpe65-Norrin-2 animals, the DKK1 injected retinae appeared more affected by light exposure than the PBS injected fellow eye, especially in the central retina. This indicated that the neuroprotective effect observed in Rpe65-Norrin-2 animals following light exposure might be mediated through an activation of the Wnt-/β-catenin pathway.

When comparing the outer nuclear layer thickness of PBS and DKK1 injected eyes of wild-types, there was no difference, neither in the central, nor in the peripheral part of the retina. This result was not surprising, since the Dkk-1 injections in wild-types did not reduce the β-catenin level significantly (see Figure 43).

2.5 Neuroprotective factors

2.5.1 Transgenic Norrin overexpression and neuroprotective factors

The previous results (Figure 44) showed that the neuroprotective effect of Norrin overexpression is at least partly mediated through an activation of the Wnt-/β-catenin signaling. In the following, the expression profiles of various neuroprotective factors were analyzed to investigate if the activation of the Wnt-/β-catenin signaling would lead to an increased expression of neuroprotective factors. To this end, quantitative real-time RT-PCR was performed of retinal RNA samples from untreated (no light damage) Rpe65-Norrin-2 and wild-type littermates. Several neuroprotective factors like *leukemia inhibitory factor (Lif), fibroblast growth factor 2 (FGF2), brain derived neurotrophic factor (Bdnf), lens epithelium derived growth factor (Ledgf), ciliary neurotrophic factor (Cntf)* and *pigment epithelium derived growth factor (Pedf)* were not differentially regulated. On the other hand, factors like *glial fibrillary acidic protein (Gfap), endothelin2 (Edn2)* and *endothelin receptor type B (Ednrb)* were significantly upregulated in Rpe65-Norrin-2 animals compared to their wild-type controls (Figure 45).

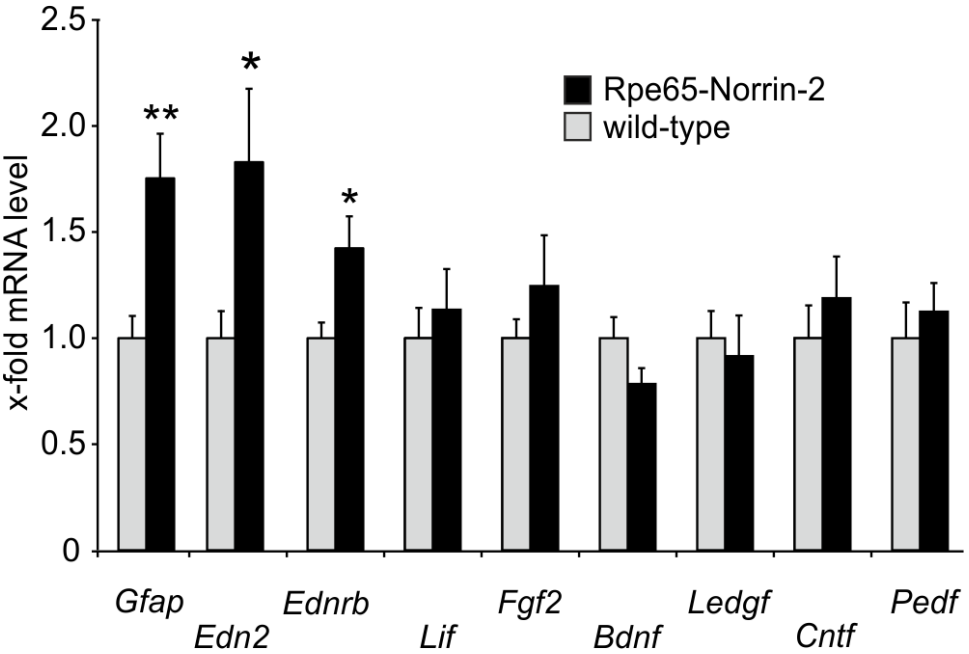

Figure 45: Realtime RT-PCR of untreated Rpe65-Norrin-2 and wild-type animals
Quantitative real-time RT-PCR for mRNA for neuroprotective factors: *Gfap, Edn2, Ednrb, Lif, Fgf2, Bdnf, Ledgf, Cntf* and *Pedf* in untreated adult wild-type and Rpe65-Norrin-2 retinae. Data is mean ± SEM, n≥ 6, **p<0.01, *p<0.05. Experiment published in (107), performed by Barbara Braunger.

To gain more insight into the localization of the dysregulated factors GFAP, EDN2 and EDNRB, immunohistochemical staining were performed. GFAP is a marker for astrocytes and activated Müller glia cells. As expected, staining for GFAP was detected on top of the retinal ganglion cell layer in wild-type mice, whereas in Rpe65-Norrin-2 animals, an intense immunoreactivity was detected along the inner retinal surface and an additional labling in the inner plexiform layer (Figure 46, upper

panel). Double immunohistochemical staining with antibodies against GFAP and glutamine synthetase (GS), a marker for Müller glia cells, revealed a partly overlap of the immunoreactivity at the inner retinal surface, but not a complete overlap layer (Figure 46, lower panel). This indicated an expression of GFAP in both Müller glia cells, especially their end feet, and astrocytes.

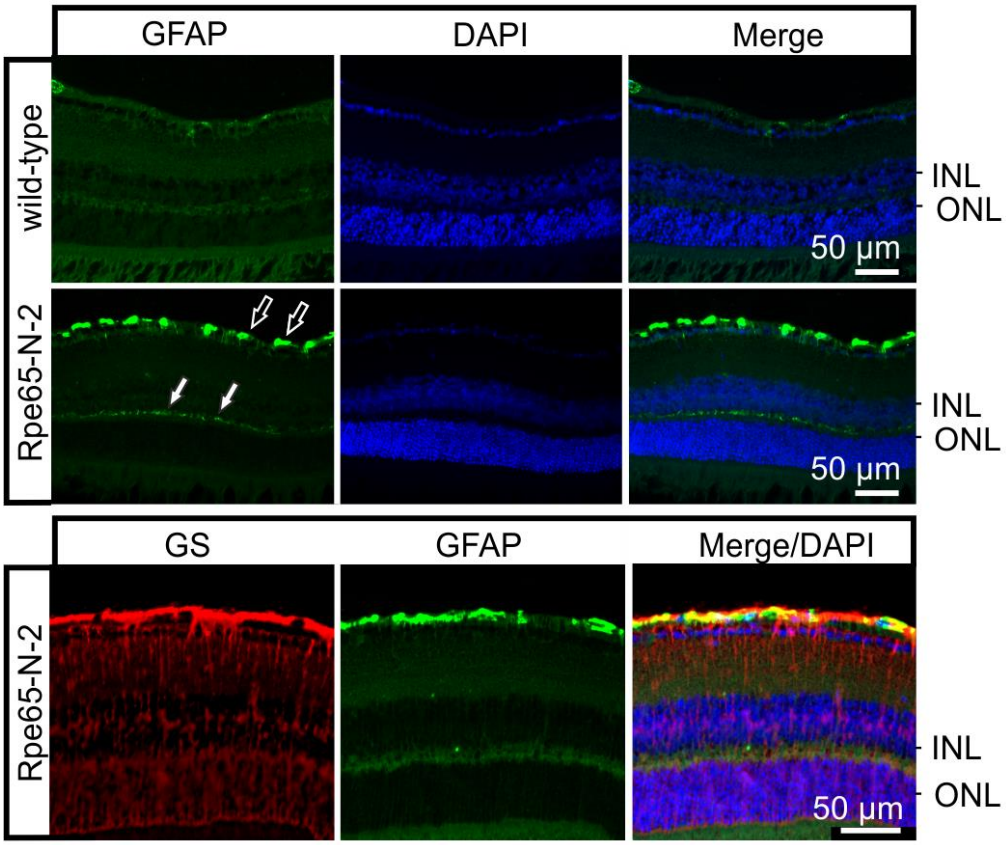

Figure 46: Immunohistochemical staining for GFAP in Rpe65-Norrin-2 animals
Top: GFAP (green) immunohistochemical staining of an adult wild-type retina. Cell nuclei were stained with DAPI (blue). Wild-type animals showed a discrete patchy staining in the inner side of the retina, whereas the Rpe65-Norrin-2 animal showed a distinct immunolabeling at the inner side of the retina and in the outer plexiform layer.
Bottom: GFAP and GS double labeling. Rpe65-Norrin-2 animals displayed the regular pattern of GS Müller glia staining with a distinct staining along the elongated glia processes stretching through the entire retina front the inner limiting membrane to the outer limiting membrane. The GFAP double labeling showed a partly overlap with the GS staining on the inner side of the retina, indicating an GFAP staining in both, Müller glia end feet and astrocytes. INL= inner nuclear layer; ONL= outer nuclear layer. Experiment published in (107), performed by Barbara Braunger.

Immunohistochemical staining for EDN2 revealed a discrete immunolabeling at the ganglion cell layer and in the retinal pigment epithelium (RPE). In Rpe65-Norrin-2 animals, the immunolabeling was particularly strong in the ganglion cell layer with an additional intense staining of the photoreceptor inner segments and in the retinal pigment epithelium (RPE) and an additional patchy immunostaining in the outer and inner plexiform layer (IPL/OPL).

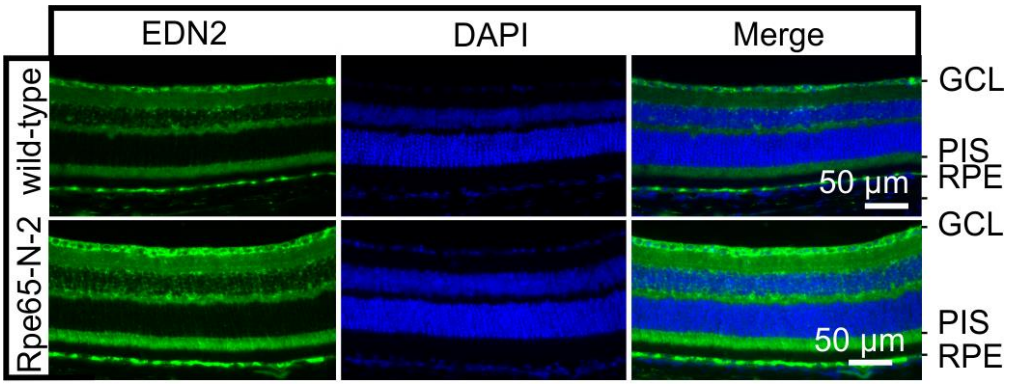

Figure 47: Immunohistochemistry of EDN2 in Rpe65-Norrin-2 animals
Wild-type animals showed a discrete immunolabeling in the ganglion cell layer and the retinal pigment epithelium. Rpe65-Norrin-2 animals had an additional homogenous staining of the photoreceptor inner segment and a patchy distribution in the inner and outer plexiform layer and a more intense labling in the ganglion cell layer. PIS= photoreceptor inner segments; GCL= ganglion cell layer; RPE= retinal pigmented epithelium. Experiment published in (107), performed by Barbara Braunger.

In wild-type mice, endothelin receptor type B (EDNRB) immunoreactivity was detectable in the inner segments of the photoreceptors, while Rpe65-Norrin-2 animals had an additional staining for EDNRB in the ganglion cell layer.

Double labeling experiments for EDNRB and GS revealed no co-localization. Additionally, the double labeling experiments with EDNRB and rhodopsin, a marker for rod photoreceptors, showed no co-localization in the inner segments of the photoreceptors. However, co-labeling for EDNRB and peanut agglutinin (PNA), a lectin that labels the interphotoreceptor matrix that sheaths cone photoreceptor inner and outer segments (111), showed an overlap, which strongly indicates that EDNRB is localized on cone photoreceptor outer segments. In Rpe65-Norrin-2 retinae, the EDNRB staining in general was more intense compared to wild-types and it co-localized with GS, which strongly indicated a co-localization with Müller glia end feet (Figure 48). Similar to the labeling in wild-types, co-labeling EDNRB with PNA in Rpe65-Norrin-2 animals revealed a co-localization, indicating its localization on cone photoreceptor cells. Yet, the PNA signal was more extended to the outer segments in Rpe65-Norrin-2 compared to wild-type labeling (Figure 49).

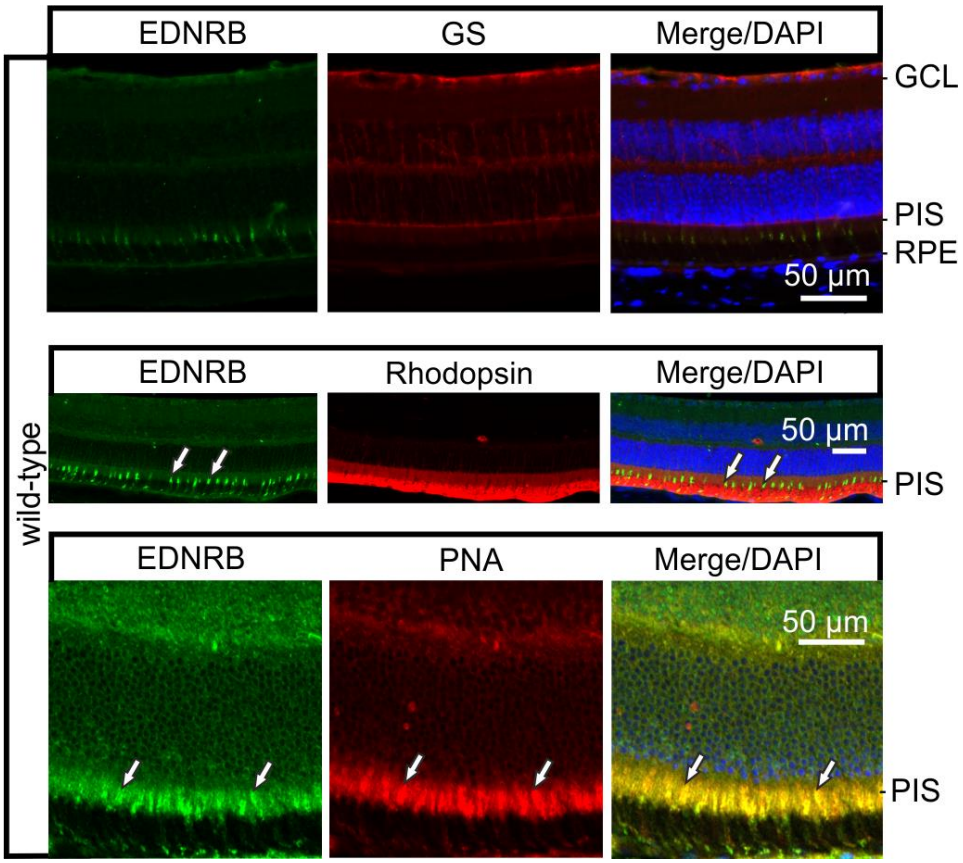

Figure 48: Immunohistochemical staining of EDNRB and co-labeling with rhodopsin and PNA in wild-type mice

Double immunohistochemical staining in wild-type animals for EDNRB (green) and either GS (red), or rhodopsin (red), or PNA (red). Nuclei were stained with DAPI (blue). Immunoreactivity for EDNRB was detectable in the inner segments of the cone photoreceptors (arrows) that are negative for GS and rhodopsin, but label positive for PNA. GCL= ganglion cell layer; PIS= photoreceptor inner segments; RPE= retinal pigmented epithelium. Experiment published in (107), performed by Barbara Braunger.

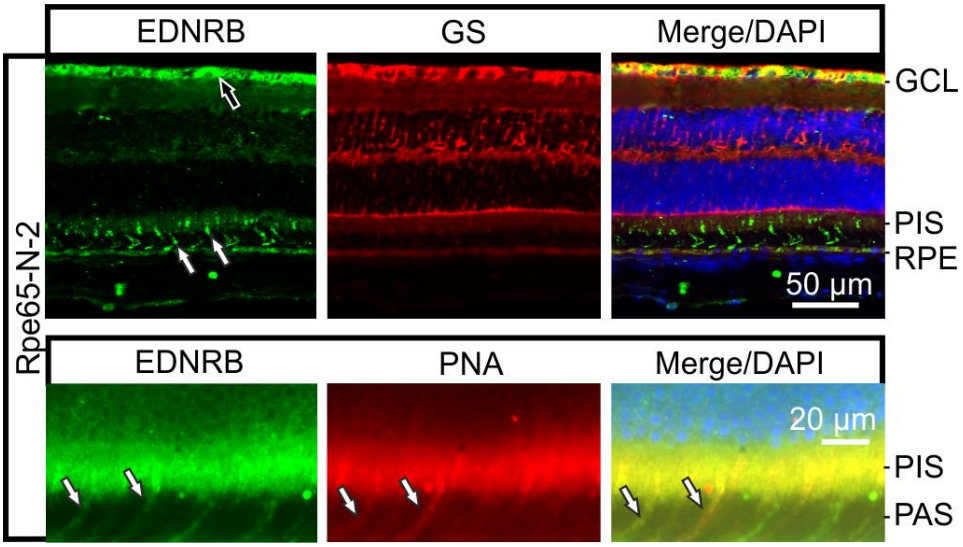

Figure 49: Immunohistochemical staining of EDNRB and co-labeling with PNA in Rpe65-Norrin-2 mice

Staining for EDNRB was more intense in Rpe65-Norrin-2 retinae than in wild-type and was additionally seen along the inner surface of the retina where it co-localized with GS. This strongly indicated its localization in Müller cell end-feet (open arrow). Staining for EDNRB was also seen in GS-negative, but PNA-positive cone photoreceptor inner and outer segments (white arrows). GCL= ganglion cell layer, PIS= photoreceptor inner segments; PAS= photoreceptor outer segments; RPE= retinal pigmented epithelium. Experiment published in (107), performed by Barbara Braunger.

So far, the data show that Norrin overexpression from the retinal pigment epithelium leads to a significant upregulation of the neuroprotective factor EDN2 and its receptor EDNRB (Figure 45). This factor is localized in the inner segments of the photoreceptors, the ganglion cell layer, the inner and outer plexiform layer and the retinal pigment epithelium. The receptor is localized on the photoreceptor inner and outer segments and the Müller glia end feet at the innermost layer of the retina. The upregulation of GFAP indicates an activation of Müller glia cells and astrocytes, most likely due to the overexpression of Norrin and its higher levels in the retina (Figure 17).

2.5.2 Correlation between Norrin induced Wnt/β-catenin activation, EDN2 upregulation and light induced apoptosis

Next, the correlation between EDN2 upregulation and Wnt/β-catenin signaling was analyzed. To this end, DKK1 was injected into the vitreous before taking the retinae for mRNA analysis. Prior to the actual experiments the influence of vitreal injections themselves on the expression levels of neuroprotective factors of interest were investigated. To this end the mRNA expression levels of *Ledgf, Edn2* and *Bdnf* were compared from sham injected (PBS) wild-types retinae and control (no injection) wild-types. The injection led to a significant increase in the expression of *Ledgf* and *Edn2* but not *Bdnf* (Figure 50). In the following inhibitor injected eyes were always compared with sham injected fellow eyes. The injection induced upregulation was therefore comparable in both eyes and detected differences are most likely due to the inhibitor.

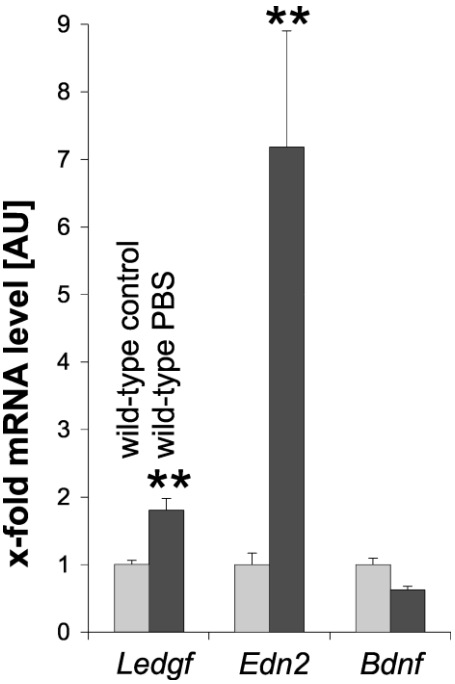

Figure 50: Influence of injections on the expression levels of *Ledgf, Edn2* and *Bdnf*
Quantitative realtime RT-PCR of wild-types control retinae (no injection) and PBS injected fellow eyes. Control: n= 3, PBS: n= 7; **p<0.01.

Wnt/β-catenin inhibition lead to a significant reduction of the *Edn2* expression in the retinae of Rpe65-Norrin-2 animals, which strongly indicated a correlation between the Norrin mediated activation of Wnt/β-catenin signaling and retinal *Edn2* upregulation (Figure 51).

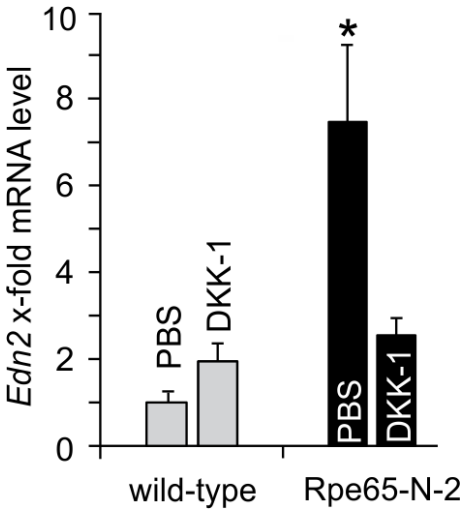

Figure 51: Wnt/β-catenin signaling and *Edn2* expression (DKK1 injections)
Quantitative real-time RT-PCR for *Edn2* mRNA in the retinae of wild-type and Rpe65-Norrin-2 mice following intravitreal injection of DKK1. The mean value obtained with RNA from PBS-injected wild-type animals was set at 1. Data is mean ± SEM, wild-type: n= 3, Rpe65-Norrin-2: n≥ 8, *p<0.05. Experiment published in (107), performed by Barbara Braunger.

Subsequently, the correlation between *Edn2* upregulation and apoptosis was analyzed. To achieve this, EDN2-signaling was inhibited prior to light exposure by using BQ788, an antagonist for endothelin receptor type B (EDNRB). BQ788 was injected into the vitreous before light exposure and the number of apoptotic (TUNEL positive) cells was investigated 30 h after light exposure. Consequently, the inhibition of EDN2 signaling led to a significant increase in the number of TUNEL positive cells in the retinae of Rpe65-Norrin-2 animals compared to the sham (5% DMSO in PBS) injected fellow eyes (Figure 52).

Taken together the obtained data so far indicate a correlation between Norrin induced Wnt/β-catenin signaling activation (Figure 19), which lead to an upregulation of EDN2 (Figure 45 and Figure 51) in the retinae of Rpe65-Norrin-2 animals, which in turn protect these animals from light induced apoptosis (Figure 52).

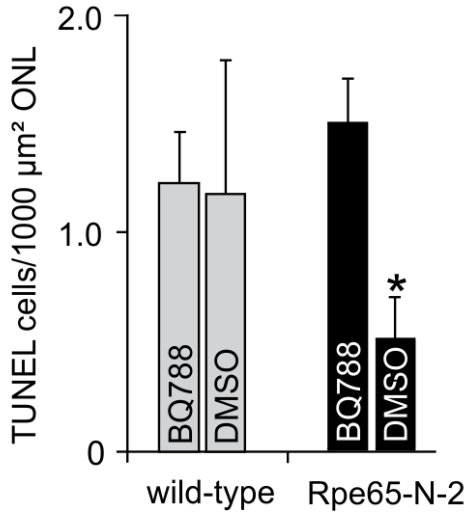

Figure 52: Light damage induced apoptotic cell death following End2 signaling inhibition (BQ788)
Quantitative TUNEL analysis, 30 h following light damage and intravitreal injection of BQ788 (left eye) or 5% DMSO in PBS (right eye, control). Data is mean ± SEM, n≥ 4, *p<0.05. Experiment published in (107), performed by Barbara Braunger.

Neuroprotective factors like LIF, EDN2 and FGF2 are well described in the context of light exposure and neuroprotection (99,100,112,113). Hence, the levels of these and other neuroprotective factors following light exposure were analyzed. Comparable to published results, a significant increase in the expression of both *Lif* and *Edn2* in wild-type retinae after light damage (Figure 53) was observed. Surprisingly, the increase in *Lif* and *Edn2* expression was significantly (p<0.05) less in light-damaged Rpe65-Norrin-2 animals (Figure 53).

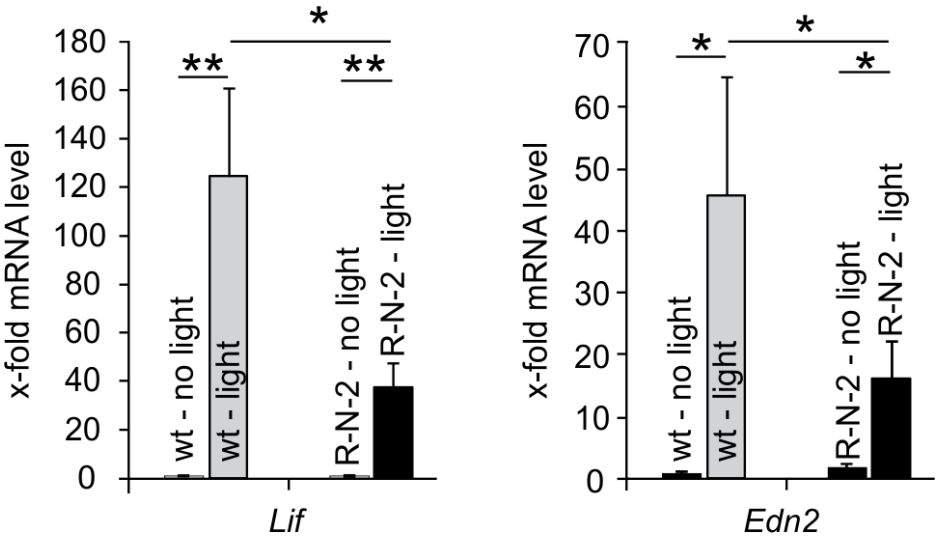

Figure 53: Expression levels of *Lif* and *Edn2* before and after light exposure.
Realtime RT-PCR for *Lif* and *Edn2* in wild-type (wt) and Rpe65-Norrin-2 (R–N-2) retinae before and 6 h after light damage. The mean value of the untreated (no light) wild-type animals was set at 1. Data is mean ± SEM, n≥ 5, *p<0.05, **p<0.01. Experiment published in (107), performed by Barbara Braunger.

GFAP, a marker for activated Müller glia cells, was significantly upregulated following light exposure in wild-types and Rpe65-Norrin-2 animals, but when comparing light exposed wild-types with light exposed Rpe65-Norrin-2 animals, Rpe65-Norrin-2 animals showed a significant lower induction of *Gfap* (Figure 54). FGF2, a marker expressed from Müller glia cells following light damage, was significantly upregulated in both wild-types and Rpe65-Norrin-2 animals following light exposure (Figure 54).

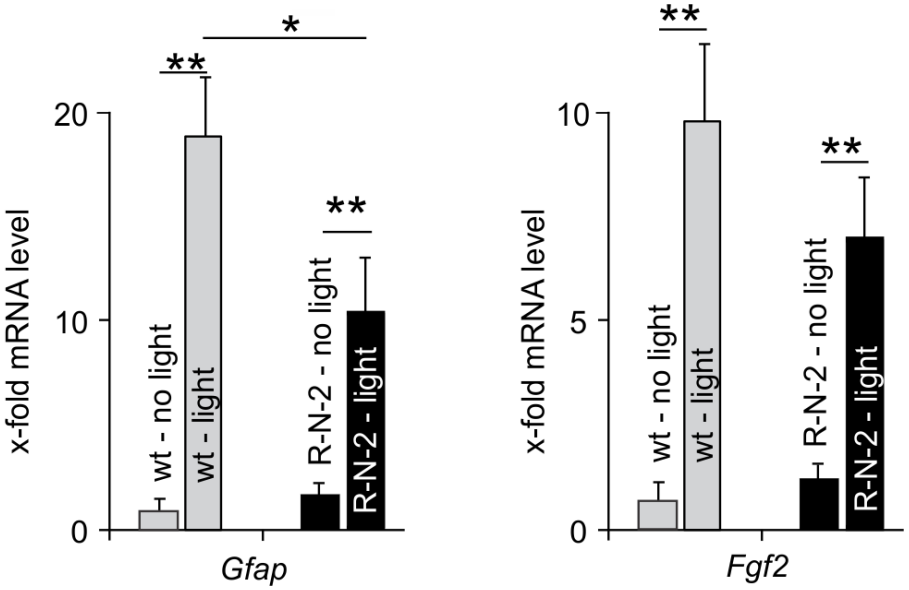

Figure 54: Expression levels of *Gfap* and *Fgf2* before and after light exposure
Realtime RT-PCR for *Gfap* and *Fgf2* in wild-type (wt) and Rpe65-Norrin-2 (R–N-2) retinae before and 6 h after light damage. Mean ± SEM, n≥ 5, *p<0.05, **p<0.01. The mean value from untreated (no light) wild-type animals was set at 1. Experiment published in (107), performed by Barbara Braunger.

When other neuroprotective factors like *Cntf* and *Pedgf* were analyzed after light exposure, there were no differences between Rpe65-Norrin-2 and wild-types. (*Cntf*: wild-types: 1 ± 0.31, n= 6, Rpe65-Norrin-2: 0.71 ± 0.15, n= 5, p= 0.50; *Pedgf*: wild-types: 1 ± 0.45, n= 8, Rpe65-Norrin-2: 0.27 ± 0.04, n = 5, p = 0.27 (mean ± SEM)).

2.5.3 Brain-derived neurotrophic factor and the protective effects of Norrin

However, when expression levels of *Bdnf* and *Ledgf* were investigated, significant differences in the amounts of mRNA between light-damaged wild-type and transgenic mice were detected. *Bdnf* and *Ledgf* levels were significantly lower (p<0.01) in light-damaged wild-type mice as compared to untreated wild-type mice, while the expression of *Bdnf* was significantly higher (p<0.05) in light-damaged Rpe65-Norrin-2 mice as compared to untreated Rpe65-Norrin-2 mice (Figure 55). These differences in both *Bdnf* and *Ledgf* levels were most probably due to a stabilization or upregulation respectively of their mRNA in Rpe65-Norrin-2 animals after light exposure.

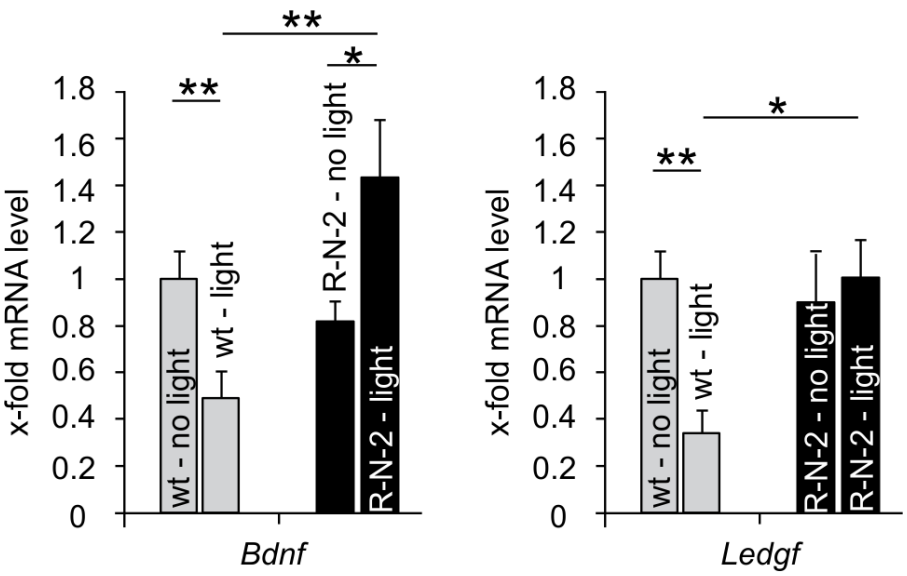

Figure 55: Expression levels of *Bdnf* and *Ledgf* before and after light exposure
Realtime RT-PCR for *Bdnf* and *Ledgf* in wild-type (wt) and Rpe65-Norrin-2 (R–N-2) retinae before and 6 h after light damage. Mean±SEM, n≥ 5, *p<0.05, **p<0.01. The mean value from untreated (no light) wild-type animals was set at 1. Experiment published in (107), performed by Barbara Braunger.

This data point was of high interest, because Norrin overexpression in Rpe65-Norrin-2 animals led to an upregulation of the neuroprotective factor *Bdnf* (Figure 55) without involving the upregulation of the neuroprotective key factors *Lif* or *Fgf2* (Figure 53), factors that are described to consitute an instrinsic protective signaling mechanism in the mouse retina following light exposure (100).

In the following we focused on the neuroprotective factor BDNF. This factor is expressed in retinal ganglion cells as well as transported retrograde from the superior colliculus back into the retina. The protein level of BDNF in Rpe65-Norrin-2 and wild-type retinae was investigated using western blot analysis 6h after light exposure. The densitometric analysis showed a significant upregulation of BDNF in Rpe65-Norrin-2 animals compared to wild-types following light exposure (Figure 56).

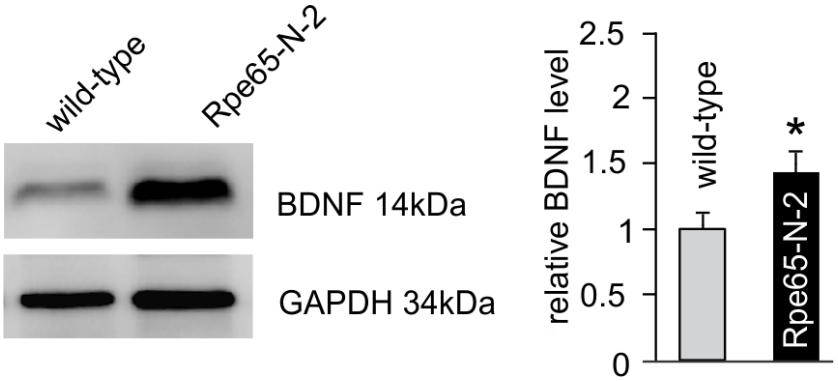

Figure 56: Western Blot analysis of BDNF protein levels following light exposure
BDNF (14 kDa) Western blot analysis and relative densitometry in wild-type and Rpe65-Norrin-2 (Rpe65-N-2) retinae 6 h after light damage. Data is mean ± SEM, n≥ 7, *p<0.05. Experiment published in (107), performed by Barbara Braunger.

Next, immunohistochemical staining for BDNF was performed to assay the protein localization. Wild-type mice showed no specific signal in their retinae 6 h after light exposure, while light-damaged Rpe65-Norrin-2 mice revealed a positive immunoreactivity for BDNF throughout the entire retina, which was especially intense on the retinal surface (Figure 57, upper panel). Double labeling experiments with antibodies against either BDNF and GFAP (astrocytes, activated Müller glia), or BDNF and GS (Müller glia) indicated that BDNF immunoreactivity in the innermost layer of the retina was localized to glia cells (Figure 57, lower two panels).

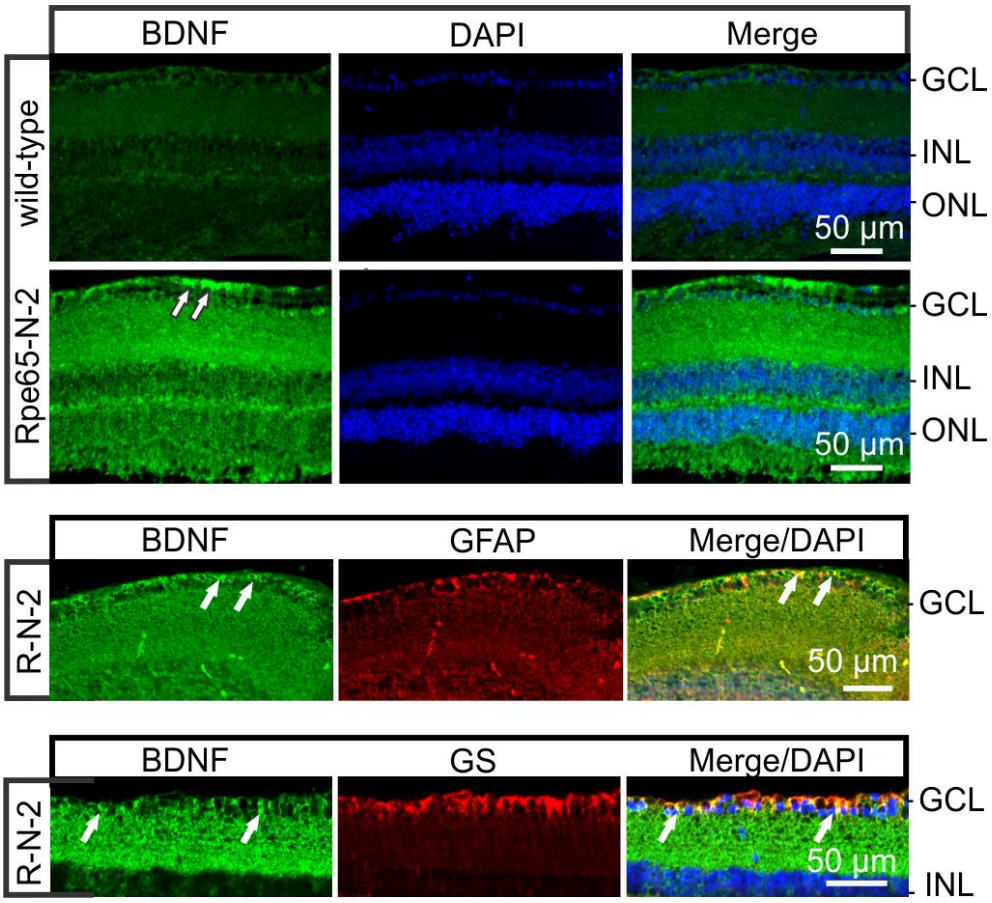

Figure 57: Immunohistochemical staining of BDNF after light damage
Immunohistochemistry of BDNF (green) 6 h after light damage. Nuclei are stained with DAPI (blue). No immunoreactivity for BDNF was observed in the wild-type (top row) animals. However, the Rpe-65-Norrin-2 mice showed immunolabeling throughout the entire retina (second row), which was especially intense on the retinal surface (arrows). Double labeling of Rpe65-N-2 (R–N-2) retinae with antibodies against BDNF and GFAP, or BDNF and GS showed partial co-localization (arrows) and indicates that BDNF immunoreactivity localizes to glial cells. GCL= ganglion cell layer; INL= inner nuclear layer; ONL= outer nuclear layer. Experiment published in (107), performed by Barbara Braunger.

To analyze if there is a possible underlying correlation between the higher amounts of BDNF in light-damaged Rpe65-Norrin-2 mice and the increase in Wnt/β-catenin and EDN2 signaling, mice were treated with intravitreal injections of DKK1 (inhibition of Wnt/β-catenin signaling), or BQ788 (inhibition of EDN2 signaling), prior to light damage. In light damaged Rpe65-Norrin-2 mice both injections caused a significant lower *Bdnf* expression, while no differences were observed in injected

and light-damaged wild-type mice (Figure 58). Concerning the retinal expression level of *Ledgf*, neither the injection of DKK1, nor of BQ788 caused any significant differences (Figure 58).

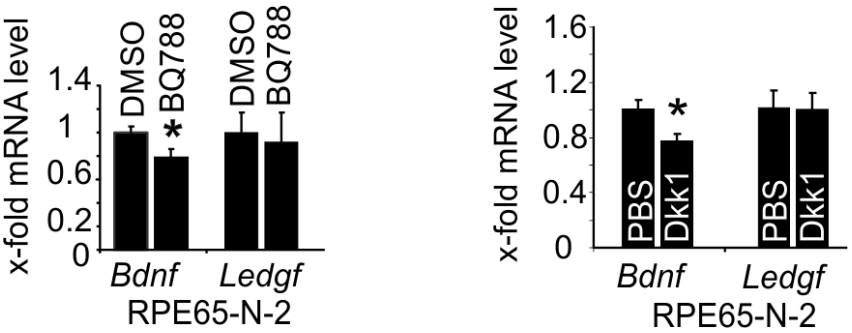

Figure 58: *Bdnf* and *Ledgf* in the context of Wnt/β-catenin and EDN2 signaling.
Left: Quantitative real-time RT-PCR of mRNA for *Bdnf* and *Ledgf* in Rpe65-Norrin-2 retinae 6 h after light exposure and intravitreal injection of BQ788 (left eye) or DMSO (right eye). Data is mean ± SEM, n= 8, *p<0.01. **Right:** Quantitative real-time RT-PCR of mRNA for *Bdnf* and *Ledgf* in Rpe65-Norrin-2 retinae 6 h after light exposure and intravitreal injection of DKK1 (left eye) or PBS (right eye). Data is mean ± SEM, n= 16, * p<0.05. Experiment published in (107), performed by Barbara Braunger.

Receptor-binding of BDNF activates the PI3K-Akt signaling pathway to mediate its neuroprotective characteristics. Therefore, the amounts of Akt/phospho-Akt (pAkt) were investigated using Western blot analysis of Rpe65-Norrin-2 retinae and wild-types after light-damage. Densitometric analysis showed an almost 4-fold ($p<0.05$) higher amount of phosphorylated Akt in Rpe65-Norrin-2 animals compared to wild-type littermates after light exposure (Figure 59).

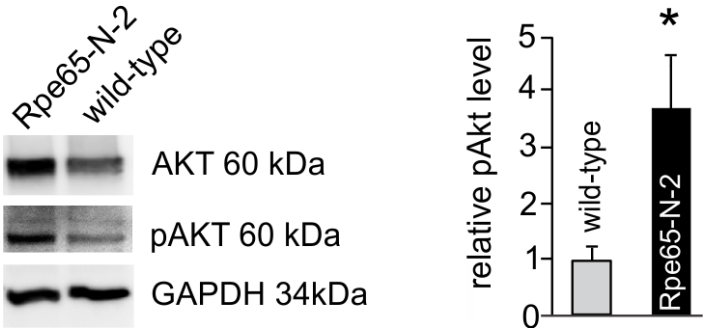

Figure 59: Akt and pAkt protein levels following light exposure.
Left: Western blot analysis for Akt and pAKT of wild-type and Rpe65-Norrin-2 retinae 6 h after light damage. **Right:** Relative densitometry for pAKT levels. Data is mean ± SEM, n≥ 7, * p<0.05. Experiment published in (107), performed by Barbara Braunger.

One possible explanation for the elevated BDNF protein level in Rpe65-Norrin-2 animals might be a reduced degradation of this factor. A first hint towards this was the significant reduced expression of *Smurf1*, an ubiquitin ligase, in untreated Rpe65-Norrin-2 animals (Figure 60) as well as in light damaged animals (data not shown).

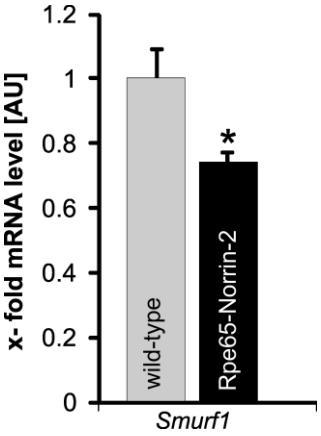

Figure 60: *Smurf1* expression levels in Rpe65-Norrin-2 animals
Quantitative realtime RT-PCR for *Smurf1* in retinae of untreated Rpe65-Norrin-2 animals and wild-types. Data is mean ± SEM, n> 5, p=0.04.

In summary, the analyzes of the neuroprotective factors in the retina before and after light exposure strongly indicated that the Norrin mediated neuroprotective effect was most likely due to an constitutive upregulation of EDN2 (see Figure 45), which resulted in an upregulation or stabilization (see Figure 55) of the neuroprotective factors *Bdnf* and *Ledgf* in the light damaged retinae.

3 Discussion

3.1 Norrin in the context of neuroprotection

The hypothesis that Norrin might have neuroprotective effects originated from the observation that Norrin knockout mice *Ndp*$^{y/-}$ had a reduction in retinal ganglion cell number (74) and the fact that mice that overexpressed Norrin in the lens (Nor-29) had more retinal ganglion cells and a higher number of cells in the developing retina (73). An *in vivo* study showed that intravitreal injections of recombinant human (rh) Norrin were neuroprotective for retinal ganglion cells, using the NMDA induced excitotoxic cell death model (80). This study showed that the neuroprotective effects were mediated through Wnt/β-catenin signaling, followed by an upregulation of neuroprotective factors (80).

The aim of the current study was to investigate, if a constitutive overexpression of Norrin would have neuroprotective effects on photoreceptor cells in the light damage model.

3.1.1 Characterization and morphology of Rpe65-Norrin-2 mice

We obtained 2 transgenic founder lines, but only Rpe65-Norrin-2 animals did show a positive signal in Northern and Southern Blot analysis. Despite the overexpression of Norrin in the Rpe65-Norrin-2 line, these transgenic animals did not show an obvious phenotype. In contrast, another transgenic mouse line, which overexpresses Norrin in the lens (Nor-29), had a significantly higher number of retinal ganglion cells and cell nuclei of neurons in the developing retina and a persistence of the hyaloid artery. This discrepancy is most likely explained through the different developmental promoter activation and their efficiency and/or the localization of the overexpression. The very strong, lens specific βB1-Crystallin promoter induces expression at E12.5 (114,115), while the moderate strong Rpe65 promoter initiates expression not before E18 (116–118). The differences in promoter efficiency became obvious, when samples from the lens specific βB1-Crystallin Norrin animals were used as positive control in Northern Blot analysis of the Rpe65-Norrin-2 eyes, and the Northern blot showed exactly this difference in Norrin RNA expression that is driven either through Rpe65 or βB1-Crystallin promoter. The higher number of retinal neurons in Nor-29 animals was clearly demonstrated to be due to an increased neuronal proliferation in the retina during embryonic development (E14.5) (73), a time point, when Norrin overexpression driven by the RPE65 promoter in Rpe65-Norrin-2 animals is not active yet. *In vitro* experiments showed that recombinant human (rh) Norrin added to RGC-5 (retinal ganglion cells) cell cultures resulted in a higher number of surviving cells (20%) indicating a more direct effect of Norrin on cell survival (80). The fact that Rpe65-Norrin-2 mice did not show an alteration in neuronal cell number might additionally be due to a different sensitivity to Norrin of photoreceptor cells in contrast to retinal ganglion cells, since the

Norrin secretion from the RPE is mostly localized around the photoreceptor cells reaching only to the outer plexiform layer.

Taken together, the characterization of the Rpe65-Norrin-2 mice demonstrated a successful overexpression of Norrin and its secretion from the RPE into the retina. The morphology of these animals was not altered.

3.1.2 Norrin and light exposure

Light damage experiments were used to induce cell death specifically to photoreceptors (97). We used cool white light at an intensity of 5000 lux for a maximum duration of 1 hour. These damage conditions were defined in dose-effect studies at the very beginning of this thesis (data not shown). In comparison to the light regimes used in other laboratories (illumination up to 24 h (122), intensities up to 15000 lux (37)), ours is rather mild. However, we observed an intense signal increase in the TUNEL labeling and strong effects on the retinal structure. The effects are more pronounced compared to light damages using e.g. another albino strain, the Balb/c mice. Different susceptibility of mouse strains to light exposure is well reported (123), but to our understanding, the heterozygous rd1 mutation (originating from the FVB/N) present in our F1 generation of FVB/N;CD1 animals might additionally boost the effect.

Following light exposure, the transgenic Norrin overexpressing animals showed a thicker outer nuclear layer, less apoptosis following light exposure, a better preserved retinal function in the ERG analysis and less autofluorescence in SLO in vivo imaging, which correlates with retinal degeneration. Taken together, the results strongly indicate a neuroprotective role of Norrin on photoreceptor cells.

Similar observations have been made for retinal ganglion cells using the model of NMDA-induced excitotoxic cell death. Here they showed protective effects of intravitreal injections with rh Norrin in combination with NMDA (80). In our damage model the neuroprotective effect in the transgenic animals was most likely due to the constitutive overexpression of the Norrin and its secretion into the retina.

Yet, a minor influence of the impaired visual cycle cannot be entirely excluded. However, this contribution seems rather unlikely, since ERG analysis of the untreated animals did not reveal any significant differences between Rpe65-Norrin-2 and wild-types. ERG responses are very sensitive to impairments of the visual cycle, hence ERG is used to monitor the effect of visual cycle modification that are now for the first time tested in a pharmacological study (124,125). Briefly, in this study ACU-4429 (Emixustat), a small-molecule visual cycle modulator that inhibits the RPE65 isomerase complex, prevented the accumulation of A2E (N-retinyledin-N-retinylethanolamin) in a mouse model of retinal degeneration (124). A2E is a major fluorophore component of lipofuscin, which represent a

biomarker for cellular aging and is of interest especially in the context of age related macular degeneration (126,127). Taken together, we did not observe significant ERG alterations in our untreated animals, indicating that the visual cycle is not modified to an extent of any greater biological relevance; hence a contribution of this to the results of our light damage experiments seems rather unlikely.

In summary, the transgenic overexpression of Norrin attenuated light induced photoreceptor damage, strongly indicating a neuroprotective role of Norrin for photoreceptor cells.

3.1.3 Norrin, Wnt/β-catenin and Edn2 signaling

Norrin activates Wnt/β-catenin signaling through specific binding to the Frizzled4 receptor (Fz4) (84). In the retina, the Fz4 receptor is expressed in all layers, but most prominently in the outer nuclear layer (ONL) and the inner segments of the photoreceptors (128). In Western blot analysis of transgenic animals, we observed significant elevated levels of retinal β-catenin and confirmed the activation of retinal Wnt/β-catenin signaling in all retinal layers using TOPGAL reporter mice. Wnt/β-catenin was shown to have neuroprotective effects (129). Therefore, the continuously active Wnt/β-catenin signaling in Rpe65-Norrin-2 animals is likely an essential component of Norrin's neuroprotective effects on photoreceptor survival. Dkk1 injections which successfully reduced β-catenin levels in the retina, resulting in an effective inhibition of the retinal Wnt/β-catenin pathway, markedly reduced the protective effects of the transgenic animals in the light damage experiments.

Untreated Rpe65-Norrin-2 animals showed a significant upregulation of the Müller cell activation marker *Gfap*, the neuroprotective factor *Edn2* and its receptor *Ednrb*. GFAP is expressed in astrocytes and Müller glia cells when they become reactive. Double labeling experiments with the Müller glia marker glutamine synthetase (GS) showed that the GFAP signal is localized in astrocytes and Müller glia cells. In Müller cells it is most pronounced in their end feet at the inner limiting membrane. *Edn2* is upregulated after light damage, as well as in mouse models of inherited photoreceptor degeneration and appears to act as a stress signal (99,100). RNA *in situ* hybridization revealed its primarily expression in photoreceptors cells (99). Immunohistochemical staining for EDN2 in our untreated wild-types showed a discrete immunolabeling at the ganglion cell layer (RGC) and in the retinal pigment epithelium (RPE), where the published *in situ* hybridization did not show any reactivity in untreated animals. In Rpe65-Norrin-2 animals, the immunolabeling was particularly strong in the ganglion cell layer with an additional intense staining of the photoreceptor inner segments and in the retinal pigment epithelium and a patchy immunostaining in the outer and inner plexiform layer (OPL/IPL). One possible explanation for the differences between the *in situ* hybridization and immunohistochemical staining is that the hybridization targets a specific transcript,

while immunohistochemical staining detects the protein's localization in the cell or tissue. The mRNA might be very low expressed in this cell type and/or the protein could have a very long half-life.

The higher amounts of EDN2 in Rpe65-Norrin-2 mice are most likely mediated by the induction of continuous Wnt/β-catenin signaling, since they are reduced to levels seen in wild-type retinae after treatment with DKK1. Moreover, blocking of EDN2 signaling with an EDNRB inhibitor (BQ788) diminished the protective effects of Norrin.

One of the various functions of Müller glia cells is the secretion of neuroprotective factors (see 1.1.1.4) (19). In the context of light damage it has been proposed that the release of LIF from Müller glia cells is the essential stimulus for the induction of EDN2 in photoreceptors, as experiments with *Lif* knockout mice (*Lif*$^{-/-}$) did not show an upregulation of *Edn2* in the context of photoreceptor degeneration (100).

Since the constitutive increase in retinal Norrin levels did not result in a significant upregulation of *Lif* following light exposure, the Norrin-Wnt/β-catenin induced continuous higher expression of *Edn2* very likely does not require Müller cell-derived LIF. Our immunohistochemical staining indicated that EDNRB, the primary retinal receptor of EDN2, is mostly expressed in the inner segments of cone photoreceptors and additionally in the Müller cell end feet in Rpe65-Norrin-2 mice. Experiments with intravitreal BQ3020 injections, an endothelin receptor type B agonist, in wild-type mice showed that Endothelin signaling induces the synthesis of molecules that prevent or delay the degeneration of photoreceptors (100).

As shown in the current thesis, the constitutively elevated EDN2 and EDNRB levels in Rpe65-Norrin-2 mice might promote protective effects in a similar manner e.g. through Müller glia cells. The constitutive upregulation of GFAP, a marker for reactive Müller glia (19), and the localization of EDNRB on Müller glia end feet further support this hypothesis. Another indication for this is the significant lower neuroprotective effect of the Norrin Wnt/β-catenin/EDN2-signaling in the context of light exposure, when injecting the EDNRB inhibitor BQ788 several hours prior to light damage.

3.1.4 Norrin neuroprotection and BDNF after light exposure

Upon light exposure, Rpe65-Norrin-2 animals showed a significant mRNA upregulation of *Bdnf* and *Ledgf*. Both factors have neuroprotective effects (130–135). LEDGF was initially discovered in lens epithelial cells but is also expressed in neuronal tissues (136). BDNF is detected in the retinal ganglion cells, in Müller glia cells and cells of the inner nuclear layer (80,107,137).

The expression of other neuroprotective factors released from Müller glia following light exposure such as *Cntf* and *Fgf2* was not different in Rpe65-Norrin-2 mice than in wild-type littermates.

It is most likely that BDNF is the factor, which eventually mediates the neuroprotective effects of constitutively elevated Norrin-Wnt/β-catenin-EDN2-signaling and which is induced in Müller glia cells to rescue photoreceptors from light-induced damage. Experiments, with inhibition of either Wnt/β-catenin signaling (DKK1), or EDN2 signaling (BQ788) showed that retinal *Bdnf* expression relies upon these two pathways, strongly indicating that BDNF is a downstream target of these pathways. Immunohistochemical staining in wild-types showed no specific BDNF signal in their retinae 6 h after light exposure. In contrast Rpe65-Norrin-2 mice revealed a positive immunoreactivity for BDNF throughout the entire retina, which was especially intense on top of the retinal surface. Double labeling experiments with antibodies against either BDNF or GFAP (astrocytes, activated Müller glia), or BDNF and GS (Müller glia cells), indicated that the BDNF immunoreactivity in the innermost layer of the retina was localized to glia cells, which are most likely responsible for the initiation of further neuroprotective effects.

It is of interest to note that the amounts of mRNA for *Bdnf* were diminished in light damaged wild-type retinae when compared to untreated wild-type animals, but *Bdnf* levels were significantly increased in light-damaged transgenic mice. It is tempting to speculate that the constitutive overexpression of Norrin in Rpe65–Norrin-2 mice does not only affect the transcription of *Bdnf* mRNA, but also its stability on protein level. To venture a guess, Norrin might interact with the proteasomal machinery which might explain a potential stabilization of BDNF following light exposure. The significant reduction of *Smurf1*, an ubiquitin ligase 3, in Rpe65-Norrin-2 animals supports this assumption. However, the *Smurf1* downregulation is very likely the cellular response of the constitutively elevated Norrin levels in the retina, since Norrin inhibits BMP signaling by acting as an antagonist of BMP2 and 4 (89,90). Smurf1 ubiquitin ligase, together with inhibitory SMAD 6/7, forms a negative feedback loop for the attenuation of bone morphogenic proteins (BMP) signals by downregulating BMP-receptor and signaling molecules (140). Another observation heading in the same direction are the elevated β-catenin levels in Rpe65-Norrin-2 animals. β-catenin is ubiquitinylated through the E3-ubiquitin-ligase β-Trcp (β-transducin repeat containing) and then degraded by the proteasome. Therefore, the E3-ubiquitin-ligase β-Trcp might also be involved in this effect of Norrin. There are numerous ubiquitin ligases in a cell, so the downreguation of other E3 ligases in these animals is very well possible, which might lead to a further stabilization of proteins like β-catenin and BDNF.

After BDNF binding to its TrkB receptor (138), the receptor dimerizes and autophosphorylates the cytoplasmatic kinase domain. Briefly, this results in an activation of Ras, which then triggers PI3K, p38MAPK and c-Raf/ERK pathways (139). The phosphatidylinositol 3-kinase (PI3K) pathway leads to the activation of Akt through its phosphorylation. Activated Akt in turn phosphorylates and inhibits

pro-apoptotic Bcl-2 family members like BAD, BAX or Caspase-9. Following light exposure, Rpe65-Norrin-2 animals showed elevated levels of phosphorylated Akt, highlighting an activation of Akt signaling in the transgenic animals. The activation of Akt signaling, a major pathway mediating neuronal survival, following receptor-binding of BDNF (141) in retinae of Norrin overexpressing mice is consistent with the assumption that BDNF mediates the neuroprotective effects in transgenic animals. BDNF binds to TrkB receptor (138). In mouse photoreceptors, the TrkB receptor is not expressed. Its expression had been investigated in close detail using single cell RT-PCR (142), immunohistochemical staining (143,144), or by assessing TrkB promoter activity with reporter genes (145). Different results have been reported for immunohistochemical TrkB staining in the rat retina. In contrast to murine photoreceptors, rat green–red sensitive cones are immunoreactive for TrkB (146,147). Thus, it appears to be unlikely that BDNF directly influences photoreceptor survival in Rpe65-Norrin-2 animals via binding to its receptor TrkB. This strongly argues for an important role of the TrkB carrying Müller glia cells in mediating the protective effects of BDNF on photoreceptor survival. Observations that intravitreal injections of BDNF activate intracellular signaling pathways in Müller cells, further support this hypothesis (142,144). Either BDNF acts on Müller glia cells in an autocrine manner, or BDNF acts paracrine on certain retinal cell types, other than the photoreceptors, to induce the release of a so far unknown neuroprotective molecule that promotes photoreceptor survival. The deletion of TrkB in Müller glia inhibited the protective effects of BDNF on photoreceptor degeneration, which supports an autocrine mechanism (143).

To sum up, the elevated BDNF levels are very likely involved in the photoreceptor protection following light exposure in Norrin overexpressing mice. Yet other, currently unknown signaling factors, which are for example released from Müller glia cells, might play a role, as well.

3.2 Norrin in the context of angiogenesis

3.2.1 Vascular phenotype of Rpe65-Norrin-2 animals

Norrin has angiogenic effects and is essential for retinal angiogenesis. The transgenic overexpression of Norrin in the lens (Nor-29) caused a persistence of the hyaloid vasculature and tunica vasculosa lentis during development (73).

The hyaloid vessel system is a compact, temporary intraocular blood circulatory system (150). It undergoes progressive and nearly complete regression during the latest stage of ocular development when the lens, the vitreous and the retina mature (150). When the vasculature of Rpe65-Norrin-2 mice was analyzed, we did not observe a persistence of the hyaloid vasculature or tunica vasculosa lentis. The difference to the Nor-29 animals can again be explained most likely through the different localization of the Norrin overexpression (lens versus retinal pigment epithelium) and the more moderate Norrin expression from the Rpe65 promoter in Rpe65-Norrin-2 animals. In addition, the immunohistochemical staining in Rpe65-Norrin-2 animals showed that the Norrin secretion reached only to the outer plexiform layer and thus may not reach the vitreous where the hyaloid artery is situated. The intraretinal vasculature in both animal models, Nor-29 and Rpe65-Norrin-2, is normal. The fact that Rpe65-Norrin-2 animals showed such a normal vascular morphology made them an even more promising model to investigate the influence of Norrin on angiogenesis, because the initial situation between transgenic and wild-type animals are absolutely comparable, suggesting that possible effects during the experiments are most likely due to Norrin and not due to a different vascular situation from the starting.

The choriocapillaris is the adjacent vascular bed to the RPE, the cell population in which Norrin is overexpressed in the Rpe65-Norrin-2 animals. Therefore this is a comparable situation to the Norrin overexpression in the lens and its effect on the hyaloid artery and tunica vasculosa lentis. However, when the endothelium of the choriocapillaris was labeled with Plasmalemma vesicle-associated protein (PLVAP), a marker for fenestrated capillaries (151), no differences were detected between Rpe65-Norrin-2 mice and wild-type littermates. There are several possible explanations for this observation: first, in contrast to the hayloid vasculature the choriocapillaris does not degenerate during development, meaning that if Norrin has anti-degenerative effects on vascular cells, this effect will not be seen in an non-degenerative situation like the choriocapillaris. Second, the promoter activity of the RPE65 starts in late embryonic development and Norrin might therefore have other effects on choroidal vascular cells than on hyaloidal vascular cells that are under the influence of Norrin as early as E12.5. Third, it might be possible that Norrin is not secreted in the same manner in the direction of the choriocapillaris than it is secreted into the retina, a finding that is supported by our immunohistochemical staining.

3.2.2 Norrin in the ROP model

To further validate the protective effects of Norrin in the context of angiogenesis, the model of retinopathy of prematurity (ROP) was used in the current thesis. This model is a well-established damage model (see 1.3.1) (152) that was used to induce vascular damage in transgenic Norrin overexpressing mice (βB1-Crystallin Norrin and Rpe65-Norrin-2) and wild-type littermates. Norrin overexpression protects mice from oxygen induced vaso-obliteration and this effect is mediated through the Wnt/β-catenin pathway. The influence upon vaso-obliteration was more pronounced in the βB1-Crystallin Norrin mice than it was in the Rpe65-Norrin-2 mice. These differences can be explained most likely due to the stronger expression of Norrin in the lens driven βB1-promoter compared to the moderate expressing from the Rpe65 promoter.

Moreover, Norrin was able to induce the re-growth of retinal capillaries and the formation of the intra-retinal vasculature after oxygen mediated vascular damage. Again the effect was more prominent in the βB1-Norrin mice than in Rpe65-Norrin-2 mice. Again, most likely due to the stronger expression of Norrin in the lens driven βB1-promoter compared to the moderate expressing from the Rpe65 promoter.

Additionally, Norrin prevented the development of preretinal tufts (neovascularization) (106). This reduction of neovascularization following ROP might be a consequence of the greater density of intravitreal vessels in a smaller eye (βB1-Norrin) and the Norrin induced increase in the number of intra-retinal capillaries. This in turn might lead to less hypoxia in the tissue and to a reduced expression of hypoxia induced angiogenic factors that stimulate neovascularization. But it is also possible that Norrin directly influences the direction of vessel growth. Experiments with $Ndp^{y/-}$/Nor-29 mice support this hypothesis, since the ectopic Norrin expression restored normal intraretinal capillarization in $Ndp^{y/-}$ mice that normally lack intraretinal vasculature (73).

In summary, Norrin is not only a protein that is primarily involved in the formation of the final capillary architecture in the retina but also reduced the ROP induced vaso-obliteration and prevented the formation of preretinal tufts.

3.3 Future directions

It is worthwhile to mention, that overexpression of Norrin in the retinal pigment epithelium, concomitant with an activation of Wnt/β-catenin pathway in the retina and constitutive elevated retinal EDN2 levels did not result in any gross phenotypic changes. Neither Norrin, nor Frizzled4 deficient mice show morphological changes of their photoreceptors, indicating that these factors are not essential for photoreceptor development, or their maintenance (71,73). Since photoreceptors express high amounts of Frizzled4 (129) and Norrin is continuously expressed even in adulthood (71), both molecules may be part of a neuroprotective pathway in the retina, although they are not required for photoreceptor maintenance. Taken together it is tempting to speculate that this pathway and Norrin could be used to delay or prevent inherited photoreceptor degeneration.

4 Summary – Zusammenfassung

4.1 Summary

Norrin is a secreted protein that binds to the frizzled-4 receptor to activate the canonical Wnt/β-catenin signaling pathway. Norrin is critical for normal vascular development in the retina. In addition, Norrin has neuroprotective properties.

The aim of the current thesis was to investigate if Norrin has neuroprotective effects on photoreceptor survival following light exposure, if this neuroprotective effect is independent of its angiogenic component and which molecular mechanisms mediate its neuroprotective properties.

To this end, transgenic mice were generated with a cell specific overexpression of Norrin in the retinal pigment epithelium (RPE). The overexpression led to a secretion of Norrin into the retina and subsequently the activation of the Wnt/β-catenin signaling pathway. The transgenic animals did not show obvious alterations in phenotype and retinal function. However, transgenic animals showed less photoreceptor vulnerability after light induced photoreceptor apoptosis. The neuroprotective effect of Norrin is most likely mediated through the Wnt/β-catenin signaling pathway, since intravitreal injections of the Wnt/β-catenin signaling inhibitor, Dickkopf1 (Dkk1) did reduce the neuroprotective effect significantly. Our data further indicate that endothelin2, which is expressed to a higher amount in transgenic animals, is involved in these neuroprotective effects, too. Intravitreal injections of an inhibitor for endothelin signaling (BQ788) did reduce the neuroprotective effect in the transgenic animals as well. Most likely, Wnt/β-catenin and endothelin2 influence the synthesis of brain derived neurotrophic factor (BDNF), whose mRNA expression was significantly reduced after intravitreal injections using both inhibitors either Dkk1 (Wnt/β-catenin pathway) or BQ788 (Endothelin signaling). Furthermore, transgenic animals showed an activation of the Akt pathway (pAkt), a signaling pathway that is activated through BDNF.

In conclusion, constitutive elevated Norrin levels in the retina protect photoreceptors from light damage, an effect that involves Wnt/β-catenin/EDN2-signaling and results in higher amounts of BDNF and pAkt in light damaged retinae, which might mediate the observed neuroprotective effects.

4.2 Zusammenfassung

Norrin ist ein sezerniertes Signalprotein, das über eine Bindung an den Frizzled-4 Rezeptor den kanonischen Wnt/β-catenin Signalweg aktiviert. Während der Entwicklung ist Norrin essentiell für die Ausbildung eines intraretinalen Kapillargebiets in der Netzhaut. Weiterhin gibt es Hinweise für eine direkte neuroprotektive Wirkung von Norrin.

Ziel der vorliegenden Doktorarbeit war es, zu untersuchen, ob Norrin Photorezeptoren vor einem experimentellen Schaden schützen kann, ob diese neuroprotektive Wirkung unabhängig von seiner angiogenen Wirkung ist und welche molekularen Mechanismen daran beteiligt sind.

Dazu wurden transgene Mäuse generiert mit einer Zell-spezifischen Überexpression von Norrin im retinalen Pigmentepithel. Diese Überexpression führte zu einer Sekretion von Norrin in die Netzhaut und zu einer Aktivierung des kanonischen Wnt/β-catenin Signalwegs. Bei den trangenen Tieren fanden sich keine offensichtlichen Veränderungen in Struktur und Funktion der Netzhaut. Nach einem experimentellen Lichtschaden der Photorezeptoren zeigte sich bei den transgenen Tieren ein deutlicher Schutz der Photorezeptoren vor einem apoptotischen Zelltod nach Lichtschaden. Diese neuroprotektive Wirkung von Norrin wird wahrscheinlich durch den Wnt/β-catenin Signalweg vermittelt, da eine intravitreale Injektion mit dem Inhibitor des Wnt/β-catenin Signalwegs, Dickkopf1 (Dkk1), den protektiven Effekt von Norrin aufhob. Weiterhin deuten unsere Daten darauf hin, dass auch Endothelin2, welches in der Netzhaut transgener Tiere in größeren Mengen nachweisbar war, an der neuroprotektiven Funktion von Norrin beteiligt ist. Die intravitreale Injektion des Endothelin2-Inhibitors BQ788 führte ebenfalls zu einer Aufhebung des neuroprotektiven Effektes von Norrin. Vermutlich wirkt Wnt/β-catenin und Endothelin2 auf die Synthese von brain derived neurotrophic factor (BDNF), dessen mRNA Expression nach Gabe von Dkk1 oder BQ788 signifikant reduziert war. Weiterhin zeigten transgene Tiere eine Aktivierung des Akt Signalwegs (pAkt), der über brain derived neurotrophic factor aktiviert wird.

Zusammenfassend kann gesagt werden, dass ein konstitutiv erhöhter Norrinspiegel in der Netzhaut Photorezeptoren vor einem Schaden schützt. An diesem neuroprotektiven Effekt sind der Wnt/β-catenin/Endothelin2- Signalweg beteiligt, welche eine Erhöhung von BDNF bedingen und zu einer Aktivierung des Akt Signalwegs (pAkt) führt.

5 Material and methods

5.1 Methods

5.1.1 Animal models.

All procedures conformed to the tenets of the National Institutes of Health Guidelines on the Care and Use of Animals in Research, the EU Directive 2010/63/E, and the Uniform Requirements for manuscripts submitted to Biomedical journals. All mice were kept in cyclic light (12 h on/12 h off) with lights on at 7 am and a light intensity of approximately 400 lux. The mice had access to food and water ad libitum.

5.1.1.1 Rpe65-Norrin-2 mice

Rpe65-Norrin mice were generated as described previously (153). These mice express ectoptic Norrin in the retinal pigment epithelium (RPE) under the control of the RPE specific promoter RPE65 (116). The animals were bred on a mixed FVB/N × CD1 background (F1). They were albino and homozygous for the L450 variant of RPE65 (36).

Figure 61: Schematic of the Rpe65-Norrin construct

5.1.1.2 βB1-Crystallin Norrin mice

Transgenic βB1-Crystallin Norrin mice were generated as described previously (73). These animals express ectoptic Norrin in the lens under the control of the lens specific βB1-crystallin promoter (114). The mice were bred in a FVB-N background.

Figure 62: Schematic of the βB1-Crystallin Norrin construct

5.1.1.3 Wnt-Reportermice: TOPGAL mice

TOPGAL mice were purchased from Jackson Laboratories (http://jaxmice.jax.org, strain name: STOCK Tg(Fos-lacZ)34Efu/J). These mice express a β-galactosidase gene under the control of a Lef/Tcf and β-catenin inducible promoter (Figure 63) (154). After performing LacZ staining, the bluish colour of the LacZ stain indicates cells/tissues with an active Wnt/β-catenin pathway.

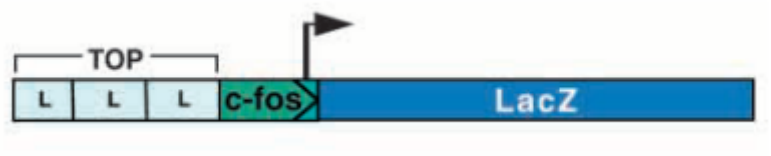

Figure 63: Schematic of the TOPGAL construct
The promoter encloses three consensus Lef-1/Tcf binding motifs (L) followed by a minimal c-fos promoter to drive the transcription of the LacZ gene, which encodes for the β-galactosidase protein. Figure taken from (154).

Some of the data of the current project are already published, hence the description of the following methods is partly published in (107,153).

5.1.2 DNA analysis

5.1.2.1 DNA isolation

To obtain a tissue sample for the extraction of genomic DNA, the mice were anaesthetized with isoflurane and 0.3-0.5 cm of the mouse tail tip was cut. The tissue sample was transferred to a 1.5ml tube and 200 µl mouse tail lysis buffer (see buffer and diluaions) was added. Afterwards the samples were incubated at 55°C overnight in a thermomixer shaker at 600 rpm (rounds per minute). The next day, the proteinase K was inactivated by heating the lysate up to 95°C for 15 min. Then the samples were centrifuged at 14000 rpm for 10 minutes. 2 µl (concentration: approximately 30 ng/µl) of the supernatant was taken as DNA template for PCR analysis.

5.1.2.2 Genotyping: Polymerase chain reaction (PCR)

5.1.2.2.1 Genotyping for the transgenes: Norrin and LacZ

This method was developed by K. Mullis and is used to a large extend in molecular biology to amplify certain DNA sequences (155). The PCR analysis in this project was used for the genotyping of the transgenic Rpe65-Norrin, βB1-Crystallin Norrin and TOPGAL animals (Figure 64). The detailed protocols are shown in Table 1 and primer sequences are given in

Table 2. For all genotyping protocols mouse tail DNA was used as a template.

Table 1: Standard PCR protocol and program for Rpe65-Norrin, β-B1-Norrin and TOPGAL genotyping

10x PCR buffer	2.5 µl	temperature	duration	
$MgCl_2$ (25 mM)	1.5 µl	94°C	2 min	
dNTPs (10 mM)	0.5 µl	94°C	30 s	34x
Primer F (10 µM)	0.5 µl	55°C (SV40)	30 s	
Primer R (10 µM)	0.5 µl	60°C (TOPGAL)	30 s	
Taq DNA polymerase	0.5 µl	72°C	1 min	
H_2O	17 µl	72°C	5 min	
DNA template	2 µl	10°C	hold	

Table 2: Genotyping primer

Primername	Mouseline	Sequence	Product size
SV40-F	Norrin	5'-GTGAAGGAACCTTACTTCTGTGGTG-3'	300 bp
SV40-R	(RPE, βB1)	5'-GTCCTTGGGGTCTTCTACCTTTCTC-3'	
Rosa-LacZ -F	TOPGAL	5'-ATCCTCTGCATGGTC AGG TC-3'	315 bp
Rosa-LacZ -R		5'-CGTGGCCTGATTCATTCC-3'	
MwoI-F	leu/met	5′- CACTGTGGTCTCTGCTATCTTC-3′	674bp
MwoI-R	mutation	5′- GGTGCAGTTCCACTTCAGTT-3′	

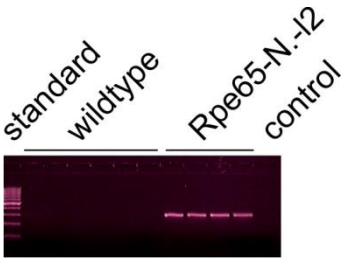

Figure 64: Genotyping for transgene Rpe65-Norrin-2 animals
Standard: 100bp, control = H_2O control

5.1.2.2.2 Genotyping for the leucine variant of Rpe65

Since a point mutation at position 450 in the Rpe65 gene (resulting in a base exchange from methionine to leucine) has major influence on the susceptibility to light damage, all out animals were genotyped and bred for the leucine variant of this point mutation (35–38,156).

Table 3: PCR protocol and PCR program for leucin/methionin genotyping of Rpe65 gene

		temperature	duration	
10x PCR buffer	5 µl	94°C	2 min	
$MgCl_2$ (25 mM)	3 µl	94°C	30 s	34x
dNTPs (10 mM)	2 µl	55°C	45 s	
Primer F (10 µM)	2 µl	72°C	1 min	
Primer R (10 µM)	2 µl	72°C	5 min	
Taq DNA polymerase	2 µl	10°C	hold	
H_2O	29 µl			
DNA template	4 µl			

12µl of PCR product (see Table 3) was digested with 8 µl H_2O and 0.3µl MwoI at 37°C for 3h. The leucine codon generates a restriction site for MwoI, which results after digestion in 2 DNA products of 437 bp and 236 bp (Figure 65).

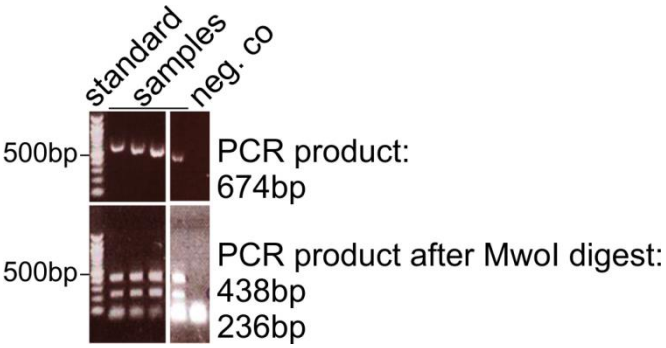

Figure 65: Leucin/methionin PCR before (upper panel) and after (lower panel) MwoI digest
Standard: 100bp, neg. co = negative control (H_2O control)

5.1.2.3 Agarose gel electrophoresis

To visualize and analyse the amplified PCR products, gel electrophoresis was used. For the gel 1 g of agarose was dissolved in 100 ml TBE buffer and heated up in a microwave oven for 5 min. After letting the solution cool down, 3 µl of ethidium bromide was added. Ethidium bromide intercalates in the DNA and fluoresces when excited with UV light. Loading dye was added to the PCR product and the samples were loaded in the gel. The DNA products were separated through the electric field in the gel according to their molecular size. A standard with defined molecular size was added at the very left pocket of the gel. That allows the verification of the correct molecular size of the amplified PCR product.

5.1.2.4 Southern blot analysis

To perform southern blot analysis mouse tail and spleen DNA was isolated using the Bio-sell tissue DNA isolation kit. Subsequently 10 µg of the isolated mouse tail and spleen genomic DNA were digested with 20 U EcoRV (+ 1 µl BSA (1:10), 1 µl buffer 3) at 37°C overnight. After inactivating the enzyme with heating the samples up at 80°C for 20 min, DNA sample buffer was added and the samples were pipetted into a 1% agarose gel, supplemented with ethidium bromide, that run for 2.5 h at 120 V. Afterwards the gel was washed under gentle shaking with the chemicals and durations as listed in Table 4.

Table 4: Wash steps for southern blot analysis: day 1 (all steps: room temperature)

20 minutes	250 mmol HCL	depurination
2x 15 minutes	0.5M NaOH + 1.5M NaCl	denaturation
2x 15 minutes	0.5M Tris-HCL + 1.5M NaCl	neutralisation
10 minutes	20x SSC	equilibration

Then gel was blotted via capillary blot overnight onto a nylon membrane. The next day the membrane was dried and crosslinked with an intensity of 1600 Joule with a Stratagene Crosslinker. Afterwards, the crosslinked membrane was pretreated with DIG easy Hyb for 30 minutes at 49°C

(prehybridisation). In the meanwhile the probe (concentration: 20 ng/µl) was prepared: 10 µl of the probe were diluted in 100 µl H_2O heated up to 95°C for 5 minutes and then left on ice for 2 minutes. Then the probe was added to the membrane with fresh DIG easy Hyb for hybridisation at 49°C overnight. The next day, the membrane was washed as listed in Table 5 and finally detection of the membrane was performed in a LAS 3000 Intelligent Dark Box.

Table 5: Wash steps and detection for southern blot analysis: day 2

2x 5 minutes	2xSSC + 0.1% SDS	room temperature
2x 15 minutes	0.1xSSC + 0.1% SDS	70°C
2 minutes	Wash buffer	room temperature
30 minutes	Blocking: 1xDIG	room temperature
30 minutes	1xDIG + AP fragment (1:10000)	room temperature
3x 10 minutes	Wash buffer	room temperature
5 minutes	Detection buffer	room temperature
5 minutes	Detection buffer + CDP star (1:100)	room temperature
X minutes	Detection: LAS imager	

5.1.2.5 Southern and northern blot probe

The generation of the Southern and northern respectively blot probe is described in (106) (see also Table 6).

Table 6: Primer sequences for southern and northern blot probes

name	Sequence	Product size:
Norrin - F	5'- AGCTCAAAGATGGTGCTCCT-3′	490 bp
Norrin - R	5'- TAGAGCCAACAGGGGAAATG-3′	

5.1.3 RNA analysis

RNA was isolated from dissected retinae. To obtain the retina, the mice were killed with cervical dislocation and the eyes were enucleated. The eye ball was carefully cut with a razor blade on top of the cornea without bruising the lens. The lens was removed as well as the anterior part of the globe and the retina was detached from the RPE and sclera with gentle brushes from the position of the optic nerve head.

5.1.3.1 RNA isolation

Following preparation, the retinae were put in a 2 ml Eppendorf tube on ice immediately and 250 µl TRIzol (Invitrogen) was added. TRIzol contains phenol and guanidine isothiocyanate and is broadly used for cell lysis, inactivation of RNAses and stabilisation of the RNA. Shortly after adding the TRIzol the samples were homogenized and further RNA isolation was performed as described in Table 7.

Remark: after adding chloroform (step 2 of the protocol in Table 7) and centrifugation the TRIzol lysate appears in 3 phases. The upper aqueous phase contains the RNA, the middle interphase contains precipitated proteins and the lower (organic) phase contains DNA, dissolved proteins and lipids.

Table 7: RNA isolation protocol

5 minutes	Incubate at room temperature	Cell lysis
	add chloroform (1/4 of the sample volume) to the lysed tissue, vortex	Protein precipitation
20 minutes	Incubate on ice	
20 minutes	Centrifuge at 14.000 rpm, 4°C	Phase separation
	Transfer the upper transparent aqueous phase to a new cup (1.5ml)	
	add isopropanol (1/1 of the sample volume) to the upper phase, vortex	RNA precipitation
overnight	Freeze at -20 °C	
20 minutes	Centrifuge at 14.000 rpm, 4°C	
	Remove supernatant	
	Add 500 µl 70% ethanol, vortex	Wash step
5 minutes	Centrifuge at 14.000 rpm, 4°C	
1-2 minutes	Dry the pellet for approximately 2 minutes	
	Add 15 µl RNAse free water, store at -80°C	RNA dissolving

The integrity of the obtained RNA was checked on a 1% agarose gel prior to further experiments like cDNA synthesis or Northern blotting (Figure 66).

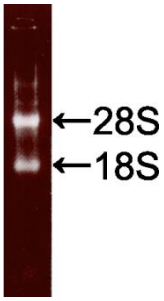

Figure 66: Agarose gel electrophoresis to prove RNA quality
Intact RNA sample exhibit a 2:1 ratio of 28S to 18S ribosomal RNA signal intensities.

5.1.3.2 Complementary DNA (cDNA) synthesis

cDNA is synthesized from a messenger RNA (mRNA) template using the enzyme reverse transcriptase. The enzyme reverse transcriptase operates on the single strand of mRNA and generates its complementary DNA. This process is based on the coupling of RNA base pairs (A, U, G and C) to their DNA counterparts (T, A, C and G). First-strand cDNA synthesis was performed using iScript cDNA Synthesis Kit (Bio-Rad) according to manufacturers' instructions. Briefly, 1 µg of RNA in H_20 was inserted into the reaction mix listed in Table 8 and cDNA amplification program was performed (Table 8).

Table 8: cDNA synthesis: reagents and amplification program

reagents	+RT	-RT	temperature	duration
iScript reverse transcriptase	1 µl	-	25°C	5 min
5x script	4 µl	4 µl	42°C	30 min
1 µg RNA in H_2O	15 µl	16 µl	85°C	5 min
			4°C	hold

5.1.3.3 Quantitative realtime RT-PCR

Quantitative real-time RT-PCR analyses were performed with the reversed transcribed samples (+RT) using the Bio-Rad iQ5 Real-Time PCR Detection System. A H_2O control and RNA that was not reverse transcribed (–RT) served as negative control for real-time RT-PCR. See Table 9 for mix and conditions.

Table 9: Realtime RT-PCR: PCR protocol and program

reagent	volume	temperature	duration	
Sample (+RT, -RT, H_2O)	0.15 µl	95°C	15 minutes	
10x PCR buffer	1.5 µl	95°C	10 seconds	40x
$MgCl_2$ (25 mM)	0.6 µl	60°C	40 seconds	
dNTPs (25 mM)	0.12 µl	72°C	10 seconds	
Taq DNA polymerase (5 U/µl)	0.06 µl	95°C	1 minute	
SYBR-Green I (7.4% (v/v) in DMSO)	0.19 µl	55°C	1 minute	
Fluorescein	0.015 µl	55°C + 0,5°C per cycle	6 seconds	81 x
H_2O	12.03 µl	(melt curve)		
Primer F (1 µM)	0.17 µl			
Primer R (1 µM)	0.17 µl			

5.1.3.4 Primer for real-time RT-PCR

All oligonucleotides were purchased from Invitrogen (Table 10) and were intron spanning (except GAPDH).

Table 10: Primer pairs for real-time RT-PCR (published in (107)).

Product	Sequence	Position	Tm [°C]	Product size
BDNF	5`- agtctccaggacagcaaagc -3`	614 – 633	59	94
	5`- tgcaaccgaagtatgaaataacc -3`	685 - 707	60	
EDN-2	5`- acctcctccgaaagctgag -3`	502–520	59	76
	5`- tttcttgtcacctctggctgta -3`	556 –577	59	
FGF2	5`- cggctctactgcaagaacg -3 `	285 – 303	59	108
	5`- tgcttggagttgtagtttgacg -3`	371 - 392	60	
GFAP	5`- acagactttctccaacctccag -3`	1217 – 1238	59	63
	5`- ccttctgacacggatttggt -3`	1260 – 1279	59	
LEDGF	5`- ggccagcagtaagacaaagc -3`	1513 – 1532	60	92
	5`- tgaagctgccgacctagttat -3`	1584 – 1604	59	
LIF	5`- aaacggcctgcatctaagg -3`	172–190	60	93
	5`- agcagcagtaagggcacaat -3`	245–264	59	

CNTF	5`- ttgattccacaggcacaaaa-3`	42 – 61	60	62
	5`- ccctgcctgactcagaggt -3`	85 - 103	60	
EDN-R-B	5`- cggtatgcagattgctttga -3`	1023 – 1042	59	92
	5`- aacagagagcaaacacgagga -3`	1094 – 1114	60	
PEDGF	5`- ggactctgatctcaactgcaag- 3`	795 – 816	59	93
	5`- aagttctgggtcacggtcag- 3`	868 – 887	60	
GAPDH	5`- tgtccgtcgtggatctgac -3`	763–781	60	75
	5`- cctgcttcaccaccttcttg -3`	818–837	60	

To allow relative quantification GAPDH was used. Quantification was performed using BioRad iQ5 Standard-Edition (Version 2.0.148.60623) software (BioRad).

5.1.3.5 Northern Blot analysis

For Northern blot analysis retinal RNA was isolated as described above. Northern blot sample buffer was added to 10 µg of each RNA sample, the mixture was heated to 65°C for 5 minutes and then quickly cooled down on ice for 2 minutes. Afterwards, the samples were loaded onto the northern blot agarose gel (see Table 11) and run at 100 V for 60 minutes. Then RNAs were transferred by capillary blot onto a positively charged nylon membrane and Norrin RNA was detected by forming a RNA/DNA hybrid with the probe. The Digoxigenin (DIG) labeled probe was prepared according to the manufacturer's manual and as described in detail in (153). Prior to hybridization the membrane was pre-incubated for 1 h at 60°C in hybridization buffer. Then the probe was added for hybridization and the blot was incubated with gentle turning in a hybridization oven at 60°C overnight to form the RNA/DNA hybrid. After hybridization the blot was washed 2x with hybridization buffer and two times with 0.1xSSC, 0.1%SDS at the used temperature. Subsequently, the membrane was shortly in DIG washing buffer (100 mM maleic acid, 150 mM NaCl, pH 7.5 and 0.3% N-lauroylsarcosin) and afterwards blocked for 1 hour with 1x blocking reagent (Roche) in 100 mM maleic acid, 150 mM NaCl, pH 7.5. Next, 0.75 U/ml of anti-DIG antibody conjugated to the alkaline phosphatase (Roche) in blocking buffer was added and incubated for further 45 minutes at RT. The membranes were washed three times in DIG washing buffer and incubated for 5 minutes in detection buffer (100 mM Tris pH 9.5, 100 mM NaCl, 5 mM MgCl2). 1% CDP-star in detection buffer (Roche) was added and the chemiluminescence signals were detected with a Fuji LAS Reader 3000.

Table 11: Northern blot gel (150ml)

Agarose	1.50 g
DEPC-H_2O	109.5 ml
10x MOPS	15 ml
Formaldehyde	25.5 ml
Ethidium bromide	3 µl

5.1.4 Protein analysis

5.1.4.1 Protein isolation

After TRIzol (Invitrogen) based RNA isolation the remaining lysates of neuronal retinae were treated following the manufacturer's instructions for protein isolation. The detailed steps are listed in Table 12.

Table 12: Protocol for protein isolation

Optional (DNA isolation):	Add 375 µl 100% ethanol to the interphase and phenol-chloroform
10 minutes incubation,	phase of the previously performed TRIzol based RNA isolation (original
room temperature	TRIzol volume 250µl)
15 minutes, 4°C	Centrifuge at 12000 x g
	Transfer the supernatant in a new reaction tube and discharge the former tube with the DNA pellet
Protein isolation:	Add 375 µl 100% isopropanol to the supernatant
10 minutes incubation, room temperature	
10 minutes	Centrifuge 12000 x g, discharge the supernatant
3x 20 minutes wash	Wash the precipitated protein pellet in 1 ml 0.3 M guanidine
buffer and	hydrochloride (in 95% ethanol) and
3x 5 minutes centrifugation, 4°C	centrifuge at 7600 x g
20 minutes incubation	Add 1 ml 95% ethanol, vortex
5 minutes, 4°C	Centrifuge 7600 x g, discharge the supernatant
1 minute	Dry the protein pellet
overnight 50°C	Dissolve the protein pellet
or	either in 1% SDS + protease inhibitors (1:1000) and incubate at 50°C overnight
65°C 15 minutes	or in urea buffer at 65°C, 15 minutes
optional: 5 minutes, RT	Centrifuge insoluble contains down and transfer the protein lysate in a new reaction tube
-80°C	storage

5.1.4.2 Western blot analysis

For Norrin Western Blots, the supernatant was separated by Urea-PAGE (4/3 16% Acrylamid + 6 M Urea). For other proteins, Proteins were separated by SDS-PAGE (10%, BDNF: 15% gel) and transferred to a polyvinyl difluoride membrane (Milipore), which was incubated with PBS containing 0.1% Tween 20 (PBST; pH 7.2) and 3% bovine serum albumin or 5% non-fat dry milk overnight. Antibodies were used as described in Table 13. After washing with PBS-T, secondary antibodies (1:2000) were added. Chemiluminescence was detected on a BAS 3000 imager work station (Fujifilm). For normalization, blots were re-probed for glyceraldehyde 3-phosphate dehydrogenase

(GAPDH). Western blot signals were evaluated by relative densitometry with the Aida Image Analyzer v.4.06 software (Raytest).

5.1.4.3 Antibodies and blocking solutions for Western blot analysis

Table 13: Antibodies and blocking solutions for western blot analysis (published in (107)).

Primary antibody	Blocking	Secondary antibody
Norrin (R&D Systems) 1:1000	3% bovine serum albumin	chicken anti-goat coupled to horseradish peroxidase (Millipore)
β-catenin (Cell Signaling) 1:2000	5% non-fat dry milk	chicken anti-rabbit coupled to horseradish peroxidase (Santa Cruz Biotechnology)
pAkt (Cell Signaling) 1:500	3% bovine serum albumin	chicken anti-mouse coupled to alkaline phosphatase (Santa Cruz Biotechnology)
Akt (Cell Signaling) 1:1000	5% non-fat dry milk	goat anti-rabbit coupled to horseradish peroxidase (Rockland)
Brain-derived neurotrophic factor (Alomone) 1:200	3% bovine serum albumin	goat anti-rabbit coupled to horseradish peroxidase (Rockland)
Glyceraldehyde 2-phosphatase dehydrogenase (Abcam) 1:10.000, HRP conjugated	5% non-fat dry milk	

5.1.4.4 Apoptosis: cell death detection ELISA

Apoptotic cell death was analysed by Cell Death Detection ELISA (Roche Diagnostics) which determines histone-associated DNA fragments (mono- and oligonucleosomes) in the cytoplasmatic fraction of cell lysates. To this end, the retinae of animals 30 h after 30 min light damage were investigated following manufacturers' instructions. The methodical principle of this ELISA is shown in Figure 67. In brief, the ELISA plate was coated with streptavidin and incubated with an anti-histone-biotin conjugated antibody. This led to the formation of a streptavidin-biotin complex. In general, the proteins avidin or streptavidin respectively are used to a broad extend in molecular biology or histology because of their potent binding ability of biotin. Avidin is found in chicken egg white while streptavidin is expressed in the bacteria Streptomyces avidinii (157). These two proteins have a molecular mass of approximately 60 -75 kDa and consist of 4 identical subunits which each can bind the vitamin biotin with very high affinity (158). That is why they are useful tools in molecular biology. In the cell death detection ELISA, the principle strepatividin-biotin method was used to detect the grade of light induced apoptosis. During apoptosis DNases cut the genomic DNA in the linker region (inter nucleosomal region) which results in an appearance of mono- and oligonucleosomes. Subsequently, the sample solution containing nucleosomes in the retinal lysates of light exposed and

non-light exposed transgene and wild-type animals was pipetted into the ELISA plate. During incubation the mono- and oligosomes in the retinal lysates bind to the anti-histone-biotin, which is already bound covalent to the streptavidin coated ELISA plate. After incubation an anti-DNA-peroxidase solution was added, followed by ABTS substrate. This led to a colorimetric change in the wells containing the light damaged samples. They appeared in a dark green color. Then colorimetric analysis was performed using an ELISA reader (Sunrise-Basic) and maghellan software.

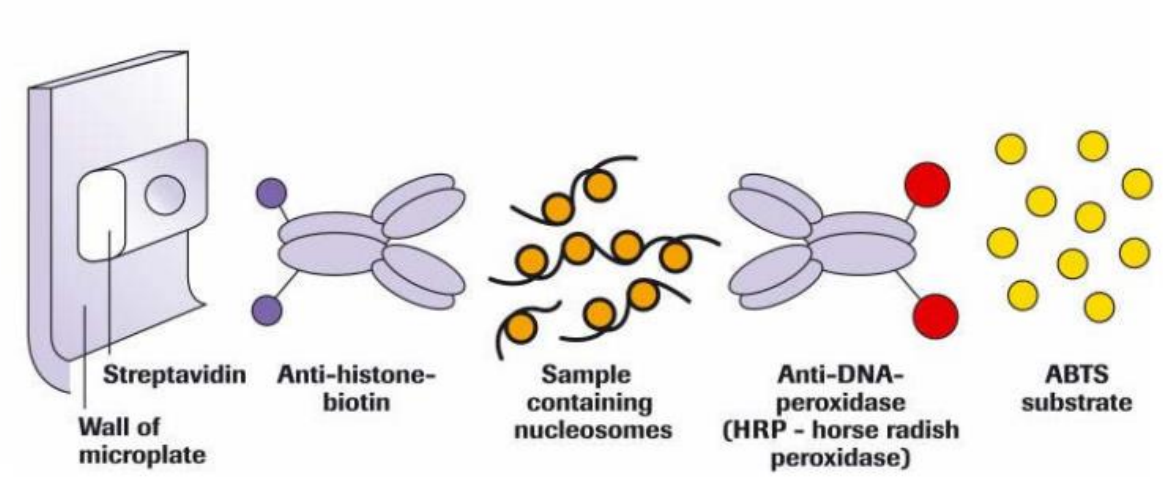

Figure 67: Schematic of the methodical principle of the Cell death detection ELISA^{plus}
(picture taken from: https://cssportal.roche.com/LFR_PublicDocs/ras/11774425001_en_11.pdf, PDF, page 13)

5.1.5 Histology

5.1.5.1 Phenotype analysis

For phenotype analysis, the eyes of untreated Rpe65–Norrin mice were investigated at postnatal day (P) 5, 10, 15, and 20, as well as at 6 weeks, 3 and 6 month of age. Eyes of light-exposed animals were analyzed 7 d and 14 d after light damage. Before enucleation, a mark was set at the superior limbus. The eyes were then fixed for 24 h in Ito's fixative (Karnovsky, 1965) and embedded in Epon (Serva). Semithin sections of 1.0 µm thickness were cut along the mid-horizontal (nasal-temporal) plane and stained by Richardson's stain (159). Further analysis was performed by semithin section light microscopy and transmission electron microscopy according to protocols published previously (80). The detailed morphometric analysis procedure following light exposure is explained in: animal experiments – light damage – light damage and morphometric read out: the spider diagram.

5.1.5.2 Immunohistochemistry

Norrin, endothelin-2 (EDN2), endothelin-receptor type B (EDN2-RB), plasmalemma vesicle-associated protein (PLVAP) immunohistochemistry and staining with IsolectinB4 was performed on frozen sections (12 µm). Eyes were fixed for 4 h in Methyl Carnoy's (10% glacial acetic acid, 60% methanol,

and 30% chloroform), transferred to 50% and 25% methanol 30 min each, washed in phosphate buffer (0.1 M, PhP), incubated in 10%, 20%, 30% sucrose/PBS overnight at 4°C and shock frozen in tissue mounting medium (DiaTec). For glial fibrillary acidic protein (GFAP) and BDNF, paraffin sections (6 µm) were used. Eyes were fixed for 4 h in 4% paraformaldehyde (PFA) and embedded in paraffin. Paraffin sections were deparaffinized and washed in water for 5 minutes. Then, sections were washed for 5 minutes in PhP, blocked with 2% BSA in 0.1M PhP for 45 minutes, and incubated with primary antibodies (Table 14) in 0.2 % BSA at 4°C overnight. After three washes in PhP (5 minutes each), secondary antibodies (Table 14) were applied for 1 h at room temperature. Lac-Z-staining was performed in mixed Rpe65-Norrin-2 mice/TOP-Gal mice (The Jackson Laboratory) as described previously (154). Paraffin sections (6.0 µm) were cut, placed on glass slides (SuperFrost/Plus; Menzel) and analyzed by light microscopy (Carl Zeiss).

5.1.5.3 Antibodies for immunohistochemistry

Table 14: Antibodies for immunohistochemistry (published in (107)).

Primary antibody	Fixation	Secondary antibody
Norrin (R&D Systems) 1:25	Methyl Carnoy's	goat anti-rabbit IgG Alexa 488 highly cross adsorbed (Invitrogen) 1:1000
Endothelin-2 (Prestige) 1:50	Methyl Carnoy's	goat anti-rabbit IgG Alexa 488 highly cross adsorbed (Invitrogen) 1:1000
Endothelin-Receptor Type B (Alomone Labs) 1:50	Methyl Carnoy's	goat anti-rabbit IgG Alexa 488 highly cross adsorbed (Invitrogen) 1:1000
Glial fibrillary acidic protein (Dako) 1:500	4% paraformaldehyde	goat anti-rabbit + Biotin 1:500 (Vector) Streptavidin Alexa 488 1:1000 (Molecular Probes)
Brain-derived neurotrophic factor (Alomone Labs) 1:20	4% paraformaldehyde	goat anti-rabbit + Biotin 1:500 (Vector) Streptavidin Alexa 488 1:1000 (Molecular Probes)
Biotinylated Griffonia (Bandeira) Simplicifolia LectinI IsolectinB4 (Vector) 1:20	Methyl Carnoy's	Streptavidin Alexa 555 (Invitrogen) 1:1000
Plasmalemma vesicle-associated protein (pan-ECA, Santa Cruz) 1:50	Methyl Carnoy's	Donkey anti rat Cy3 (Jackson ImmunoResearch) 1:2000

5.1.5.4 Apoptosis: TUNEL analysis

DNA fragmentation is a characteristic of apoptosis. Terminal deoxynucleotidyl transferase dUTP nick end labeling (TUNEL) is an established method to detect DNA fragments. Apoptotic cell death was analyzed by TUNEL labeling using the Apoptosis Detection System (DeadEnd Fluorometric TUNEL, Promega). To this end the retinae of animals 30 h after 30 min light damage were investigated following manufacturers' instructions (Figure 68).

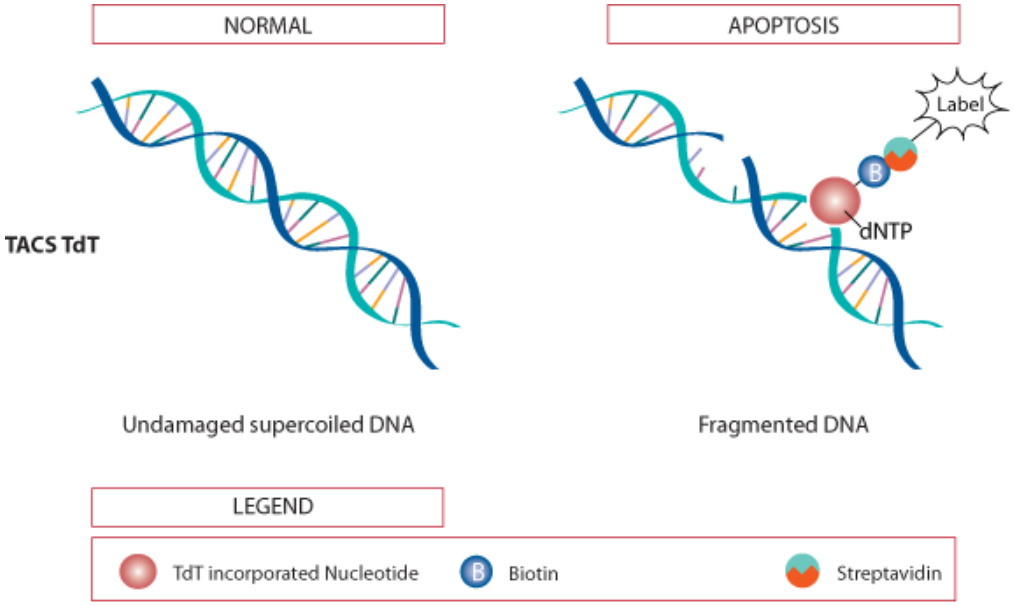

Figure 68: Schematic of the methodical principle of the TUNEL assay
The enzyme TdT incorporates Biotin or – as in the TUNEL assay used in this project- FITC coupled nucleotides in the fragmented DNA. If biotin is used, streptavidin –horseradish peroxidase and colorimetric substrates like diamanobenzidin (DAB) are added in a second step. (picture taken from: http://www.rndsystems.com/product_detail_objectname_tunel_assay_principle.aspx)

For quantitative analysis, the number of TUNEL-positive nuclei in mid-horizontal sections throughout the entire retina were counted using KatiKati2 (http://www.geocities.jp/gen_0715/softs/katikati/index2.html) cell counter and normalized to the area of the outer nuclear layer, which was determined with the Axiovision 4.8 program from Zeiss.

5.1.6 Animal experiments

5.1.6.1 Oxygen-induced retinal damage: The retinopathia praematurorum (ROP) model

To induce ROP, mice with their nursing mother were exposed to 75% oxygen for 5 d from postnatal day (P) 7 to P12 according to the described protocol (151) and as indicated in Figure 69.

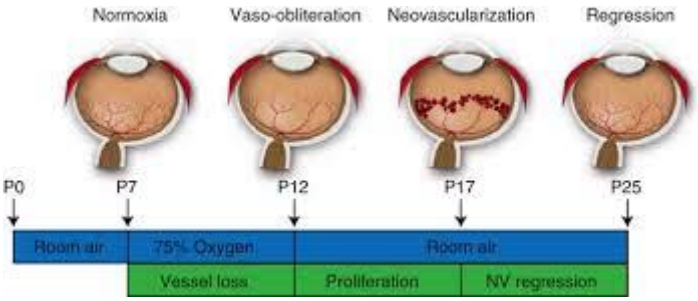

Figure 69: Schematic of the ROP model
Mice were exposed to high oxygen (75%) from d 7 to d 12. The following return to room air lead to a relative hypoxia, resulting in vessel proliferation. Figure taken from (160).

Mice were killed at P12, or returned to room air until P14, P16 or P17. The effects of Norrin on capillary re-growth into ROP induced vasobliterated areas, the formation of intraretinal vessels and the development of preretinal neovascular tufts were analysed using retinal whole mounts (for detailed whole mount method explanation, see below). To this end, light-micrographs of retinal whole mounts were taken at a 5x magnification for documentation of the superficial vascular plexus and of preretinal neovascular tufts, the deep capillary plexus were recorded at a 20x magnification using the Apotome mode of an Axiovision fluorescent microscope (Carl Zeiss). The total area of the retina, the areas of preretinal neovascular tufts, of vasobliteration, and of the deep capillary plexus were measured and calculated as area of neovascular tufts per 1000 μm^2 retina, area of vasobliteration per total retinal area as well as retinal area that was covered by deep plexus per total retinal area using the Axiovision software 4.8. To analyze the deep capillary plexus in cross sections retinal whole mounts were embedded in Tissue Tek and subjected to cryosectioning.

5.1.6.2 Light damage

Rpe65-Norrin mice, 6–9 week old, were transferred to cyclic dim light (<100 lux) for 5 days followed by a dark-adaption period of 12 h. Mice with dilated pupils (one drop Mydriaticum Stulln/eye) were then placed in reflective cages and exposed to diffuse cool, white fluorescent light coming from the top of the cage with an intensity of 5000 lux for 30 min (detection of apoptosis) or 1 h (other experiments). Average intensity was measured on the cage floor (5000 lux). After light exposure, mice were allowed to recover first for 6 h in dim light, and then sacrificed (mRNA analysis) or brought back to normal cyclic light conditions. Light damage experiments were always performed in the early morning.

5.1.6.3 Light damage and morphometric read out: the spider diagram

Morphometric measurements were used to quantify the occurrence of the light damage per experimental group (wild-type versus Rpe65-Norrin-2). To this end, Richardson stained sagittal section from the nasal to temporal side through the optic nerve head were used.

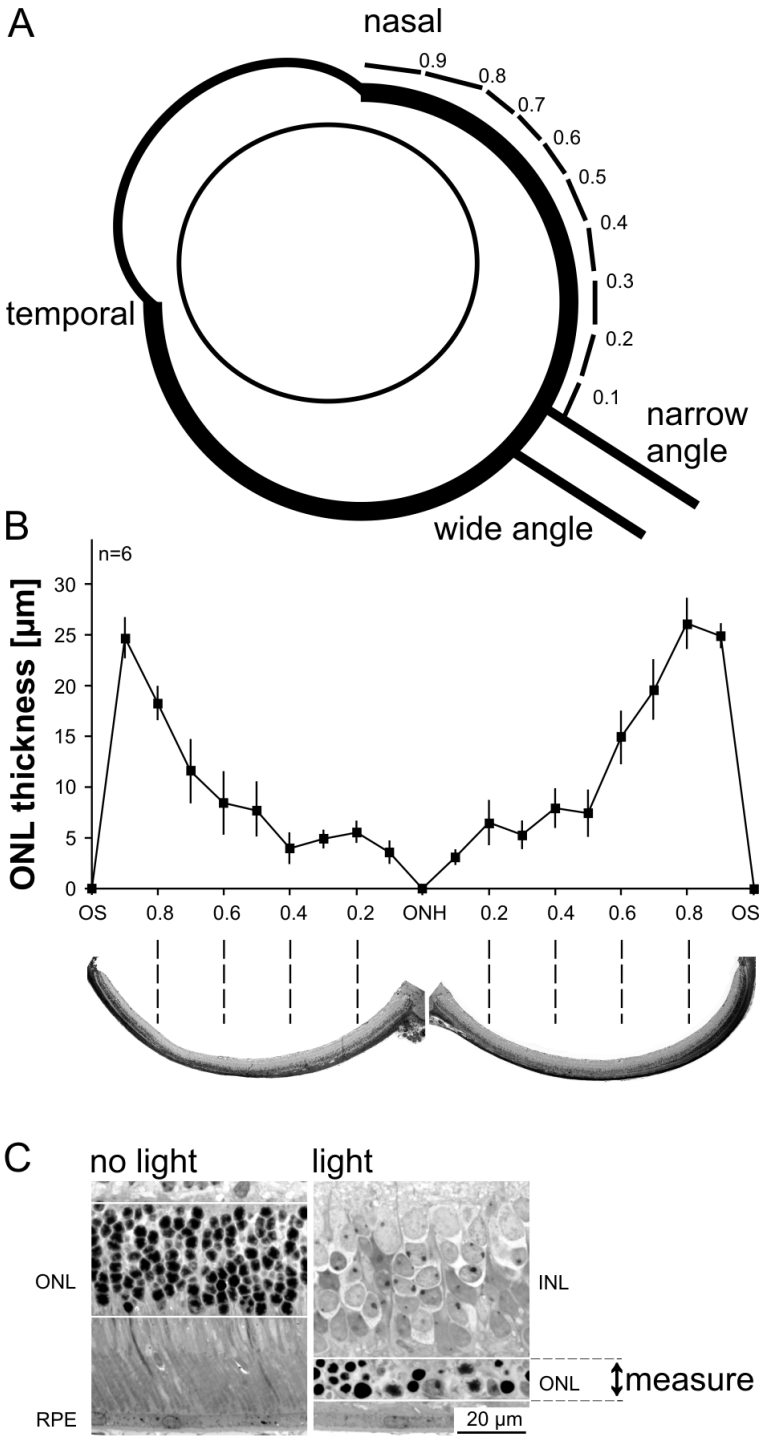

Figure 70: Morphometric analysis following light exposure
A. schematic drawing of the measure points of the experimental eye. B. Example of a spider diagram of light exposed animals, showing the thickness of the outer nuclear layer throughout the retina at 21 measure points. C. Richardson stained semithin section of a control (no light) and a light exposed (light) animal to show the measure technique on the section. Figure taken from a manuscript in preparation: Barbara M. Braunger, Daniela Kawall and Ernst R. Tamm: Light-induced photoreceptor damage.

The length of the hemispheres of these sections was measured; the total length divided through 10 and the thickness of the outer nuclear layer was measured between each 10th of the hemisphere. The means of the measure points were blotted in a so called spider diagram and statistical analysis was performed to compare single measure points throughout the entire retina between wild-type and Rpe65-Norrin-2 animals (Figure 70).

5.1.6.4 Intravitreal injections

In the ROP model, some of the animals were injected with 3 µl of Dickkopf-1 (DKK-1) [10 ng/µl] once into the vitreous of anesthetized mice after hyperoxia at P12. For light damage experiments and morphometry, DKK1 (R&D Systems) was injected 3 times (12 h before, and 2 and 4 d after light damage). Mice were anesthetized using isofluran (Baxter) and 3 µl DKK1 (10 ng/µl) or PBS (contralateral eye) were injected through the basal limbus using a 33 gauge needle. Animals were killed 7 days after light damage. For analysis of β-catenin or neuroprotective molecules, DKK1 or PBS were injected twice (15 and 3 h before light damage, or enucleation of the eyes in non-light damaged animals). BQ788 (1 µg/µl diluted in 5% DMSO in PBS) or 5% DMSO (contralateral eye), 2 µl each, were injected twice (15 and 3 h before light damage). Light-damaged animals were killed 6 h after light exposure.

5.1.6.5 Fundus imaging and angiography

Fundus imaging and angiography were performed in cooperation with Prof. Jägle, Regensburg. Retinal imaging was performed with a commercially available imaging system (Micron III; Phoenix Research Laboratories, Inc.). Light source path and imaging path filters (low pass and high pass at 500 nm) were used for fluorescein angiography (FLA). Mice were anesthetized by s.c. injection of ketamine (65 mg/kg) and xylazine (13 mg/kg), and their pupils were dilated with tropicamide eyedrops (Mydriaticum Stulln; Pharma Stulln) before image acquisition. FLA was performed using a s.c. injection of 75 mg/kg body weight fluorescein-Na (Alcon).

Laser scanning ophthalmoscopy (SLO) and optic cohaerence tomography (OCT) were performed in cooperation with Prof. Seeliger, Tübingen. Mice were anesthetized with ketamine (66.7 mg/kg b.w.) and xylazine (11.7 mg/kg b.w.), and the pupils were dilated with tropicamide eye drops prior to examination.

5.1.6.6 Retinal whole mounts

To analyze the vascular phenotype of 6-week-old Rpe65-Norrin mice, mice were deeply anesthetized with ketamine (120 mg/kg body weight, i.m.) and xylazine (8 mg/kg body weight) and perfused through the left ventricle with 1 ml of phosphate buffered saline (PBS) containing 50 mg high molecular weight (MW = 2,000,000) FITC-dextran (Sigma). The eyes were enucleated and placed in

4% paraformaldehyde for 4 hrs. Retinae were dissected and flat mounted using fluorescent mounting medium (Dako). Lightmicrographs of retinal whole mounts were taken at a 5x magnification to achieve an overview of retinal vasculature by using an Axiovision fluorescent microscope (Carl Zeiss). Retinal whole mount preparation and analysis was performed with the help of Dr. Andreas Ohlmann, Regensburg.

5.1.6.7 Functional analysis: electroretinography (ERG)

The functional ERG analyses were performed in cooperation with Prof. Matthias Seeliger, Tübingen. Electroretinographies were recorded binocularly in untreated animals and light exposed mice 2 weeks after damage as described previously (161). Briefly, after overnight dark adaptation, mice were anesthetized with ketamine (66.7 mg/kg b.w.) and xylazine (11.7 mg/kg b.w.), and the pupils were dilated with tropicamide eye drops. Single-flash responses were obtained under dark-adapted (scotopic) and light-adapted (photopic) conditions. Light adaptation was achieved with a background illumination of 30 cd/m2 starting 10 min before photopic recordings. Single white-flash stimuli ranged from –4 to 1.5 log cd*s/m2 under scotopic and from –2 to 1.5 log cd*s/m2 under photopic conditions, divided into ten and eight steps, respectively. Ten responses were averaged with interstimulus interval of 5 or 17 s (for 0 to 1.5 log cd*s/m2).

5.1.6.8 Rhodopsin recovery in darkness

To determine the absolute rhodopsin content mice were dark adapted for 16 hours and all following procedures were performed under dim red light. Detailed steps are described in Table 15. To further analyze the ability of rhodopsin recovery in darkness which allows deeper conclusions of the proper function of the visual cycle, exactly the same analysis was performed as described in Table 15, except that the animals were exposed to 5000 lux for 10 minutes and either killed directly after the light exposure or after a following recovery period (10 min, 3h, 6h) in darkness. In general, all the steps of this protocol were performed according to the descriptions in (36,162).

Table 15: Protocol for absolute rhodopsin content and rhodopsin recovery in darkness

	Add both retinae to 1 ml H_2O
3 minutes, room temperature	Centrifugation, 15000 x g
	Discharge the supernatant and re-suspend the retinal pellet in 700 µl of 1% CTAB solution
	Homogenize the retinae
3 minutes, room temperature	Centrifugation, 15000 x g
	Measure the absorption of the supernatant at 500nm (plastic cuvette: 1 cm length)
90 seconds, cool white light	Expose the sample at 16000 lux to bleach all present rhodopsin and repeat the photometer measurement at 500nm

Then the amount of rhodopsin present per retina was calculated. Therefore a formula derived from the Lambert–Beer equation and as described in (162) was used:

$rho = vol \times c = \text{vol} \times [\Delta abs_{500}/(e \times l \times n)]$

rho: amount of rhodopsin per retina (in moles)

vol: sample volume (in liters)

c: rhodopsin concentration per retina (in mol/liters)

$\Delta abs_{500:}$ difference between absorption before and after bleaching measured at 500 nm

e: extinction coefficient of rhodopsin at 500 nm (4.2×10^4 cm × M)

l: path length of the plastic cuvette (in centimeters)

n number of retinae

5.1.7 Statistical analysis

Statistical differences between individual test populations were analysed by Student's t-test (heteroscedastic, two-tailed) using Ecxel software. P values < 0.05 were considered to be statistically significant. All results are expressed as mean ± SEM.

5.2 Material

5.2.1 Chemicals and reagents

10x PCR-buffer	Qiagen, Hilden
2-mercaptoethanol	Roth, Karlsruhe
Acetic acid, glazial	Merck, Darmstadt
Albumin fraction V (BSA)	Roth, Karlsruhe
Ammoniumperoxidisulfat (APS), 10% (w/v)	Roth, Karlsruhe
BC Assay reagent A+B	Interchim, Wörgl, AUS
Bromphenolblue	Sigma-Aldrich, Taufkirchen
BQ788	Sigma-Aldrich, Taufkirchen
CDP star	Roche, Mannheim
Chloroform	Roth, Karlsruhe
Coomassie Brillant Blue R-250	Sigma-Aldrich, Taufkirchen
CTAB: hexadecyltrimethyl-ammoniumbromide	Fluka Chemie, Buchs, Switzerland
DAPI: see Vectashield	Linaris
Deoxycholacid	Roth, Karlsruhe
DEPC (Diethylpyrocarbonat)	Roth, Karlsruhe
Diethylether	Roth, Karlsruhe
Dig Easy Hyb	Roche, Mannheim
di-Natriumhydrogenphosphat-Dihydrat	Merck, Darmstadt
Dkk-1	R&D Systems
DMSO	Roth, Karlsruhe
dNTPs	Qiagen, Hilden
Dodecylsulfat (Na_2-salt)	Serva Electrophoresis GmbH, Heidelberg
Dry milk	Roth, Karlsruhe
Ethanol, absolute	Roth, Karlsruhe
Ethidium bromide	Serva, Heidelberg
FBS	Invitrogen, Karlsruhe
FITC-Dextrane (MW: 200000)	Sigma-Aldrich, Taufkirchen
Fluoresceine	Qiagen, Hilden
Flouresceinisothiocyanat (FITC) Dextran	Sigma-Aldrich, Taufkirchen
Fluorescent Mounting Medium	DakoCytomation, Hamburg
Formaldehyde	Roth, Karlsruhe
Formamide	Sigma-Aldrich, Taufkirchen
Guanidin-HCL	Roth, Karlsruhe
Glycerine	Roth, Karlsruhe
Glycine	Merck, Darmstadt
Hycdrochloric acid 37 % (HCl)	Merck, Darmstadt
Immobilon Western HRP substrate	Millipore Corporation, Billerica, USA
Isoflurane	Baxter, Unterschleißheim
Isopropanol	Roth, Karlsruhe
Kaliumchloride	Roth, Karlsruhe
Kaliumdihydrogenphosphat	Roth, Karlsruhe

Ketamin	WDT, Garbsen
Linde Gas (75% oxygen)	Linde Gas GmbH
Magnesiumchloride (25 mM)	Qiagen, Hilden
Maleic acid	Roth, Karlsruhe
Methanol	Merck, Darmstadt
MOPS	Roth, Karlsruhe
Mydriaticum Stulln (Tropicamide) eye drops	Pharma Stulln Gmbh
Na_2HPO_4 x H_2O	Roth, Karlsruhe
Natriumchloride	Roth, Karlsruhe
Natriumhydrogenphosphat-monohydrate	Merck, Darmstadt
Nonidet P-40 = Tergitol	Sigma-Aldrich, Taufkirchen
Osmiumtetroxide	Merck, Darmstadt
Paraformaldehyd (PFA)	Sigma-Aldrich, Taufkirchen
PBS	Invitrogen, Karlsruhe
Protease-inhibition-Mix M	Serva Electrophoresis GmbH, Heidelberg
Rotiphorese Gel 30 (30 % acrylamide-stock solution with 0,8 % bisacrylamid proportional 37,5:1)	Roth, Karlsruhe
SYBR-Green	Qiagen, Hilden
Urea	Sigma-Aldrich, Taufkirchen
TEMED	Roth, Karlsruhe
Tergitol	Sigma-Aldrich, Taufkirchen
Tissue-Tek	Sakura, Zoeterwoude, NL
Tris Ultrapure, MB Grade	Usb Corporation, Cleveland, USA
Tris	Roth, Karlsruhe
TRIzol-Reagenz	Invitrogen, Karlsruhe
Trypan blue solution (0,08 %)	Sigma-Aldrich, Taufkirchen
Tween 20	Roth, Karlsruhe
Vectashield Mounting Medium for Fluorescence with DAPI	Vector Laboratories, Burlingame, USA
Water Rotisolv (Rnase-frei)	Roth, Karlsruhe
Xylazine	Serumwerk Bernburg, Bernburg

5.2.1.1 Enzymes and Taq polymerase

Restriction endonucleases	New England Biolabs
Taq Polymerase	New England Biolabs
BioThermRed Taq DNA Polymerase	NatuTec, Frankfurt
Proteinase K	Roth, Karlsruhe

5.2.1.2 Kits

Cell death detection ELISA	Roche, Mannheim
DeadEnd™ Fluorometric TUNEL System	Promega, Madison, Wisconsin, USA
iScript cDNA Synthesis Kit	BioRad Laboratories, München, Deutschland
HotStarTaq® DNA Polymerase	Qiagen, Valencia, CA
Nexttec mouse tail kit	Bio-sell, Nürnberg

5.2.2 Consumable supplies and equipment

5.2.2.1 Consumable supplies

Conical tubes 15 ml, 50 ml	Sarstedt, Nürnbrecht
3 MM blotting papers	Neolab, Heidelberg
Biosphere filter tips	Sarstedt, Nürnbrecht
Ear clips	Hauptner & Herebrholz, Solingen
Epon	Serva, Heidelberg
Cover slides, 24 x 60 mm	Menzel-Gläser, Braunschweig
Dispomed single use syringe	Dispomed Witt oHG, Geinhausen
Ecoflo perfusion set	Dispomed Witt oHG, Geinhausen
Laboratory glass	Schott, Roth, VWR
Liquid blocker PAP-Pen	SCI Science Services, München
Microseal „B“ Film	Biorad, München
Multi-reaction tubes 0,5 ml; 1,5 ml; 2,0 ml	Roth, Karlsruhe
Omnifix sterile single use syringes	B. Braun, Wertheim
Parafilm	Pechiney Plastic Packaging, Chicago, USA
Pasteurpipettes	Brand, Wertheim
PCR Plates, 96 well iCycler IQ	Biorad, München
Personna razor blades	American Safety Razor Company, Verona, USA
Pipet tips	Sarstedt, Nürnbrecht
Nitrile glooves	VWR, Darmstadt
Nylone membrane	Roche, Mannheim
PVDF-western blotting membrane	Roche, Mannheim
Serological pipettes	Sarstedt, Nürnbrecht
Sterican single use-injection needle	B. Braun, Wertheim
SuperFrost® Plus glas slide	Menzel-Gläser, Braunschweig

5.2.2.2 Equipment

Axiovert 40 CFL	Zeiss, Göttingen
BioPhotometer	Eppendorf, Hamburg
Electrophoresis power supply E835	Biorad, Hercules, USA
Electron microscope 10A	Zeiss, Göttingen
Gel chamber for electrophoresis	Peqlab Biotechnologie GmbH, Erlangen

Inolab pH-meter	WTW GmbH, Weilheim
IQ5 Multicolor Real-time PCR Detection System + iCycler	BioRad, München
Julabo SW20 waterbath	Julabo Labortechnik GmbH, Seelbach
Kern PJL 2100-2M balance	Kern & Sohn GmbH, Balingen-Frommern
LAS 3000 Intelligent Dark Box	Fujifilm, Düsseldorf
Mastercycler gradient, personal	Eppendorf, Hamburg
Memmert waterbath	Memmert GmbH, Schwabach
Mettler AE 163 special accuracy weighting machine	Mettler Toledo, Gießen
Microm HM 500 OM cryostats	Microm International, Walldorf
Microscope Axio Imager Z1	Zeiss, Göttingen
MilliQ Plus PF water destill machine	Millipore Corporation, Billerica, USA
Model 45-101-i class II electrophoresis system	Peqlab Biotechnologie GmbH, Erlangen
Pipetman Pipetten	Gilson, Middleton, USA
Polymax 1040 shaker	Heidolph, Kelheim
Research Pipets	Eppendorf, Hamburg
Semi-dry electrophoretic transfer cell	Peqlab Biotechnologie GmbH, Erlangen
Sunrise-Basic ELISA-Reader	Tecan Austria GmbH, Grodig, AUS
Systec V75 autoclave	Systec GmbH, Wettenburg
Thermomixer comfort	Eppendorf, Hamburg
Vortex Genie 2	Scientific Industries Inc., New York, USA
Ultrospec 3100pro spectrophotometer	Amersham, GE healthcare, USA
Centrifuge 5415D, 5415R, 5804R, 5810R	Eppendorf, Hamburg
Stratagene Crosslinker	Herolab, Wiesloch
HB-1000 Hybridizer	UVP Laboratory Products, Cambridge, UK
Ultracut microtome	Reichert-Jung, Kirchseeon

5.2.3 Gels, buffers, dilutions

5.2.3.1 Buffers and dilutions

5.2.3.1.1 Histology

EM-fixation	10 ml paraformaldehyde 25 % 50 ml 0,2 M cacodylate buffer pH 7,6 30 ml H_2O
Lac-Z-fixation	48.4 ml 0.1 M phosphate buffer pH 7.3 100 µl 1 M $MgCl_2$ 1.0 ml 0,250 M EGTA pH 7.3 0.4 ml 25 % glutaraldehyde
Lac-Z-staining	72.0 ml Lac-Z wash-buffer 3.0 ml X-Gal (25 mg/ml in DMSO) 0.159 g K4Fe(CN)63H2O 0.123 g K3Fe(CN)6
Lac-Z-wash-buffer	1 ml 1 M MgCl2 5.0 ml 1 % NaDC 5.0 ml 2 % tergitol 489 ml 0.1 M NaPO4-buffer
0,1 M phosphate buffer, pH 7.4	Buffer 1: buffer 2 (see table rows below) 5:1, pH 7.4
Buffer 1: 0,1 M Na_2HPO4 x 2 H_2O	35.6g in 2l H_2O
Buffer 2: 0.1M NaH_2PO_4 x 1 H_2O	13.8g in 1l H_2O
Natriumcacodylate buffer	0,1 M natriumcacodylate buffer 0.1 M HCl, pH 7,4
Osmiumferrocyanide	1 % osmiumtetroxide 0,8 % kaliumhexacyanoferrat (II)
Richardson stain	Stock 1: 5 g (1 %) azur in 500 ml aqua dest. Stock 2: 5g in 500 ml 1% methylenblue in 1 % Natriumtetraborat solution Mix stocks: 1:1 ad 2 vol. H_2O
PFA-solution (4 %)	Paraformaldehyde 4 % 0,1 M phosphate buffer pH 7,4

5.2.3.1.2 Protein analysis

10x elektrode buffer	250 mM Tris/HCl 400 mM Glycin 1 % (w/v) SDS solve in H_2O; ad 1 l
Coomassie-destain	500 ml methanol 10 ml acetic acid Ad H_2O to 1 l

Coomassie-stain	40 ml Methanol
	2 ml acetic acid
	0,2 g Coomassie-Brilliant Blue R-250
	Ad H2O to 100 ml
0,9 % NaCl	0,9 % (w/v) in dH_2O, autoclave
PBS, 10x, pH 7,4	80 g Natriumchloride
	2 g Kaliumchloride
	4,4 g Na_2HPO_4
	2,4 g KH_2PO_4
	ad dH_2O to 1 l, autoclave
Urea-buffer	25 ml 10 % SDS
	10 ml 1 M TRIS pH 6,8
	100 µl 0,5 M EDTA pH 8
	750 µl β-mercaptoethanol
	24 g urea
SDS-solution, 10 % (w/v)	10 g SDS
	Solve in dH_2O; ad 100 ml
SDS-PAGE-buffer, 10x	250 mM Tris/HCl
	400 mM glycine
	1 % (w/v) SDS
	Solve in H_2O; ad 1 l
SDS-sample buffer, 4x	0,25M Tris/HCl, pH 6,8
	30 % glycerin
	8 % (w/v) SDS
	0,02 % (w/v) bromphenolblue
	0,3 M DTT bzw. 10 % β-mercaptoethanol
TBS, 10x, pH 7,4	30 g Tris
	80 g Natriumchlorid
	2 g Kaliumchlorid
	Solve in H_2O ad 1 l, autoclave
TBST, 1x	100 ml 10x TBS
	0,05 % (v/v) tween 20
	Solve in H_2O ad 1 l
Transfer buffer, 10x	5,8 g tris
	2,9 g glycin
	200 ml methanol
	3,7 ml 10 % (w/v) SDS
	Solve in H_2O ad 1 l
Tris/HCl, 1,0 M, pH 6,8	121,14 g Tris
	Solve in H_2O ad 1 l
Tris/HCl, 1,5 M, pH 8,8	181,71 g Tris
	Solve in H_2O ad 1 l
Wash buffer for protein isolation	0,3 M Guanidin HCL
	Solve in 95 % Ethanol

Detection buffer, pH 9	0,1 M Tris-HCl 0,1 M NaCl
Urea-page: collection gel 4/3 4% acrylamide + 6M urea	17.7 ml Rotiphorese Gel30 36.03g urea Ad 100 ml H_20
Urea-page: separation gel 4/3 16% acrylamide + 6M urea	71.1 ml Rotiphorese Gel30 36.03g urea Ad 100 ml H20
4x lower tris	1.5M Tris-Cl pH=8.8 0.4% SDS
4x upper tris	0.5M Tris-Cl pH=6.8 0.4% SDS

5.2.3.1.3 DNA analysis

Mouse tail lysis buffer	50 mM KCl 10 mM Tris-HCl, pH 8.3 2 mM $MgCl_2$ 0.1 mg/ml gelatine 0.45 % Nonidet P-40 0.45 % Tween 20 Ad proteinase K before use 20 mg/ml
DNA loading dye	Bromphenol blue 0.25% (w/v) Xylene cyanol FF 0.25% (w/v) Ficoll 15% (w/v)
10x TBE buffer	TRIS 108g Borate 55g EDTA (0.5M), pH8 40ml Ad H_2O (destilled) ad 1l
Southern blot wash buffer, pH 7,5	100 mM maleic acid 150 mM NaCl 0.3 % Tween-20
Southern blot blocking, pH 7,5 1x DIG	100 mM maleic acid 150 mM NaCl 1 % blocking reagent, Roche Mannheim, Germany

5.2.3.1.4 RNA analysis

Northern blot sample buffer	110µl DEPC-H_2O 50µml 10x MOPS 90µl formaldehyde 250µl formamide
Northern blot buffer (for electrophoresis)	70ml 10xMOPS 630ml H_2O 3,85ml formaldehyde

10x MOPS	41.9g MOPS 4.1g Natriumacetate 4.45g Natrium$_2$acetate Sterile filtration, store in dark bottle

5.2.3.1.5 Animal experiments

1% CTAB	1g CTAB solve in 100ml H_2O
Dkk-1	Concentration: 10 ng/µl, injection volume: 3µl/eye Dilute stock solution (100ng/µl in PBS) 1:10 in PBS
BQ788	Concentration: 1µg/µl, injection volume: 2µl/eye Dilute stock solution (20µg/µl in 100%DMSO) 1:20 in PBS

5.2.3.2 Polyacrylamide gel electrophoresis

Table 16: SDS gels for western blot analysis

	Stacking gel	Resolving gel 10 %	Resolving gel 15 %
H_2O	0,68 ml	1,9 ml	1,3 ml
Rotiphorese® Gel 30	0,17 ml	1,7 ml	2,3 ml
Tris/HCl, 1 M, pH 6,8	0,13 ml	-	-
Tris/HCl, 1,5 M, pH 8,8	-	1,3 ml	1,3 ml
10 % SDS	0,01 ml	0,05 ml	0,05 ml
10 % APS	0,01 ml	0,05 ml	0,05 ml
TEMED	0,001 ml	0,002 ml	0,002 ml

Table 17: Gels for Urea page

	Collection gel	Separation gel
4/3 4% acrylamide + 6 M Urea	750 µl	-
4/3 16% acrylamide + 6 M Urea	-	3,75 ml
4x lower Tris	-	1,25 ml
4x upper Tris	250µl	-
APS (25%)	10 µl	50 µl
Temed	1 µl	5 µl

6 References

1. Kolb H. Simple Anatomy of the Retina. In: Kolb H, Fernandez E, Nelson R, Herausgeber. Webvision Organ Retina Vis Syst [Internet]. Salt Lake City (UT): University of Utah Health Sciences Center; 1995 [zitiert 28. Juli 2013]. Verfügbar unter: http://www.ncbi.nlm.nih.gov/books/NBK11533/
2. Gray H, Clemente CD. Anatomy of the human body. Philadelphia: Lea & Febiger; 1985.
3. Vaney DI, Sivyer B, Taylor WR. Direction selectivity in the retina: symmetry and asymmetry in structure and function. Nat Rev Neurosci. März 2012;13(3):194–208.
4. Crooks J, Kolb H. Localization of GABA, glycine, glutamate and tyrosine hydroxylase in the human retina. J Comp Neurol. 15. Januar 1992;315(3):287–302.
5. Lucas RJ, Douglas RH, Foster RG. Characterization of an ocular photopigment capable of driving pupillary constriction in mice. Nat Neurosci. Juni 2001;4(6):621–6.
6. Schmidt TM, Chen S-K, Hattar S. Intrinsically photosensitive retinal ganglion cells: many subtypes, diverse functions. Trends Neurosci. November 2011;34(11):572–80.
7. Kolb H, Nelson R. Amacrine cells of the cat retina. Vision Res. 1981;21(11):1625–33.
8. Voinescu PE, Emanuela P, Kay JN, Sanes JR. Birthdays of retinal amacrine cell subtypes are systematically related to their molecular identity and soma position. J Comp Neurol. 10. Dezember 2009;517(5):737–50.
9. Wässle H. Knock out of direction selectivity in the retina. Neuron. Juni 2001;30(3):644–6.
10. Masland RH. The neuronal organization of the retina. Neuron. 18. Oktober 2012;76(2):266–80.
11. Wässle H, Puller C, Müller F, Haverkamp S. Cone contacts, mosaics, and territories of bipolar cells in the mouse retina. J Neurosci Off J Soc Neurosci. 7. Januar 2009;29(1):106–17.
12. Masland RH. The neuronal organization of the retina. Neuron. 18. Oktober 2012;76(2):266–80.
13. Wässle H. Parallel processing in the mammalian retina. Nat Rev Neurosci. Oktober 2004;5(10):747–57.
14. Niesel P. [Physiologic principles of studying visual functions]. Klin Monatsblätter Für Augenheilkd. Mai 1989;194(5):294–300.
15. Haverkamp S, Wässle H. Immunocytochemical analysis of the mouse retina. J Comp Neurol. 14. August 2000;424(1):1–23.
16. García M, Vecino E. Role of Müller glia in neuroprotection and regeneration in the retina. Histol Histopathol. Oktober 2003;18(4):1205–18.
17. Gardner TW, Antonetti DA, Barber AJ, Lieth E, Tarbell JA. The molecular structure and function of the inner blood-retinal barrier. Doc Ophthalmol. 1. Januar 1999;97(3-4):229–37.
18. Scott A, Powner MB, Gandhi P, Clarkin C, Gutmann DH, Johnson RS, u. a. Astrocyte-Derived Vascular Endothelial Growth Factor Stabilizes Vessels in the Developing Retinal Vasculature. PLoS ONE. 29. Juli 2010;5(7):e11863.
19. Bringmann A, Reichenbach A. Role of Muller cells in retinal degenerations. Front Biosci J Virtual Libr. 1. Oktober 2001;6:E72–92.
20. Giaume C, Kirchhoff F, Matute C, Reichenbach A, Verkhratsky A. Glia: the fulcrum of brain diseases. Cell Death Differ. Juli 2007;14(7):1324–35.
21. Graeber MB, Stre'rt WJ. Microglia: Immune Network in the CNS. Brain Pathol. 1990;1(1):2–5.
22. Streit WJ. Microglia and neuroprotection: implications for Alzheimer's disease. Brain Res Brain Res Rev. April 2005;48(2):234–9.
23. Streit WJ. Microglia as neuroprotective, immunocompetent cells of the CNS. Glia. November 2002;40(2):133–9.

24. Hanisch U-K, Kettenmann H. Microglia: active sensor and versatile effector cells in the normal and pathologic brain. Nat Neurosci. November 2007;10(11):1387–94.
25. Karlstetter M, Ebert S, Langmann T. Microglia in the healthy and degenerating retina: insights from novel mouse models. Immunobiology. Oktober 2010;215(9-10):685–91.
26. Young RW. The renewal of photoreceptor cell outer segments. J Cell Biol. April 1967;33(1):61–72.
27. Anderson DH, Fisher SK. The photoreceptors of diurnal squirrels: outer segment structure, disc shedding, and protein renewal. J Ultrastruct Res. April 1976;55(1):119–41.
28. Palczewski K. Chemistry and biology of vision. J Biol Chem. 13. Januar 2012;287(3):1612–9.
29. Steinberg RH, Fisher SK, Anderson DH. Disc morphogenesis in vertebrate photoreceptors. J Comp Neurol. 1. April 1980;190(3):501–8.
30. Mustafi D, Engel AH, Palczewski K. Structure of Cone Photoreceptors. Prog Retin Eye Res. Juli 2009;28(4):289–302.
31. Zaidi FH, Hull JT, Peirson SN, Wulff K, Aeschbach D, Gooley JJ, u. a. Short-Wavelength Light Sensitivity of Circadian, Pupillary, and Visual Awareness in Humans Lacking an Outer Retina. Curr Biol. 18. Dezember 2007;17(24):2122–8.
32. Strauss O. The retinal pigment epithelium in visual function. Physiol Rev. Juli 2005;85(3):845–81.
33. Baylor D. How photons start vision. Proc Natl Acad Sci U S A. 23. Januar 1996;93(2):560–5.
34. Leskov IB, Klenchin VA, Handy JW, Whitlock GG, Govardovskii VI, Bownds MD, u. a. The gain of rod phototransduction: reconciliation of biochemical and electrophysiological measurements. Neuron. September 2000;27(3):525–37.
35. Grimm C, Wenzel A, Hafezi F, Yu S, Redmond TM, Remé CE. Protection of Rpe65-deficient mice identifies rhodopsin as a mediator of light-induced retinal degeneration. Nat Genet. Mai 2000;25(1):63–6.
36. Wenzel A, Reme CE, Williams TP, Hafezi F, Grimm C. The Rpe65 Leu450Met variation increases retinal resistance against light-induced degeneration by slowing rhodopsin regeneration. J Neurosci Off J Soc Neurosci. 1. Januar 2001;21(1):53–8.
37. Danciger M, Lyon J, Worrill D, Hoffman S, Lem J, Reme CE, u. a. New retinal light damage QTL in mice with the light-sensitive RPE65 LEU variant. Mamm Genome Off J Int Mamm Genome Soc. April 2004;15(4):277–83.
38. Danciger M, Matthes MT, Yasamura D, Akhmedov NB, Rickabaugh T, Gentleman S, u. a. A QTL on distal chromosome 3 that influences the severity of light-induced damage to mouse photoreceptors. Mamm Genome Off J Int Mamm Genome Soc. Juni 2000;11(6):422–7.
39. Stahl A, Connor KM, Sapieha P, Chen J, Dennison RJ, Krah NM, u. a. The mouse retina as an angiogenesis model. Invest Ophthalmol Vis Sci. Juni 2010;51(6):2813–26.
40. Fruttiger M. Development of the mouse retinal vasculature: angiogenesis versus vasculogenesis. Invest Ophthalmol Vis Sci. Februar 2002;43(2):522–7.
41. Hansen AC. Norrie's disease. Am J Ophthalmol. August 1968;66(2):328–32.
42. Warburg M. Norrie's disease. Birth Defects Orig Artic Ser. März 1971;7(3):117–24.
43. Townes PL, Roca PD. Norrie's disease (hereditary oculo-acoustic-cerebral degeneration). Report of a United States family. Am J Ophthalmol. November 1973;76(5):797–803.
44. Warburg M. Norrie's disease--differential diagnosis and treatment. Acta Ophthalmol (Copenh). März 1975;53(2):217–36.
45. Moreira-Filho CA, Neustein I. A presumptive new variant of Norrie's disease. J Med Genet. April 1979;16(2):125–8.
46. Donnai D, Mountford RC, Read AP. Norrie disease resulting from a gene deletion: clinical features and DNA studies. J Med Genet. Februar 1988;25(2):73–8.

47. Bleeker-Wagemakers EM, Zweije-Hofman I, Gal A. Norrie disease as part of a complex syndrome explained by a submicroscopic deletion of the X chromosome. Ophthalmic Paediatr Genet. November 1988;9(3):137–42.
48. Bleeker-Wagemakers LM, Friedrich U, Gal A, Wienker TF, Warburg M, Ropers HH. Close linkage between Norrie disease, a cloned DNA sequence from the proximal short arm, and the centromere of the X chromosome. Hum Genet. 1985;71(3):211–4.
49. Gal A, Stolzenberger C, Wienker T, Wieacker P, Ropers HH, Friedrich U, u. a. Norrie's disease: close linkage with genetic markers from the proximal short arm of the X chromosome. Clin Genet. März 1985;27(3):282–3.
50. Sims KB, Lebo RV, Benson G, Shalish C, Schuback D, Chen ZY, u. a. The Norrie disease gene maps to a 150 kb region on chromosome Xp11.3. Hum Mol Genet. Mai 1992;1(2):83–9.
51. Chen ZY, Hendriks RW, Jobling MA, Powell JF, Breakefield XO, Sims KB, u. a. Isolation and characterization of a candidate gene for Norrie disease. Nat Genet. Juni 1992;1(3):204–8.
52. Berger W, Meindl A, van de Pol TJ, Cremers FP, Ropers HH, Döerner C, u. a. Isolation of a candidate gene for Norrie disease by positional cloning. Nat Genet. Juni 1992;1(3):199–203.
53. Meindl A, Berger W, Meitinger T, van de Pol D, Achatz H, Dörner C, u. a. Norrie disease is caused by mutations in an extracellular protein resembling C-terminal globular domain of mucins. Nat Genet. Oktober 1992;2(2):139–43.
54. Chen Z-Y, Battinelli EM, Fielder A, Bundey S, Sims K, Breakefield XO, u. a. A mutation in the Norrie disease gene (NDP) associated with X-linked familial exudative vitreoretinopathy. Nat Genet. Oktober 1993;5(2):180–3.
55. Shastry BS. Identification of a recurrent missense mutation in the Norrie disease gene associated with a simplex case of exudative vitreoretinopathy. Biochem Biophys Res Commun. 8. Mai 1998;246(1):35–8.
56. Shastry BS, Hejtmancik JF, Trese MT. Identification of novel missense mutations in the Norrie disease gene associated with one X-linked and four sporadic cases of familial exudative vitreoretinopathy. Hum Mutat. 1997;9(5):396–401.
57. Torrente I, Mangino M, Gennarelli M, Novelli G, Giannotti A, Vadalà P, u. a. Two new missense mutations (A105T and C110G) in the norrin gene in two Italian families with Norrie disease and familial exudative vitreoretinopathy. Am J Med Genet. 17. Oktober 1997;72(2):242–4.
58. Fuchs S, Kellner U, Wedemann H, Gal A. Missense mutation (Arg121Trp) in the Norrie disease gene associated with x-linked exudative vitreoretinopathy. Hum Mutat. 1995;6(3):257–9.
59. Meindl A, Lorenz B, Achatz H, Hellebrand H, Schmitz-Valckenberg P, Meitinger T. Missense mutations in the NDP gene in patients with a less severe course of Norrie disease. Hum Mol Genet. März 1995;4(3):489–90.
60. Smallwood PM, Williams J, Xu Q, Leahy DJ, Nathans J. Mutational analysis of Norrin-Frizzled4 recognition. J Biol Chem. 9. Februar 2007;282(6):4057–68.
61. Robitaille J, MacDonald MLE, Kaykas A, Sheldahl LC, Zeisler J, Dubé M-P, u. a. Mutant frizzled-4 disrupts retinal angiogenesis in familial exudative vitreoretinopathy. Nat Genet. Oktober 2002;32(2):326–30.
62. Battinelli EM, Boyd Y, Craig IW, Breakefield XO, Chen ZY. Characterization and mapping of the mouse NDP (Norrie disease) locus (Ndp). Mamm Genome Off J Int Mamm Genome Soc. Februar 1996;7(2):93–7.
63. Meitinger T, Meindl A, Bork P, Rost B, Sander C, Haasemann M, u. a. Molecular modelling of the Norrie disease protein predicts a cystine knot growth factor tertiary structure. Nat Genet. Dezember 1993;5(4):376–80.
64. Meindl A, Berger W, Meitinger T, van de Pol D, Achatz H, Dörner C, u. a. Norrie disease is caused by mutations in an extracellular protein resembling C-terminal globular domain of mucins. Nat Genet. Oktober 1992;2(2):139–43.

65. Ohlmann A, Merkl R, Tamm ER. Focus on Molecules: Norrin. Exp Eye Res. September 2012;102:109–10.
66. Ohlmann A, Tamm ER. Norrin: Molecular and functional properties of an angiogenic and neuroprotective growth factor. Prog Retin Eye Res. Mai 2012;31(3):243–57.
67. Bernstein SL, Wong P. Regional expression of disease-related genes in human and monkey retina. Mol Vis. 5. November 1998;4:24.
68. Hartzer MK, Cheng M, Liu X, Shastry BS. Localization of the Norrie disease gene mRNA by in situ hybridization. Brain Res Bull. 15. Juli 1999;49(5):355–8.
69. Rehm HL, Zhang D-S, Brown MC, Burgess B, Halpin C, Berger W, u. a. Vascular defects and sensorineural deafness in a mouse model of Norrie disease. J Neurosci Off J Soc Neurosci. 1. Juni 2002;22(11):4286–92.
70. Luhmann UFO, Meunier D, Shi W, Lüttges A, Pfarrer C, Fundele R, u. a. Fetal loss in homozygous mutant Norrie disease mice: a new role of Norrin in reproduction. Genes New York N 2000. August 2005;42(4):253–62.
71. Ye X, Wang Y, Cahill H, Yu M, Badea TC, Smallwood PM, u. a. Norrin, frizzled-4, and Lrp5 signaling in endothelial cells controls a genetic program for retinal vascularization. Cell. 16. Oktober 2009;139(2):285–98.
72. Ye X, Smallwood P, Nathans J. Expression of the Norrie disease gene (Ndp) in developing and adult mouse eye, ear, and brain. Gene Expr Patterns GEP. Februar 2011;11(1-2):151–5.
73. Ohlmann A, Scholz M, Goldwich A, Chauhan BK, Hudl K, Ohlmann AV, u. a. Ectopic norrin induces growth of ocular capillaries and restores normal retinal angiogenesis in Norrie disease mutant mice. J Neurosci Off J Soc Neurosci. 16. Februar 2005;25(7):1701–10.
74. Richter M, Gottanka J, May CA, Welge-Lüssen U, Berger W, Lütjen-Drecoll E. Retinal vasculature changes in Norrie disease mice. Invest Ophthalmol Vis Sci. November 1998;39(12):2450–7.
75. Enyedi LB, de Juan E, Gaitan A. Ultrastructural study of Norrie's disease. Am J Ophthalmol. 15. April 1991;111(4):439–45.
76. Luhmann UFO, Lin J, Acar N, Lammel S, Feil S, Grimm C, u. a. Role of the Norrie disease pseudoglioma gene in sprouting angiogenesis during development of the retinal vasculature. Invest Ophthalmol Vis Sci. September 2005;46(9):3372–82.
77. Berger W, van de Pol D, Bächner D, Oerlemans F, Winkens H, Hameister H, u. a. An animal model for Norrie disease (ND): gene targeting of the mouse ND gene. Hum Mol Genet. Januar 1996;5(1):51–9.
78. Lenzner S, Prietz S, Feil S, Nuber UA, Ropers H-H, Berger W. Global gene expression analysis in a mouse model for Norrie disease: late involvement of photoreceptor cells. Invest Ophthalmol Vis Sci. September 2002;43(9):2825–33.
79. Lin S, Cheng M, Dailey W, Drenser K, Chintala S. Norrin attenuates protease-mediated death of transformed retinal ganglion cells. Mol Vis. 2009;15:26–37.
80. Seitz R, Hackl S, Seibuchner T, Tamm ER, Ohlmann A. Norrin mediates neuroprotective effects on retinal ganglion cells via activation of the Wnt/beta-catenin signaling pathway and the induction of neuroprotective growth factors in Muller cells. J Neurosci Off J Soc Neurosci. 28. April 2010;30(17):5998–6010.
81. MacDonald BT, Tamai K, He X. Wnt/beta-catenin signaling: components, mechanisms, and diseases. Dev Cell. Juli 2009;17(1):9–26.
82. MacDonald BT, He X. Frizzled and LRP5/6 receptors for Wnt/β-catenin signaling. Cold Spring Harb Perspect Biol. Dezember 2012;4(12).
83. Komiya Y, Habas R. Wnt signal transduction pathways. Organogenesis. April 2008;4(2):68–75.

84. Xu Q, Wang Y, Dabdoub A, Smallwood PM, Williams J, Woods C, u. a. Vascular Development in the Retina and Inner Ear: Control by Norrin and Frizzled-4, a High-Affinity Ligand-Receptor Pair. Cell. 19. März 2004;116(6):883–95.
85. Ye X, Wang Y, Nathans J. The Norrin/Frizzled4 signaling pathway in retinal vascular development and disease. Trends Mol Med. September 2010;16(9):417–25.
86. Zorn AM. Wnt signalling: antagonistic Dickkopfs. Curr Biol CB. 7. August 2001;11(15):R592–595.
87. Mao B, Wu W, Davidson G, Marhold J, Li M, Mechler BM, u. a. Kremen proteins are Dickkopf receptors that regulate Wnt/beta-catenin signalling. Nature. 6. Juni 2002;417(6889):664–7.
88. Junge HJ, Yang S, Burton JB, Paes K, Shu X, French DM, u. a. TSPAN12 regulates retinal vascular development by promoting Norrin- but not Wnt-induced FZD4/beta-catenin signaling. Cell. 16. Oktober 2009;139(2):299–311.
89. Deng C, Reddy P, Cheng Y, Luo C-W, Hsiao C-L, Hsueh AJW. Multi-functional norrin is a ligand for the LGR4 receptor. J Cell Sci. 1. Mai 2013;126(Pt 9):2060–8.
90. Xu S, Cheng F, Liang J, Wu W, Zhang J. Maternal xNorrin, a canonical Wnt signaling agonist and TGF-β antagonist, controls early neuroectoderm specification in Xenopus. PLoS Biol. 2012;10(3):e1001286.
91. Heckmann M. [Pathogenesis of retinopathy of prematurity]. Ophthalmol Z Dtsch Ophthalmol Ges. Dezember 2008;105(12):1101–7.
92. Hellstrom A, Perruzzi C, Ju M, Engstrom E, Hard AL, Liu JL, u. a. Low IGF-I suppresses VEGF-survival signaling in retinal endothelial cells: direct correlation with clinical retinopathy of prematurity. Proc Natl Acad Sci U S A. 8. Mai 2001;98(10):5804–8.
93. Stahl A, Connor KM, Sapieha P, Chen J, Dennison RJ, Krah NM, u. a. The mouse retina as an angiogenesis model. Invest Ophthalmol Vis Sci. Juni 2010;51(6):2813–26.
94. Remé CE, Grimm C, Hafezi F, Iseli HP, Wenzel A. Why study rod cell death in retinal degenerations and how? Doc Ophthalmol Adv Ophthalmol. Januar 2003;106(1):25–9.
95. Wenzel A, Grimm C, Samardzija M, Remé CE. Molecular mechanisms of light-induced photoreceptor apoptosis and neuroprotection for retinal degeneration. Prog Retin Eye Res. März 2005;24(2):275–306.
96. Hao W, Wenzel A, Obin MS, Chen C-K, Brill E, Krasnoperova NV, u. a. Evidence for two apoptotic pathways in light-induced retinal degeneration. Nat Genet. Oktober 2002;32(2):254–60.
97. Grimm C, Remé CE. Light damage as a model of retinal degeneration. Methods Mol Biol Clifton NJ. 2013;935:87–97.
98. Wenzel A, Grimm C, Samardzija M, Remé CE. Molecular mechanisms of light-induced photoreceptor apoptosis and neuroprotection for retinal degeneration. Prog Retin Eye Res. März 2005;24(2):275–306.
99. Rattner A, Nathans J. The genomic response to retinal disease and injury: evidence for endothelin signaling from photoreceptors to glia. J Neurosci Off J Soc Neurosci. 4. Mai 2005;25(18):4540–9.
100. Joly S, Lange C, Thiersch M, Samardzija M, Grimm C. Leukemia inhibitory factor extends the lifespan of injured photoreceptors in vivo. J Neurosci Off J Soc Neurosci. 17. Dezember 2008;28(51):13765–74.
101. Gao H, Hollyfield JG. Basic fibroblast growth factor: increased gene expression in inherited and light-induced photoreceptor degeneration. Exp Eye Res. Februar 1996;62(2):181–9.
102. Joly S, Pernet V, Chemtob S, Di Polo A, Lachapelle P. Neuroprotection in the juvenile rat model of light-induced retinopathy: evidence suggesting a role for FGF-2 and CNTF. Invest Ophthalmol Vis Sci. Mai 2007;48(5):2311–20.

103. Xu Q, Wang Y, Dabdoub A, Smallwood PM, Williams J, Woods C, u. a. Vascular development in the retina and inner ear: control by Norrin and Frizzled-4, a high-affinity ligand-receptor pair. Cell. 19. März 2004;116(6):883–95.
104. Yi H, Nakamura REI, Mohamed O, Dufort D, Hackam AS. Characterization of Wnt signaling during photoreceptor degeneration. Invest Ophthalmol Vis Sci. Dezember 2007;48(12):5733–41.
105. Cerpa W, Toledo EM, Varela-Nallar L, Inestrosa NC. The role of Wnt signaling in neuroprotection. Drug News Perspect. Dezember 2009;22(10):579–91.
106. Ohlmann A, Seitz R, Braunger B, Seitz D, Bösl MR, Tamm ER. Norrin promotes vascular regrowth after oxygen-induced retinal vessel loss and suppresses retinopathy in mice. J Neurosci Off J Soc Neurosci. 6. Januar 2010;30(1):183–93.
107. Braunger BM, Ohlmann A, Koch M, Tanimoto N, Volz C, Yang Y, u. a. Constitutive overexpression of Norrin activates Wnt/β-catenin and endothelin-2 signaling to protect photoreceptors from light damage. Neurobiol Dis. Februar 2013;50:1–12.
108. Yannuzzi LA, Ober MD, Slakter JS, Spaide RF, Fisher YL, Flower RW, u. a. Ophthalmic fundus imaging: today and beyond. Am J Ophthalmol. März 2004;137(3):511–24.
109. Nandakumar N, Buzney S, Weiter JJ. Lipofuscin and the principles of fundus autofluorescence: a review. Semin Ophthalmol. November 2012;27(5-6):197–201.
110. Rückmann A von, Fitzke FW, Bird AC. Fundus autofluorescence in age-related macular disease imaged with a laser scanning ophthalmoscope. Invest Ophthalmol Vis Sci. 2. Januar 1997;38(2):478–86.
111. Hageman GS, Johnson LV. Biochemical characterization of the major peanut-agglutinin-binding glycoproteins in vertebrate retinae. J Comp Neurol. 22. Juli 1986;249(4):499–510, 482–3.
112. LaVail MM, Faktorovich EG, Hepler JM, Pearson KL, Yasumura D, Matthes MT, u. a. Basic fibroblast growth factor protects photoreceptors from light-induced degeneration in albino rats. Ann N Y Acad Sci. 1991;638:341–7.
113. Wen R, Song Y, Cheng T, Matthes MT, Yasumura D, LaVail MM, u. a. Injury-induced upregulation of bFGF and CNTF mRNAS in the rat retina. J Neurosci Off J Soc Neurosci. November 1995;15(11):7377–85.
114. Flügel-Koch C, Ohlmann A, Piatigorsky J, Tamm ER. Disruption of anterior segment development by TGF-beta1 overexpression in the eyes of transgenic mice. Dev Dyn Off Publ Am Assoc Anat. Oktober 2002;225(2):111–25.
115. Duncan MK, Li X, Ogino H, Yasuda K, Piatigorsky J. Developmental regulation of the chicken beta B1-crystallin promoter in transgenic mice. Mech Dev. Juni 1996;57(1):79–89.
116. Boulanger A, Liu S, Henningsgaard AA, Yu S, Redmond TM. The upstream region of the Rpe65 gene confers retinal pigment epithelium-specific expression in vivo and in vitro and contains critical octamer and E-box binding sites. J Biol Chem. 6. Oktober 2000;275(40):31274–82.
117. Boulanger A, Redmond TM. Expression and promoter activation of the Rpe65 gene in retinal pigment epithelium cell lines. Curr Eye Res. Mai 2002;24(5):368–75.
118. Manès G, Leducq R, Kucharczak J, Pagès A, Schmitt-Bernard CF, Hamel CP. Rat messenger RNA for the retinal pigment epithelium-specific protein RPE65 gradually accumulates in two weeks from late embryonic days. FEBS Lett. 20. Februar 1998;423(2):133–7.
119. Braunger BM, Pielmeier S, Demmer C, Landstorfer V, Kawall D, Abramov N, u. a. TGF-β Signaling Protects Retinal Neurons from Programmed Cell Death during the Development of the Mammalian Eye. J Neurosci Off J Soc Neurosci. 28. August 2013;33(35):14246–58.
120. Young RW. Cell death during differentiation of the retina in the mouse. J Comp Neurol. 1. November 1984;229(3):362–73.
121. Cepko CL, Austin CP, Yang X, Alexiades M, Ezzeddine D. Cell fate determination in the vertebrate retina. Proc Natl Acad Sci U S A. 23. Januar 1996;93(2):589–95.

122. Ranchon Cole I, Bonhomme B, Doly M. Pre-treatment of adult rats with high doses of erythropoietin induces caspase-9 but prevents light-induced retinal injury. Exp Eye Res. Dezember 2007;85(6):782–9.
123. LaVail MM, Gorrin GM, Repaci MA. Strain differences in sensitivity to light-induced photoreceptor degeneration in albino mice. Curr Eye Res. Juni 1987;6(6):825–34.
124. Kubota R, Boman NL, David R, Mallikaarjun S, Patil S, Birch D. Safety and effect on rod function of ACU-4429, a novel small-molecule visual cycle modulator. Retina Phila Pa. Januar 2012;32(1):183–8.
125. Kubota R, Al-Fayoumi S, Mallikaarjun S, Patil S, Bavik C, Chandler JW. PHASE 1, DOSE-RANGING STUDY OF EMIXUSTAT HYDROCHLORIDE (ACU-4429), A NOVEL VISUAL CYCLE MODULATOR, IN HEALTHY VOLUNTEERS. Retina Phila Pa. 19. September 2013;
126. Young RW. Pathophysiology of age-related macular degeneration. Surv Ophthalmol. April 1987;31(5):291–306.
127. Iriyama A, Fujiki R, Inoue Y, Takahashi H, Tamaki Y, Takezawa S, u. a. A2E, a Pigment of the Lipofuscin of Retinal Pigment Epithelial Cells, Is an Endogenous Ligand for Retinoic Acid Receptor. J Biol Chem. 5. Februar 2008;283(18):11947–53.
128. Wang Y, Huso D, Cahill H, Ryugo D, Nathans J. Progressive cerebellar, auditory, and esophageal dysfunction caused by targeted disruption of the frizzled-4 gene. J Neurosci Off J Soc Neurosci. 1. Juli 2001;21(13):4761–71.
129. Chiang A, Priya R, Ramaswami M, Vijayraghavan K, Rodrigues V. Neuronal activity and Wnt signaling act through Gsk3-beta to regulate axonal integrity in mature Drosophila olfactory sensory neurons. Dev Camb Engl. April 2009;136(8):1273–82.
130. LaVail MM, Unoki K, Yasumura D, Matthes MT, Yancopoulos GD, Steinberg RH. Multiple growth factors, cytokines, and neurotrophins rescue photoreceptors from the damaging effects of constant light. Proc Natl Acad Sci U S A. 1. Dezember 1992;89(23):11249–53.
131. Inomata Y, Hirata A, Koga T, Kimura A, Singh DP, Shinohara T, u. a. Lens epithelium-derived growth factor: neuroprotection on rat retinal damage induced by N-methyl-D-aspartate. Brain Res. 21. November 2003;991(1-2):163–70.
132. Machida S, Chaudhry P, Shinohara T, Singh DP, Reddy VN, Chylack LT Jr, u. a. Lens epithelium-derived growth factor promotes photoreceptor survival in light-damaged and RCS rats. Invest Ophthalmol Vis Sci. April 2001;42(5):1087–95.
133. Nakamura M, Singh DP, Kubo E, Chylack LT Jr, Shinohara T. LEDGF: survival of embryonic chick retinal photoreceptor cells. Invest Ophthalmol Vis Sci. April 2000;41(5):1168–75.
134. Zhang M, Mo X, Fang Y, Guo W, Wu J, Zhang S, u. a. Rescue of photoreceptors by BDNF gene transfer using in vivo electroporation in the RCS rat of retinitis pigmentosa. Curr Eye Res. September 2009;34(9):791–9.
135. Gauthier R, Joly S, Pernet V, Lachapelle P, Di Polo A. Brain-derived neurotrophic factor gene delivery to muller glia preserves structure and function of light-damaged photoreceptors. Invest Ophthalmol Vis Sci. September 2005;46(9):3383–92.
136. Chylack LT Jr, Fu L, Mancini R, Martin-Rehrmann MD, Saunders AJ, Konopka G, u. a. Lens epithelium-derived growth factor (LEDGF/p75) expression in fetal and adult human brain. Exp Eye Res. Dezember 2004;79(6):941–8.
137. Bennett JL, Zeiler SR, Jones KR. Patterned expression of BDNF and NT-3 in the retina and anterior segment of the developing mammalian eye. Invest Ophthalmol Vis Sci. November 1999;40(12):2996–3005.
138. Klein R, Nanduri V, Jing SA, Lamballe F, Tapley P, Bryant S, u. a. The trkB tyrosine protein kinase is a receptor for brain-derived neurotrophic factor and neurotrophin-3. Cell. 26. Juli 1991;66(2):395–403.

139. Parada LF, Tsoulfas P, Tessarollo L, Blair J, Reid SW, Soppet D. The Trk family of tyrosine kinases: receptors for NGF-related neurotrophins. Cold Spring Harb Symp Quant Biol. 1992;57:43–51.
140. Murakami K, Mathew R, Huang J, Farahani R, Peng H, Olson SC, u. a. Smurf1 ubiquitin ligase causes downregulation of BMP receptors and is induced in monocrotaline and hypoxia models of pulmonary arterial hypertension. Exp Biol Med Maywood NJ. Juli 2010;235(7):805–13.
141. Brunet A, Datta SR, Greenberg ME. Transcription-dependent and -independent control of neuronal survival by the PI3K-Akt signaling pathway. Curr Opin Neurobiol. Juni 2001;11(3):297–305.
142. Wahlin KJ, Campochiaro PA, Zack DJ, Adler R. Neurotrophic factors cause activation of intracellular signaling pathways in Müller cells and other cells of the inner retina, but not photoreceptors. Invest Ophthalmol Vis Sci. März 2000;41(3):927–36.
143. Harada C, Guo X, Namekata K, Kimura A, Nakamura K, Tanaka K, u. a. Glia- and neuron-specific functions of TrkB signalling during retinal degeneration and regeneration. Nat Commun. 2011;2:189.
144. Rohrer B, Korenbrot JI, LaVail MM, Reichardt LF, Xu B. Role of neurotrophin receptor TrkB in the maturation of rod photoreceptors and establishment of synaptic transmission to the inner retina. J Neurosci Off J Soc Neurosci. 15. Oktober 1999;19(20):8919–30.
145. Grishanin RN, Yang H, Liu X, Donohue-Rolfe K, Nune GC, Zang K, u. a. Retinal TrkB receptors regulate neural development in the inner, but not outer, retina. Mol Cell Neurosci. Juli 2008;38(3):431–43.
146. Di Polo A, Cheng L, Bray GM, Aguayo AJ. Colocalization of TrkB and brain-derived neurotrophic factor proteins in green-red-sensitive cone outer segments. Invest Ophthalmol Vis Sci. November 2000;41(12):4014–21.
147. Vecino E, García-Crespo D, García-Grespo D, García M, Martinez-Millán L, Sharma SC, u. a. Rat retinal ganglion cells co-express brain derived neurotrophic factor (BDNF) and its receptor TrkB. Vision Res. Januar 2002;42(2):151–7.
148. Dorrell MI, Friedlander M. Mechanisms of endothelial cell guidance and vascular patterning in the developing mouse retina. Prog Retin Eye Res. Mai 2006;25(3):277–95.
149. Saint-Geniez M, D'Amore PA. Development and pathology of the hyaloid, choroidal and retinal vasculature. Int J Dev Biol. 2004;48(8-9):1045–58.
150. Herrnberger L, Seitz R, Kuespert S, Bösl MR, Fuchshofer R, Tamm ER. Lack of endothelial diaphragms in fenestrae and caveolae of mutant Plvap-deficient mice. Histochem Cell Biol. November 2012;138(5):709–24.
151. Smith LE, Wesolowski E, McLellan A, Kostyk SK, D'Amato R, Sullivan R, u. a. Oxygen-induced retinopathy in the mouse. Invest Ophthalmol Vis Sci. Januar 1994;35(1):101–11.
152. Seitz R, Hackl S, Seibuchner T, Tamm ER, Ohlmann A. Norrin mediates neuroprotective effects on retinal ganglion cells via activation of the Wnt/beta-catenin signaling pathway and the induction of neuroprotective growth factors in Muller cells. J Neurosci Off J Soc Neurosci. 28. April 2010;30(17):5998–6010.
153. Ohlmann A, Seitz R, Braunger B, Seitz D, Bösl MR, Tamm ER. Norrin promotes vascular regrowth after oxygen-induced retinal vessel loss and suppresses retinopathy in mice. J Neurosci Off J Soc Neurosci. 6. Januar 2010;30(1):183–93.
154. DasGupta R, Fuchs E. Multiple roles for activated LEF/TCF transcription complexes during hair follicle development and differentiation. Dev Camb Engl. Oktober 1999;126(20):4557–68.
155. Mullis K, Faloona F, Scharf S, Saiki R, Horn G, Erlich H. Specific enzymatic amplification of DNA in vitro: the polymerase chain reaction. Cold Spring Harb Symp Quant Biol. 1986;51 Pt 1:263–73.
156. Samardzija M, Wenzel A, Naash M, Remé CE, Grimm C. Rpe65 as a modifier gene for inherited retinal degeneration. Eur J Neurosci. Februar 2006;23(4):1028–34.

157. Diamandis EP, Christopoulos TK. The biotin-(strept)avidin system: principles and applications in biotechnology. Clin Chem. 5. Januar 1991;37(5):625–36.
158. Green NM. Avidin. Adv Protein Chem. 1975;29:85–133.
159. RICHARDSON KC, JARETT L, FINKE EH. Embedding in epoxy resins for ultrathin sectioning in electron microscopy. Stain Technol. November 1960;35:313–23.
160. Connor KM, Krah NM, Dennison RJ, Aderman CM, Chen J, Guerin KI, u. a. Quantification of oxygen-induced retinopathy in the mouse: a model of vessel loss, vessel regrowth and pathological angiogenesis. Nat Protoc. Oktober 2009;4(11):1565–73.
161. Tanimoto N, Muehlfriedel RL, Fischer MD, Fahl E, Humphries P, Biel M, u. a. Vision tests in the mouse: Functional phenotyping with electroretinography. Front Biosci Landmark Ed. 2009;14:2730–7.
162. Kueng-Hitz N, Grimm C, Lansel N, Hafezi F, He L, Fox DA, u. a. The Retina of c-fos−/− Mice: Electrophysiologic, Morphologic and Biochemical Aspects. Invest Ophthalmol Vis Sci. 3. Januar 2000;41(3):909–16.

The picture of Leonardo da Vinci on the third page was taken from

http://www.medicalinfo.asia/a-glimpse-into-the-archives-of-da-vincis-anatomical-drawings

7 Abbreviations

A	ampere
α	alpha/ anti
AMD	age related macular degeneration
AU	arbitrary unit
β	beta
BDNF	brain derived neurotrophic factor
bidest.	bidestillatus
BMP	bone morphogenetic protein
bp	base pair
BrdU	bromdesoxyuridine
BSA	bovin serum albumin
°C	grade Celsius
cDNA	complementary DNA
cGMP	cyclic guanosine monophosphate
CNS	central nervous system
CNTF	ciliary neurotrophic factor
d	day
da	Dalton
DAPI	4’,6-Diamidin-2-phenylindol
DNA	deoxyribonucleic acid
dNTPs	desoxyribonucleoside triphosphate
dUTP	desoxyuridine triphosphate
EDN2	Endothelin2
EDNRB	Endothelin receptor type B
ERG	electroretinography
FGF-2	fibroblast growth factor 2
FITC	fluorescein isothiocyanate-dextran
fwd	forward
g	gram
GAPDH	glycerinaldehyd-3-phosphat-Dehydrogenase
GFAP	glial fibrillary acidic protein
GFP	green fluorescent protein
GS	glutamine synthetase

h	hour
H2O	water
HRP	horseradish peroxidase
k	kilo
l	liter
LEDGF	lens epithelium derived growth factor
LIF	leukemia inhibitory factor
M	Molar
m	meter, milli
MgCl2	magnesium chloride
min	minute
mm	mus musculus
mRNA	messenger RNA
MW	molecular weight
µ	mikro
n	nano
NaCl	sodium chloride
NDP	Norrin disease pseudoglioma
Nor-29	βB1-Crystallin Norrin line 29
P	postnatal day
PBS	phosphate buffered saline
PDE	phosphodiesterase
PCR	polymerase chain reaction
PEDF	pigment epithelium derived growth factor
PFA	paraformaldehyd
PLVAP	plasmalemma vesicle-associated protein
PVDF	polyvinylfluoride
rev	reverse
RNA	ribonucleic acid
RPE	retinal pigment epithelium
rpm	revolutions per minute
rTdT	terminal deoxynucleotidyl transferase, recombinant
RT	room temperature
ROP	retinopathia of prematurity
s	second

SEM	standard error of the mean
Smad	Sma- and Mad-related Protein
SSC	Standard Saline Citrate
Taq	thermus aquaticus
TBE	TRIS-Borat-EDTA-Puffer
TBS	TRIS buffered saline
TBST	TRIS buffered saline Tween-20
TEMED	N,N,N´,N´-tetramethyl ethylendiamine
TGFβ	transforming growth factor beta
Tris	tris(hydroxymethyl)aminomethan
TUNEL	TdT-mediated dUTP-biotin nick end labelling
U	unit
V	Volt
VEGF	vascular endothelial growth factor
W	Watt
WNT	Wingless-related integration site
%	percent

8 Figure and table legend

8.1 Figure Legend

8.2 Table Legend

9 Danksagung

Bei Prof. Ernst Tamm möchte ich mich recht herzlich für das interessante Projekt, die vielen fachlich spannenden Diskussionen und für die Übernahme des Gutachtens bedanken. Ich freue mich auf die folgenden gemeinsamen Projekte und auf unsere weitere Zusammenarbeit.

Prof. Bernhard Weber danke ich für die Bereitschaft, das Zweitgutachten zu übernehmen.

Andreas Ohlmann und Roswitha Seitz möchte ich für die kollegiale Zusammenarbeit am Norrinprojekt danken.

Bei Elke, Angelika, Margit, Silvia und Katharina möchte ich mich für die hilfsbereite Unterstützung und die vielen wertvollen Tipps bei histologischen, immunhistologischen und molekularbiologischen Versuchen bedanken.

Außerdem möchte ich Markus, Walter und Marcus für ihre kompetente fachliche Unterstützung und Hilfsbereitschaft in meiner Anfangszeit und für vieles mehr danken.

Weiterhin danke ich auch allen anderen Mitgliedern des Lehrstuhls für die freundschaftliche Arbeitsatmosphäre.

Meinen Eltern, Geschwistern und vor allem meinem Mann Andreas möchte ich ganz herzlich danken, dass sie mich während dieser doch etwas stressigen Zeit unterstützt, motiviert und an mich geglaubt haben.

10 Erklärung

Hiermit erkläre ich, dass ich die vorliegende Dissertation selbstständig und ohne unerlaubte Hilfsmittel angefertigt habe.

Regensburg, den

Barbara Braunger